

DESIGN ANALYSIS OF LINE-START INTERIOR
PERMANENT MAGNET SYNCHRONOUS MOTOR

HOSSAN MOHAMMAD ZUBAYER



Design Analysis of Line-start Interior Permanent Magnet Synchronous Motor

by

Hossan Mohammad Zubayer

A thesis is submitted to the School of Graduate Studies
in partial fulfilment of the requirements for the degree of
Master of Engineering

Faculty of Engineering and Applied Science
Memorial University of Newfoundland

May 2011

St. John's

Newfoundland

Canada

Abstract

The past 25 years have been a significant period with advances in the development of interior permanent magnet machines. Over this period, line-start interior permanent magnet synchronous motors have expanded their presence in the industrial and domestic marketplace from few specialized niche markets in high efficiency machine tools, household appliances, small utility motors and servo drives to mass-produced automotive applications. A closer examination reveals that several different knowledge-based technological advancements and market forces as well as consumer demand for high efficiency requirements have combined, sometimes in fortuitous ways, to accelerate the development of the improved new small energy efficient motors.

Compared with squirrel-cage induction machines, line-start permanent magnet machines have high efficiency and high power factor because they exhibit two torque components namely the permanent magnet torque and the reluctance torque. Though the stator of a permanent magnet motor is the same as that of an induction motor, numerous configurations are possible in term of the ways the permanent magnet is placed in the rotor. In order to find the optimized structure, line-start permanent magnet synchronous machines with different rotor structures will be comparatively studied in terms of dynamics and steady state performance and transient process with finite element method.

The advances in computing power have seen numerical methods like Finite Element Analysis (FEA) being employed in various design problems of interior permanent magnet (IPM) motors. This thesis presents the design, analysis and simulation of line-start IPM synchronous motors. Analytical derivations are provided. Taking into account inherent advantages of numerical methods like FEA for optimum design, shape and orientation of IPM motors, simulation codes for Laboratory IPM motors are presented. Three sets of rotors for the IPMSM are analyzed using time-stepping FEA. This works provide cost

effective simulations. The simulated results are compared with those published in the literature for verifications.

Acknowledgement

My heart-felt gratitude goes to my supervisor Dr. M. A. Rahman for his guidance, advice and tutelage throughout my stint here in this university. It is his able care that eased my way through gruelling complicacies of investigative research.

I acknowledge the contribution of Dr. Saleh Saleh of Marine Institute, Dr. Kai Wang, post-doctoral fellow in Memorial University of Newfoundland and Dr. Ping Zhou of Ansoft Corporation for their contribution and inspiration in completing this thesis. I want to thank Dr. M. A. Rahman and the School of Graduate Studies, the Faculty of Engineering and Applied Science for their constant financial support.

Finally, I want to thank my mother Hosne Jahan for her endless inspiration all through my life. I want to dedicate this work to my father, Md. Mokhesur Rahman, who always wanted me to be an engineer.

Contents

Abstract	ii
Acknowledgement	iv
List of Symbols	xi
List of Figures	xv
1. Introduction	
1.1 Introduction	1
1.2 Literature Review	
1.2.1 History and Evolution of Permanent Magnet Materials	3
1.2.2 Permanent Magnet Synchronous Motor (PMSM)	6
1.2.3 Line Start Permanent Magnet Synchronous Motors	9
1.3 Brief Review of Numerical Techniques	11
1.4 Thesis Objective	16
1.5 Outline of Chapters	17
2. Mathematical Modeling of Interior Permanent Magnet Motor	
2.1. System Equations for Permanent Magnet motors	18
2.2 Modeling of Interior Permanent Magnet Synchronous Motor	28

2.3 Park's Transformation	31
2.4 Relationship between a-b-c axis and d-q axis quantities in stationary and synchronous reference form	36
2.5 Torque expression of PMSM	39
3. Finite Element Approach	
3.1 Finite Element Approach	42
3.1.1. Equations for magnetic field windings	43
3.2 Finite Element Formulation	
3.2.1 Discretization of the 2-D domain	47
3.2.2 Choosing an Interpolation Function	47
3.2.3 Derivation of the element matrices and vectors	48
3.2.3.1 Weighted Residual Method	48
3.2.4 Assembly of Global Matrix	49
3.2.5 Imposition of Boundary Condition	50
3.2.5.1 Dirichlet Boundary Conditions	50
3.2.5.2 Mixed Boundary Conditions	50
3.2.6 Solution of the global matrix system	51
3.3 Finite Element Formulation of Electromagnetic Field	51
3.4 Boundary Conditions	55

3.5 Forces and Torque Calculation in an Electromagnetic Field	55
3.5.1 Maxwell Stress Tensor	56
3.5.2 Arkkio's Method	56
3.5.3 Method of Magnetic Coenergy Derivation	57
3.5.4 Coulomb's Virtual Work	57
3.5.5 Magnetizing Current Method	58
3.6 Inductance and Reactance Calculation in a Electromagnetic Field	58
3.6.1 Dynamic Inductance Calculation	58
3.6.2 Steady-state Inductance Calculation	60
3.6.3 Synchronous Reactance Calculation	60
3.6.4 Leakage Reactance Calculation	63
3.7 Times-stepping finite element analysis	63
4. Design Case Studies	
4.1 Analytical vs. Finite Element Analysis	64
4.2 Computer Aided Design	65
4.3 Maxwell® Software Package for Analysis of Electric Motor	67
4.3.1 Maxwell 2D	67
4.3.2 Two Dimensional (2D) AC Magnetic	67

4.3.3 Two Dimensional (2D) DC Magnetic	68
4.3.4 Electrostatic field calculation	68
4.3.5 Magnetostatic Field Solution	69
4.3.6 Eddy Current Analysis	69
4.3.7 Transient Analysis	70
4.4 Design Components in Maxwell® package	71
4.4.1 RMXpert	71
4.4.2 External Circuit Editor	74
4.4.3 PExprt™	75
4.4.4 PEmag™	77
4.5 Design application and workflow of Maxwell 2D	77
4.5.1 Creating a project for Maxwell 2D	78
4.5.2 Drawing the Project	80
4.5.2.1 Stator Slot Design	80
4.5.2.2 Rotor Slot Design	82
4.5.2.3 Rotor Pole Geometries	82
4.5.3 Setting up the problem	85
4.5.3.1 Assign materials to objects	85
4.5.3.2 Setting up boundary condition	85

4.5.3.3 Assigning voltage and current source excitation	86
4.5.4 Defining forces, torques and related values	86
4.5.5 Setting up the analysis	87
4.5.6 Solving the problem	88
4.5.7 Post processor	88
5. Simulation and Results	
5.1 Working Model	90
5.2 Straight shape line-start IPMSM	91
5.2.1 Performance Investigation of Straight Shape line-start IPMSM	95
5.3 V- Shape line-start IPMSM	98
5.3.1 Performance Investigation	102
5.4 Partial V-shape line-start IPMSM	107
5.4.1 Loss Calculation	114
5.4.2 Airgap Flux Distribution calculation	117
5.4.3 Back-EMF Calculation	118
5.4.4 Cogging Torque Calculation	119
5.5 Partial V-shape with concentrated winding	120
6. Conclusion and Future Work	123

References	126
Appendix A	
Setting Up a Maxwell Design for IPM motors	135
Appendix B	
Results from Published Literature	154

List of Figures

1.1 History of Development of PM Materials	6
1.2 Schematic cross section of a 4-pole PMSM.	7
1.3 Different configuration of IPM rotors: a) full V-shape PM, b) surface mounted PM c) Modified hybrid PM, d) straight PM and extended rotor bars, e) U-shaped PM , f) partial V-shape PM and poles producing air gap length, g) mixed PM h) straight –mixed PM for high flux i) partial straight V-shape PM	8
2.1 Two-pole, wye-connected, salient pole synchronous machine	20
2.2 Park's model of PMSM (a) d-axis,	35
2.2 Park's model of PMSM (b) q-axis	36
2.3 Stationary d-q axis to synchronously rotating d'-q' axis transformation	39
3.1 Typical triangular element connected to other elements	52
3.2 Mesh generated by Maxwell® for one-quarter of cross-section of a motor	53
3.3 Phasor Diagram of a PM Motor	61
4.1 Winding Type for RMxp ^{rt} ™	73
4.2 Winding Editor for RMxp ^{rt} ™	74
4.3 Few components used in Maxwell Circuit Editor Schematic	75
4.4 Design window of PExp ^{rt} ™	77

4.5 Flow chart for Maxwell® 2D	78
4.6 Project window of Maxwell® 2D	79
4.7 (a, b, c, d, e, f) Six separate structure for stator slot	81
4.8 (a) Whole-coiled concentric stator winding arrangement	82
4.8 (b) Half-coiled concentric stator winding arrangement	82
4.9 (a,b,c,d) Various rotor pole structure.	83
4.10 Drawing window of Autocad®	84
4.11 Mesh plot for concentrated winding permanent magnet machine	87
5.1 Cross-section of line-start IPMSM with straight-shape magnet arrangement	91
5.2 BH curve for the material “50www470”	93
5.3(a) Flux lines for line-start IPMSM with straight magnet arrangement	94
5.3(b) Flux density of line-start IPMSM with straight magnet arrangement	94
5.4 Torque –time response for line-start IPMSM	95
5.5 Induced voltage –time response for straight shape line-start IPMSM	96
5.6 Core loss-time response for straight shape line-start IPMSM	97
5.7 Solid Loss-time response for straight shape line-start IPMSM	98
5.8 Cross-section of line-start IPMSM with V-shaped magnet arrangement	100
5.9 Flux lines for line-start IPMSM with V-shaped magnet arrangement	101

5.10 Flux density distribution for line-start IPMSM with V-shaped magnet arrangement	101
5.11 Speed – time response for V-shaped line-start IPMSM	102
5.12 Demagnetization curve of NEOREC Magnet	104
5.13 Flux density for V-shaped line-start IPMSM with an initial angle of -45°	104
5.14 Speed-time response of V-shaped line-start IPMSM	105
5.15 Torque-time response of V-shaped line-start IPMSM	105
5.16 Induced voltage- time response of V- shaped line-start IPMSM	106
5.17 Induced current-time response of V-shaped line-start IPMSM	106
5.18 Cross-section of line-start IPMSM with partially V-shaped magnet arrangement	110
5.19 Finite Elements (grid) for partial V-shaped IPMSM for magnetic flux distribution in the motor	110
5.20 Magnetic flux lines (contours) for partially V-shaped line-start IPMSM	111
5.21 Flux density for partially V-shaped line-start IPMSM	111
5.22 Speed-time response of line-start partial V-shaped IPMSM	112
5.23 Torque-time response of partial V-shaped line-start IPMSM	112
5.24 Motor current-time response partial V-shaped line-start IPMSM (Phase A)	113
5.25 Simulated voltage versus time waveforms of line-start IPMSM	113
5.26 Flux lines vs. Normalized distance for partial V-shaped IPMSM	114

5.27 Core Loss- time response for partial V-shaped line-start IPMSM	115
5.28 Standard Loss- time response of partial V-shaped line-start IPMSM	116
5.29 Loss-time report on partial V-shaped line-start IPMSM	116
5.30 Flux distribution vs. normalized distance curve	117
5.31 Back EMF- waveforms for partial V-shaped IPMSM	118
5.32 Cogging torque vs. time curve for partial V-shaped line-start IPMSM	119
5.33 Partial V-shaped line-start IPMSM with concentrated winding	120
5.34 Flux lines in partial V-shaped line-start IPMSM with concentrated winding	121
5.35 Flux density distribution in partial V-shaped line-start IPMSM with concentrated winding	121

List of Symbols

v_a, v_b and v_c	A, B and C phase voltage respectively
i_a, i_b, i_c and i_f	A, B, C phase and field current respectively
r_{as}, r_{bs} and r_{cs}	A, B and C phase stator resistance respectively
v_{as}, v_{bs} and v_{cs}	A, B and C phase stator voltage respectively
V_{dq0}	vector of d, q and 0 axis voltages
V_{abc}	vector of a, b and c axis voltages
i_{dq0}	d or q or 0 axis current respectively
λ_{dq0}	d or q or 0 axis flux-linkage respectively
v_d and v_q	d and q axis voltages respectively
i_d and i_q	d and q axis current respectively
N_s	is the number of conductors in stator per phase
N_p	is the maximum no. of conductor in turn/ phase
MMF	Magnetomotive force
MMF_{as}	Magnetomotive force created by phase A of stator winding
MMF_{bs}	Magnetomotive force created by phase B of stator winding
MMF_{cs}	Magnetomotive force created by phase C of stator winding
MMF_s	Magnetomotive force created by phase stator winding

MMF_f	Magnetomotive force created by field winding
X	widest gap approximated in airgap
Y	narrowest gap approximated in airgap
α_1 & α_2	two constants used to explain the airgap
i_{as}	current due to phase A of stator winding
i_{bs}	current due to phase B of stator winding
i_{cs}	current due to phase C of stator winding
λ_{as}	Flux linkage due to phase A of stator winding
λ_{bs}	Flux linkage due to phase B of stator winding
λ_{cs}	Flux linkage due to phase C of stator winding
λ_{fs}	Flux linkage due to stator winding and field winding
$\lambda_a, \lambda_b, \lambda_c$ and λ_f	A, B, C phase and field flux linkages respectively
$\lambda_{aas}, \lambda_{bbs}, \lambda_{ccs}$	self flux linkage for phase A, B and C respectively
λ_{abs} or λ_{bas}	mutual inductance between phase A and B of stator winding
λ_{acs} or λ_{cas}	mutual inductance between phase A and C of stator winding
λ_{bcs} or λ_{cbs}	mutual inductance between phase B and C of stator winding
λ_{asf} or λ_{fas}	mutual inductance between phase A of stator winding and field winding
λ_{bsf} or λ_{fbs}	mutual inductance between phase B of stator winding and field winding

λ_{csf} or λ_{fcs}	mutual inductance between phase C of stator winding and field winding
$L_{aas}, L_{bbs}, L_{ccs}$	self-inductance for phase A, B and C respectively
L_{ff}	leakage inductance due to field winding
L_{sf}	leakage inductance between stator and field winding
λ_m	Mutual flux linkage on a whole
L_{md} and L_{mq}	d and q axis magnetizing inductance
L_d and L_q	d and q axis inductance
M_{abs} or M_{bas}	mutual inductance between phase A and B of stator winding
M_{acs} or M_{cas}	mutual inductance between phase A and C of stator winding
M_{bcs} or M_{cbs}	mutual inductance between phase B and C of stator winding
M_{asf} or M_{fas}	mutual inductance between phase A of stator winding and field winding
M_{bsf} or M_{fbs}	mutual inductance between phase B of stator winding and field winding
M_{csf} or M_{fcs}	mutual inductance between phase C of stator winding and field winding
g	airgap length
N_f	number of conductors in field winding
N_{as}	number of conductors in phase A of stator winding
H	magnetic field intensity
B_f	magnetic flux density

μ_0	permeability of free space ($4\pi \times 10^{-7}$ H/m)
μ_r	relative permeability
Φ	magnetic flux for a single turn
θ_r	rotor position
P_d	developed power
P_{in}	input power
T_m	electromagnetic torque
J	current density
E	electric field strength
EMF	Electromotive Force
A	Magnetic vector potential
F	energy functional
x_d, x_q and x_0	d, q and 0 axis reactance respectively
x_a, x_b and x_c	a, b and c axis reactance respectively
χ	any variable, such as voltage, current or flux linkage
$[c_1]$	the co-efficient matrix of transformation
V_{dq0}	d or q or 0 axis voltage respectively
i_{abc}	vector of A, B and C axis currents

λ_{abc}	vector of A, B and C axis flux-linkages
r_{abc}	vector of A, B and C axis resistances
ω_r	angular speed of rotor
v_d^r, v_q^r and v_0^r	d or q or 0 axis rotor voltage respectively
v_d^s, v_q^s and v_0^s	d or q or 0 axis stator voltage respectively
i_d^r, i_q^r and i_0^r	d or q or 0 axis rotor current respectively
λ_d^r, λ_q^r and λ_0^r	d or q or 0 axis rotor flux linkage respectively
x_d^s, x_q^s and x_0^s	d, q and 0 axis stator reactance respectively
σ	electric conductivity
P_a	input active power
e	EMF according to Faraday's law
I_{eo}	current in an enclosed loop
W_m	stored magnetic energy
\mathbf{J}	applied current density
Ω	domain of the area for an element
μ	magnetic permeability
$N(x, y)$	interpolation function

x, y	x and y co-ordinates for a node
c_1, c_2 and c_3	three scalars
u	unknown quantity for an element
u_j^e	unknown quantity for j -th node
N_j	interpolation function for j -th node
n	number of nodes
$\alpha_x, \alpha_y, \beta$ and g_l	constants
r^e	residual of a 2 nd order differential equation
ω_d	weight function
Ω^e	domain area
Γ_e	contour bounding the area under the triangular element
A_x, A_y, n_x and n_y	scalars used to explain weighted residual method
$[M_{ij}^e], [T_{ij}^e], [f_i^e], [p_i^e]$ and $[b_i^e]$	matrix used to explain weighted residual method
$[K_{ij}^{ee}], [u_i^e]$ and $[b_i^e]$	matrix used to explain weighted residual method
ε	permittivity of the medium
m	constant used to explain boundary condition
A_l, A_m and A_n	magnetic vector potential in scalar form for node l, m and n respectively

x_l, x_m and x_n	x co-ordinate for node l, m and n respectively
y_l, y_m and y_n	y co-ordinate for node l, m and n respectively
Δ	area of the triangle
$\widehat{u}_x, \widehat{u}_y$ and \widehat{u}_z	three unit vectors
$[R], [M]$ and $[C]$	generalized matrix used for finite element formulation of electromagnetic field
θ_0	angle of radial boundary
\mathbf{F}	total planar force
L_i	length for the surface S
r_i	radius of the circumference
W	magnetic co-energy
δ_a	represents the displacement.
$[G]$	Jacobian matrix
\mathbf{r}	vector to connect origin to midpoint of $d\Gamma_c$
v_j	terminal voltage for the j-th winding
R_j	resistance for j-th winding
i_j	current for j-th winding
λ_j	flux linkage for j-th winding

L_{jk}^{inc}	instantaneous inductance for j-th winding
P_j	instantaneous terminal power for j-th winding
Δi_j and Δi_k	small perturbation current for j and k-th winding
X_l	leakage reactance
V	terminal voltage
E_0	excitation voltage due to permanent magnet flux alone
r_1	stator resistance for a permanent magnet synchronous motor
δ	torque angle for a permanent magnet synchronous motor
E_i	back-EMF at any time i
δ_i	interior torque angle of rotor position at time i
l_i	length of the airgap
K_w	product of stator winding distribution
Δt	time step for time-stepping finite element analysis
B	magnetic flux density
P	no. of poles
L_{ff}	self-inductance for field winding
l	stack length
r	mean radius of airgap

ξ	dummy variable for integration
L_b	stator leakage inductance due to leakage flux at ending ring
e_{af}	voltage induced by field winding flux
ω_e	angular electrical frequency
δ_{e0}	electrical angle of rotor at time 0
p	differential operator $\frac{d}{dt}$
ω	angular frequency
a_k, b_k and c_k	scalars
Γ_c	all interfaces between the iron or permanent magnet and the airgap
B_{ti}, B_{ni}	tangential and normal components of flux density
x_d, x_q	d and q axis synchronous reactances respectively
x_{md}, x_{mq}	d and q axis magnetizing reactances respectively
L_A, L_B, L_F and L_f	constants of machine inductances as given in equations (2.49) - (2.51) and (2.56) respectively

Chapter 1

1.1 Introduction

Electric Power systems form the backbone of modern society. Electricity and its accessibility are the greatest engineering achievements in the past century. In the 21st century, global warming has become an important issue. Modern life needs electric energy technologies for climate controlled home and work place environment. In order to maintain and develop these energy-consuming technologies, availability of sustainable energy sources and their effective utilization through efficiency improvements are of significant importance. Over 60% of the generated energy is consumed by electric motors [29]. AC motors are widely used in all aspects of industrial, commercial, domestic, utility and special-purpose commercial markets. Thus improvements in efficiency of small electric motors are one of the most effective measures to reduce primary energy consumption, which cause global warming. Interior permanent magnet (IPM) synchronous motors are the latest choice of researchers due to their high efficiency, high power density, quiet operation, compact size, high reliability and low maintenance requirements.

Interior permanent magnet synchronous motor drives have been increasingly developed and widely used to meet the high efficiency and performance requirements. This motor type exhibits asymmetrical and nonlinear characteristics, resulting in an additional reluctance torque, which has to be exploited in order to tap the full power and torque capabilities of the IPM motor [1-10]. Performance analyses of three phase IPM motors are extensively reported in the literature [11-12, 13, 14, 15]. However, the single-phase IPM motors have received little attention from the researchers to date. This is attributed to the starting problem

associated with these single phase motors [2, 8]. Both polyphase and single phase IPM motor drives are suitable for many applications. However, the choice of the motor including the rotor, its configuration, permanent magnet (PM) materials, magnet locations and orientations, control scheme and topology depends on the specifications, cost, complexity, accuracy and reliability of the IPM motor drive system. From utilization point of view, more than 50% of consumed energy in electrical networks is utilized by electrical machines and mostly by induction motors which offer high reliability and improved operating efficiencies. Therefore, the effective energy saving solution of the greatest consumption devices in electrical networks is to improve the efficiency of electrical induction motors among all electrical machines. In the past attempts to increase the efficiency of induction motors were focused on design optimization of these induction machines.

Design optimization to increase efficiency is to minimize the internal losses, such as the stator copper losses and rotor slip losses. This can be done by increasing the slot area so that more copper can be used. The result is a larger cross-sectional area of windings and a reduction in the stator resistance. Rotor copper losses in squirrel cage induction motors can be reduced by modifying the shape and size of the rotor bars. Core losses can be reduced by decreasing the magnetic flux density in the iron of the machine. This can be done by increasing the volume or quality of iron used in the machine. Also, for a given flux density, eddy current losses can be reduced by using thinner iron laminations. A downside of these efficiency improvement techniques is that they cannot be easily done without over-sizing the original motor. Therefore, resizing the machine is not a viable solution to improve the efficiency and has limited degrees of success. An alternative solution is using other type of machines that achieves higher power efficiencies without overly increasing physical size. One such machine is the permanent magnet synchronous machine (PMSM) which contains permanent magnets embedded in the rotor. It combines permanent magnet and induction torques for a better motor efficiency during synchronous operation within a standard ac motor stator frame and a rotor having permanent magnets below the conducting squirrel cages to permit the motor starting by direct coupling to an ac power source. In fact, it presents an

alternative to the induction machine. This solution may lead to important technical advantages in industrial applications such as reduced manufacturing costs and/or better performances as well as reduced running costs [1-4].

1.2 Literature Review

1.2.1 History and Evolution of Permanent Magnet Materials

The history of application of permanent magnets (PM) in the rotating machines is linked to the development of high-energy permanent magnet materials [1,12] in industrial scale. Magnetic materials with a possibility of synthetic magnetism saw the most changes in laboratory and demonstrating prototypes during the early period of the twentieth century. This history can be reviewed by coursing through the technical and scientific publications of this period and pertinent patents filed worldwide.

The literature review takes us back to 1920 when methodic contributions on PM principles and application by S. Evershed [17] formed the stepping stone for modern research on PM machines. The next decade and a half saw some sporadic improvements on harnessing the knowledge in this technology and justifying the economic aspect as the cost of materials was not being recouped by the performance improvements. In 1941, G. J. Wey from Westinghouse Company reported the problem of shielding PMs against external transient magnetic fields [16]. He proposed to solve this problem by using the copper-plating process invented by the E. I. du Pont of Nemours Company in the USA. During the late 50's Alnico (Aluminum, Nickel and Cobalt alloy) hogged the interest of the researchers as it provided, until then the highest energy product upto 5.5 MG-Oe..

A vital contribution on putting this Alnico material in PM alternators was first made by R.M. Saunders from University of California, Berkeley and R. H. Weakley from U.S. Electric Motors, Los Angeles in 1951 [18]. Their narration included both the design of stator and rotor and operational aspects of Alnicos based electric machines. A flurry of papers followed afterward on the same topic.

In 1952 Maurice W. Brainard proposed a precise description on synchronous machines with rotating permanent magnet fields [19]. His work which was published in two parts also made comparison between PM machines and wire-wound field machines using charts and design formulae. Later he patented PM excitation for synchronous generators [20]. A flurry of papers followed afterward on the same topic in the technical literature.

The development of PM excited machines had its fair share of criticism too. R. C. Byloff severely criticized the design parameter calculation for permanent magnet generators by D. Ginsberg and L.J. Misenheimer [21] which was reportedly based on manual spreadsheet and experimental verification. Byloff stated that PM machines exhibit a much larger tolerance in the rated values to be adopted which he partly explained by the large variability in PM materials, non repeatability of the magnetizing process and effects of operating conditions and so on [22]

In the same year, D. Hershberger of General Electric Company of USA [23] extended the Alnico excitation to dc machines. In 1954, F. W. Merrill broadly described the development of the permanent magnet synchronous motor which he named as "Permasyn Motor" [1]. He listed eight ideal characteristics of PM synchronous motors and explained the effect of PM in achieving those. This paper was technically appreciated by P. L. Algers from the General Electric Company of USA.

In 1957, D. J. Hanrahan and D. S. Toffolo proposed a theory which can lead to optimum design of a permanent magnet generator where they used a demagnetization effect for air stabilization, short-circuit stabilization, or full load stabilization [24]. The paper which acknowledged the contribution of Italian engineer, P. Gozzoli also commented by Gordon R. Slemon from the University of Toronto. Gozzoli's work analyzes the magnetic field around rotor poles both with and without stator windings [25].

Although ferrite magnets first made inroads in the early 1950's, the first substantive papers on ferrite ceramic magnets and describing their application on electric machinery appeared in the early years of the

1960's. The ferrite magnets had a low ($\mathbf{B.H}$) energy product, especially low remanence. These barium ferrite magnets are hard and brittle in their anisotropic form and very hard to machine. However, these ferrite permanent magnets are widely adopted for rotating electric machine applications because of their relatively high coercivity in spite of low remanence and most importantly low market price [26].

In 1970's Rare Earth based materials were first introduced. The samarium cobalt materials (such as SmCo_5) had both high remanence and high coercivity. The per unit cost of SmCo_5 was high. But they did not have the market share of ferrite magnets having low cost. Furthermore, price swings of materials like Cobalt and very expensive Samarium (Sm) stunted the economic prospect of this magnet for wide scale applications in electric machines. Moreover, like ferrite magnets the SmCo_5 was very hard and brittle, thus these are not amenable to machining and so difficult to work with.

The popularity of IPM synchronous motors is largely due to the availability of modern permanent magnets with high $(\mathbf{B.H})_{\text{max}}$ energy product and cost effective newer rare earth PM materials like Neodymium Boron Iron (NdBFe) which also enhance the performance of ac motor drives and reduce its size and losses in PM motors. In their anisotropic and fully dense form, these (NdBFe) magnets are ductile and easily machineable. They also exhibit an energy product up to 60MGOe with high remanence (> 1 Tesla) and extra-ordinarily large coercivity exceeding 10kA/m. The minor loop excursion is almost linear in the second quadrant of the B-H characteristic curve. Sustained and extensive research, development, analysis, control and application of IPM motors with these high energy magnets are progressing in leaps and bounds for the past 25 years [27], perhaps even exceeding Merrill's dream [1] and Veinott's [28] expectation. The rapid development of the PM technology is best illustrated in Fig 1.

In the 20th century, squirrel cage induction motors have been the most popular electric motors, due to their simple and rugged construction. An induction motor is a singly-fed motor [29]. Advancements in electronics and control technology have added more features to both the polyphase and single phase

induction motor drives to make them more prevalent in industrial, commercial and domestic motors markets. It is well known that induction motors suffer from relatively poor power factor, slip losses and

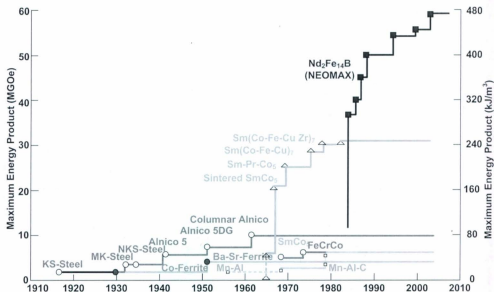


Fig 1.1: History of Development of PM Materials

low efficiency as compared to conventional dc-wire wound synchronous motors, which are doubly-fed machines. Typical synchronous and dc commutator motors have limitations such as extra dc power source noise, EMI, wear and tear, etc. due to the use of commutator and brushgear assemblies. The above mentioned problems have led to the development of permanent magnet brushless dc as well as IPM synchronous motors which have PM excitation in the rotor. The inherent disadvantages of induction motors and conventional synchronous motors are overcome by singly-fed IPM synchronous motors.

1.2.2 PERMANENT MAGNET SYNCHRONOUS MOTOR (PMSM)

The structure of a permanent magnet synchronous motor (PMSM) is similar to the induction motor structure but with permanent magnets inserted in the rotor [30-32]. The most basic construction of a

PMSM consists of poly-phase wound stator windings which in some cases may be identical to an induction motor stator, with a rotor consisting of permanent magnets within a laminated iron core mounted on a shaft. Fig. 1.2 shows a schematic cross section of a 4-pole PMSM.

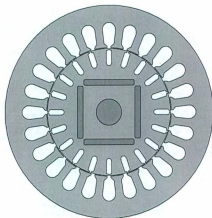


Fig 1.2. Schematic cross section of a 4-pole PMSM.

Fig. 1.3 displays a variety of permanent magnets and their orientations and configurations within the rotor structure. All the magnet arrangements are broadly called interior permanent magnet (IPM) types. The original IPM machines evolved over the years by many innovators of IPM technology.

The rotor structure of Fig. 1.3 (a) was proposed by Kurihara and Rahman [33], while the rotor structure of Fig. 1.3(b) was proposed by Smith in 2006 [34]. The rotor structure of Fig. 1.3 (c) was proposed by Binns in 1992 [35], while the rotor structure of Fig. 1.3(d) was proposed by Rahman in 1993 [36]. The rotor structure of Fig. 1.3 (e) was proposed by Libert in 2006 [37], while the rotor structures of Fig. 1.3(f), The rotor structure of Fig. 1.3 (h) was proposed by Binns in 1994 [38], while the rotor structure of Fig. 1.3(i) was proposed by Rahman and Kurihara in 2004[39].

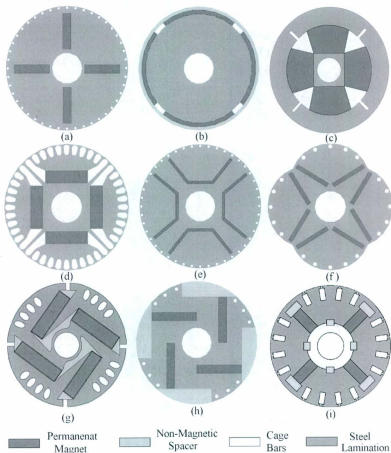


Fig. 1.3: Different configuration of IPM rotors: a) full V-shape PM, b) surface mounted PM c) Modified hybrid PM, d) straight PM and extended rotor bars, e) U-shaped PM, f) partial V-shape PM and poles producing air gap length, g) mixed PM h) straight –mixed PM for high flux i) partial straight V-shape PM

There have been many types of configurations since the inserted PMs may have different shapes, materials, sizes and positions which deeply influence the performances of the machine. It can thus be classified according to the rotor structure. Some different types of IPM rotors are shown in Fig. 1.3. The

most common structures of the line-start interior permanent magnet synchronous motors (IPMSM) are of figures 1.3 (d, g, i) where the PMs are embedded below the rotor squirrel-cages.

The interior PMSM has a more complex design; however the physical nature of the rotor provides protection to the magnets at higher operating speeds. They are designed thus to produce reluctance torque and electrical torque [4]. Most IPMSMs need an inverter for starting which is not economical for single constant speed applications. Cage-equipped PM motors are an alternative, to overcome this issue. These sorts of machines are called line start interior permanent magnet motors. The line start property is obtained due to the design of the rotor with starting aluminum cage. The inverter-fed IPM motor can be started with position sensor or sensorless means, in which the starting conduction cage winding bars can be dispensed with [15, 22]. This is not covered in this thesis, because the topic of this thesis is on line-starting from the main power supply source without going through a feedback system using sensor(s) or otherwise indirectly. In the indirect sensorless process, a high frequency signal is imposed on the stator coils at stationary condition to determine the position of the rotor axis for starting of the IPM motor through signal processing.

1.2.3 LINE START PERMANENT MAGNET SYNCHRONOUS MOTORS

A line-start interior permanent magnet synchronous machine (LSIPMSM) is characterized by squirrel cage bars or damper windings in the rotor for asynchronous starting, as shown in Fig. 1.2 and Fig. 1.3. It is an induction machine with added permanent magnets in the rotor, but it has a higher efficiency than an induction machine. The fact that the magnetizing field generated by permanent magnets means the magnetizing current is not necessary, leads to a much higher power factor in full load operation. In addition the absence of field ohmic losses and the much lower rotor losses once synchronized make the machine highly efficient.

The starting performance of a LSIPMSM from the moment of switch-on to the onset of stable synchronous running forms an important part of the assessment of this machine especially for practical applications. The motor can be self-starting when connected to supply mains directly [30]. However, a few aspects during the self-starting process have to be considered, including starting current, starting torque, the demagnetization of permanent magnet, run-up time, etc. The maximum current occurs at run-up as in a normal induction machine. The heavy inrush current at starting may cause demagnetization of the magnets unless suitable precautions are taken in the design of IPMSM. Although the squirrel cage bars can protect the magnets from demagnetization during the transients associated with the start-up, the magnet thickness must be designed such that it can withstand the maximum possible demagnetization current. In practice, this high starting current should be prevented from happening often so as to protect the permanent magnet. Therefore frequent self-starting of the machine should be avoided or the machine should be started at low voltage and light loads. In this paper direct online starting of the motor has been considered.

Starting torque is another important issue during the starting of a LSIPMSM. Three different torques appear in the process of starting [41]:

- Braking torque due to the magnet;
- Pulsating torque due to rotor saliency acting as a braking torque;
- Accelerating torque due to the rotor squirrel cage bars.

The squirrel cage bars in the rotor can provide the accelerating torque that drives the machine to near synchronous speed. The magnet torque is a braking torque that opposes the cage torque during run-up. The stronger the magnet field, the greater the braking torque. The accelerating torque must overcome, not only the applied load torque, but also the generated magnet braking torques due to the presence of the permanent magnet flux and the rotor saliency. As the motor approaches synchronous speed, the level of accelerating cage torque is lowered and the magnet torque reverses its role and becomes the sole source of accelerating torque. This synchronizing torque from the permanent magnet must be big enough so as to

pull the machine into synchronism. For large capacity machines, a stronger magnet field is needed for the successful synchronism. However, this high magnetic field will result in a big braking torque at low run-up speed and prevent the machine from starting.

Pulsating torque is another issue of a LSIPMSM. That is caused by the machine saliency during the run-up. It will bring oscillation to the speed and hence mechanical variation to the shaft. Such oscillation may be severe and cause damage to the shaft during the starting process. The pulsation torque persists right up to the moment of pull-in.

Finally, the generated heat in the cage of the line start machines during start-up is more of a problem in permanent magnet machines because of the proximity of the cages to the magnets. Both the residual flux density and coercivity of some permanent magnets reduce as a function of temperature. Indeed if the temperature excursion is beyond a certain value, permanent demagnetization can happen. Therefore for permanent magnet synchronous machines with very high rotor bar current during the self-starting process, the heat effects brought along by the current may cause the demagnetization of the permanent magnet. For such machines frequent self-starting should not be applied.

There are different ways to study the starting up process of LSIPMSM. The traditional way is to divide it into two different regions: 1) the start up response up to an operating point, 2) the transition process from that operating point to synchronism [39-42]. During synchronism, the cogging torque is another drawback of LSIPMSM which is considered to be eliminated or reduced in many research papers [43-47].

1.3 Brief Review of Numerical Techniques

The IPM synchronous motors have been extensively analyzed by various analytical and numerical methods over the past 30 years. There exist exhaustive analytical methods to determine the bulk parameters of IPMSM and the steady state terminal performances of the line-start IPMSM. In order to obtain the steady state, dynamic and transient performances of modern IPMSM motor drives, finite element analysis (FEA) has emerged as the standard numerical tool in recent years.

Analytical procedures solve the unknown field by experimental measurements on analogous field regions i.e. fields having the same equations or the same boundary and interface conditions. For this it has been virtually impossible to model the inhomogeneities, nonlinearities and so on by means of solving techniques already in vogue in the real problem. Numerical methods came to eliminate these flaws in analytical methods.

Since about 1940, finite difference schemes started to be used in practice. These methods replace a continuous domain with a grid of discrete points or nodes for which unknown values are computed. But in fields with higher field gradients like magnetic fields, these grids increase computation time. Moreover they are not suitable for boundaries with curves and interfaces. To overcome these shortcomings, civil engineers started using alternative variational method, Finite Element. The term "Finite Element Analysis" was first used by Clough in 1960 [48]. Silvester and Chari then brought it to alternators or motors [49]. In fiercely competitive world markets with pressure of increased cost of electricity and relatively high price of permanent magnets, building a prototype is costlier than ever. To avoid miscalculation that can prove costly once the motor is manufactured, it is necessary to accurately predict the synchronous and dynamic performances of the proposed design of a PM machine. The topic of both synchronous and steady-state analyses has been treated extensively in this literature.

However linear coupled circuit analysis and lumped parameter model cannot easily calculate IPM machine characteristics without taking into account magnetic saturation, complex configuration, eddy currents and external system parameters. Finite Element among other numerical methods can be a suitable candidate because the elements used can be easily adapted to the shape of boundaries and interfaces.

In their paper [49] Chari et al. showed how the finite element can be used in non linear saturable magnetic material analysis. In their book and another paper [50, 51] Chari et al. employed the triangular finite elements for determining the eddy current distribution in current carrying conductors. In 1981 Dr. Demerdash et al. brought the finite element analysis to permanent magnet synchronous machine analysis

where they modeled the permanent magnet as a simple magnetic circuit consisting of permanent magnet in series with an iron core and airgap. Then they replaced the magnet by a coil in series with the same iron core and airgap. This coil had the same dimension and magnetization profile as the permanent magnet. They created the flux density profiles for various parts like stator core, stator tooth, stator slot tip, slot stem etc. These ideas are indeed very innovative and went a long way in shaping the finite elements for line-start permanent synchronous motors.

P. Silvester from McGill University proposed that the process employed for finite element analysis (FEA) can be divided in two phases, a preprocessor phase and a solver phase. The preprocessor phase should include the operations carried out once. For example discretization of regions, assigning boundary conditions, modeling of magnetic characteristics is dealt with in the preprocessor phase [52]. The post processing technique based on finite element analysis (FEA) proposed by both Chari [49] and Silvester was helpful in predicting model performance and design optimization.

Since FEA is a time consuming process, a technique combining the equivalent field or electrical circuit analysis to accurately predict the machine performance has been the source of considerable efforts [52, 53]. Demerdash tried to bring the power conditioner network under the span of analysis [54]. This power conditioner network can be nonsinusoidal voltage or current source inverter-converter. FEA can be easy to implement for interior permanent magnet motors fed by current source inverter [55] but it is difficult for voltage source inverters. Voltage source inverters see voltage as a cause and current is an effect which is contrary to Maxwell's theory, based on which the Finite Element theory is developed.

The measurements of saturable parameters like back-EMF, d -axis reactance, q -axis reactance were reported by Chalmers et al. [56], where on a sample commercial motor, the variation of parameters was studied over 360° of load angle.

Ping Zhou and M. A. Rahman from Memorial University used a different method to extract saturable parameters direct-axis inductance, quadrature-axis inductance permanent magnet induced flux linkage at arbitrary load conditions [57]. Their procedure started with extraction of these parameters from the $a-b-c$ reference frame using transient time stepping FEA solution in time domain and not using BH curve associated with the frequency domain. They applied a total of 16 transient solutions to a three phase line-start IPM motor within the range of torque angle 0° to 150° with an interval of torque angle 10° . Then they converted the parameters to the $d-q$ axis reference frame using Park's Transformation theory. This method shows a better accuracy as extracted $d-q$ axis parameters have taken into account the effects of the slot leakage and phase-spread harmonic fields and eliminated the uncertainty due to the arbitrary choice of a small angle displacement.

But Demerdash et al. reported in their paper [58], with a rapid increase of power conditioning circuit like an inverter or converter, the current and magnetomotive force (MMF) are no longer sinusoidal in many cases and armature MMF no longer rotates uniformly. As the relative angular position of stator MMF with respect to the rotor d -axis is cyclically rotating between upper and lower bounds, the concept of a uniformly rotating $d-q$ -o frame of reference, and its associated direct and quadrature axis inductances is not so well suited. They proposed a new approach to accurately calculate of the apparent and incremental self and mutual inductances of rotating machinery. This approach is based on the perturbation of the magnetic field distribution inside the machine. The magnetic field distributions and the energy perturbations due to small current increments are determined by means of the finite element method. Using these inductances for a series of current sets spanning one complete ac cycle of operation, they calculated the variation of these inductances during both normal and abnormal modes of operation.

However, both of these methods are refuted by Bianchi et al. by saying that these methods take actual values of the currents thereby neglecting the cross-coupling inductances and these methods are time consuming [59]. They proposed a method to allow the PM flux-linkage and the d - and q -axis inductances

to be determined at different load conditions, taking into account the iron saturation. They also modeled the interaction between the d- and q-axis fields. The new procedure involves only one Finite element solution for each operating time and thus takes less time. After solution it transforms the non-linear problem into a linear but non-homogeneous one, to separate current contributions of the magnetic flux. Determination of machine inductances requires another two Finite Element solutions.

The common methods of torque calculation in Finite Element Analysis are the Lorentz force method, virtual work principle method and the Maxwell stress tensor method. Lorentz force is the most straightforward way to establish magnitude and direction of force on a coil. Force intensity is obtained by multiplying \vec{B} found from Finite Element and current density normal. For interior permanent magnet motors where torque producing conductors are only in the stator, this method is not so effective [60, 61]. In 1983 Fitzgerald et al. [70] showed that the total force in a system can be calculated from rate of change of co-energy, but this technique heavily relies on two almost similar quantities, which can nullify each other. Maxwell stress tensor, where force is calculated accurately by integration of force intensity around the surface, depends on the discretization of the surface area which has arcs, angles etc. So the elements or component size in Finite Element Analysis is important in the boundary of the surface. More elements can result in longer processing time. However Maxwell stress tensor gives the best result in post processing calculation [62, 63, 64].

Andy Knight et al. made a comparison between line-start permanent magnet motor and induction motor [65]. Using time-stepped finite element eddy current formulation they carried out detailed simulation of the performance of both the induction motor and line-start permanent magnet machines. In steady-state solution they set the rotor speed at 1500 rpm for a 4-pole 50 Hz system and the initial angle of the rotor mesh was compared to that of the stator mesh. They predicted an efficiency much better than the efficiency predicted by the analytical method at 81% for the line-start permanent magnet synchronous motor. This efficiency which they predicted to improve further with the increase of power factor shows a

peak of 89% under certain output power condition. For dynamic behavior simulation, they showed with the introduction of a permanent magnet in the rotor, the peak speed in a line-start permanent magnet motor increases to 2110 rpm, in comparison with 1680 rpm for a 4-pole 60 Hz IPM motor.

Kurihara and Dr. M. A. Rahman in their paper [39] proposed a new rotor structure for line-start interior permanent magnet synchronous motors which show high efficiency in synchronous speed and when connected to a line frequency can go to synchronism with a large load attached. Using a time stepping FEA they could successfully predict the dynamic and transient behavior which shows a good agreement with the experimental results.

From the discussions above, it will only be fair to say, although much of the past research has used finite element analysis to successfully predict the dynamic and transient behavior of line-start permanent magnet synchronous motors for various rotor structures, more investigations are needed to consider various rotor configurations and PM orientations as well as stator shape, winding arrangements and overall size and rating of the IPM motor.

1.4 Thesis Objectives

The objectives of the thesis are:

- (a) Design analysis for various types of rotor magnets of line-start IPM motors.
- (b) Develop Finite Element Models for major types of IPM motors.
- (c) Write the design codes to successfully model the steady state, dynamic and transient performances.
- (d) Document all the necessary steps to successfully run the special finite element software packages.
- (e) Provide comparative performance results including losses.

(f) Provide evidence of the validity of computer-aided simulation results with the experimental results of a line-start interior permanent magnet synchronous motor.

1.5 Outlines of Chapters

Chapter one contains the introduction and the objective of this thesis.

Analytical formulations are provided in Chapter two. A per-phase equivalent circuit model is developed for a generalized lumped parameter model. Based on two axis theory, torque expression is also built.

Chapter three contains the finite element equations for simulating the flux profiles of different types of IPM rotors.

Chapter four introduces a new computer aided technique for employment of finite element method in motor analysis.

Chapter five shows the simulation results of a line-start interior permanent magnet synchronous motor with straight-shape, V-shape and partial V-shape permanent magnet motor.

Chapter six has the conclusion and suggestions for future work.

Chapter 2

Mathematical Modeling of Interior Permanent Magnet Motor

In this chapter a generalized lumped parameter model is obtained. A per-phase equivalent circuit is proposed to account for the saliency of a PM motor and the influence of core losses. Finally a torque equation is developed.

2.1. System Equations for Permanent Magnet motors

We used a 3-phase motor for analytical modeling as this type of motors is widely used for industrial drive applications. The standard two axis theory with fixed rotor reference frame is best suited for analytical modeling. A number of transformation methods are available to transform from three- phase model to two phase model but for my case I used the Park's transformation [66] for the voltage and currents to accommodate a better representation of electrical power in the machine. As a result, the developed torque is invariant over transformation. A two pole, three phase, wye connected salient pole machine is chosen for analysis as shown in Fig 2.1 [67]

The MMF (magneto motive force) created in the motor bore by stator winding is mostly sinusoidal as we assume that the stator winding is sine-distributed without any short-pitching and skewing. This winding produces an air gap MMF which is displaced by angle ϕ_s from a fixed axis. The rotor with an angular speed of ω_r is displaced by angle θ_r . For a given angular displacement relative to the given axis ϕ_s , ϕ_r and θ_r are connected by,

$$\phi_s = \phi_r + \theta_r \quad (2.1)$$

The ampere conductor distribution of a sine-distributed winding is expressed by

$$N_m = N_p \sin \phi_s \quad 0 \leq \phi_s \leq \pi \quad (2.2)$$

$$N_m = -N_p \sin \phi_s \quad \pi \leq \phi_s \leq 2\pi \quad (2.3)$$

where N_p is the maximum no. of conductor in turn/ phase. The number of conductors per pole is [68]

$$\frac{N_p}{2} \times \frac{2}{\pi} \times \frac{\pi}{P} = \frac{N_p}{P} \quad (2.4)$$

where P is the number of poles. So the total number of conductors per phase is

$$\frac{N_p}{P} \times 2P = 2N_p \quad (2.5)$$

If N_s is the number of conductors per phase, the total number of turns per phase is half the number of conductors per phase

$$N_p = \frac{N_s}{2} \quad (2.6)$$

The analysis may be simplified by considering only one of the stator windings at a time and assuming that the winding may be approximated as a sinusoidally distributed winding. The MMF waveform of the equivalent phase A winding is

$$\text{MMF}_{as} = \frac{N_s}{2} i_{as} \cos \phi_s \quad (2.7)$$

where “a” stands for phase A and “s” stands for stator. Similarly for other two phases “bs” and “cs” it can be written as

$$\text{MMF}_{bs} = \frac{N_s}{2} i_{bs} \cos\left(\phi_s - \frac{2\pi}{3}\right) \quad (2.8)$$

$$\text{MMF}_{cs} = \frac{N_s}{2} i_{cs} \cos\left(\phi_s + \frac{2\pi}{3}\right) \quad (2.9)$$

By adding the MMFs in (2.7) to (2.9) we get the MMF produced by stator currents in the air gap

$$\text{MMF}_s = \frac{N_s}{2} \left[i_{as} \cos \phi_s + i_{bs} \cos\left(\phi_s - \frac{2\pi}{3}\right) + i_{cs} \cos\left(\phi_s + \frac{2\pi}{3}\right) \right] \quad (2.10)$$

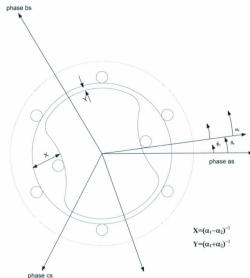


Fig 2.1: Two-pole, wye-connected, salient pole synchronous machine

For a magnetically linear system, the flux linkages with armature phases a, b, c and field winding f are expressed in terms of inductance and currents as follows,

$$\lambda_{as} = L_{sas}i_{as} + M_{abs}i_{bs} + M_{acs}i_{cs} + M_{af}s i_f \quad (2.11)$$

$$\lambda_{bs} = M_{bas}i_{as} + L_{bsb}i_{bs} + M_{bcs}i_{cs} + M_{bf}s i_f \quad (2.12)$$

$$\lambda_{cs} = M_{cas}i_{as} + M_{cbs}i_{bs} + L_{ccs}i_{cs} + M_{cf}s i_f \quad (2.13)$$

$$\lambda_f = M_{fas}i_{as} + M_{fbs}i_{bs} + M_{fcs}i_{cs} + L_{ff}s i_f \quad (2.14)$$

Here L with two like subscripts denote a self-inductance and M with two different subscripts denote mutual inductances. Self-inductance of a winding is computed using the ratio of the flux linked by a winding to the current flowing in the winding with all other winding currents zero. Mutual inductance is the ratio of flux linked by one winding due to current flowing in a second winding with all other winding currents zero including the winding for which the flux linkages are calculated [69]. Though the air gap length g is uniform for a synchronous machine, for a particular rotor position it is approximated as,

$$g(\phi_r) = \frac{1}{\alpha_1 - \alpha_2 \cos 2\phi_r} \quad (2.15)$$

and
$$g(\phi_s - \theta_r) = \frac{1}{\alpha_1 - \alpha_2 \cos 2(\phi_s - \theta_r)} \quad (2.16)$$

where the minimum air gap length is approximated as

$$Y = \frac{1}{(\alpha_1 + \alpha_2)} \quad (2.17)$$

and the maximum length is

$$X = \frac{1}{(\alpha_1 - \alpha_2)} \quad (2.18)$$

where α_1 and α_2 are two constants used for explaining the air gap length.

The airgap magnetomotive force (MMF) is given as

$$\text{MMF} = \mathbf{H} \times g = \frac{B_r}{\mu_r \mu_0} g \quad (2.19)$$

where \mathbf{H} is the magnetic field intensity, B_r is the magnetic flux density and μ_0 is the permeability of free space ($4\pi \times 10^{-7}$ H/m) and μ_r is the relative permeability. Since MMF is a function of ϕ_s , for a small stator flux in comparison with a fixed frame the eqn. (2.19) is given as,

$$\text{MMF}(\phi_s) = \mathbf{H} \times g = \frac{B_r(\phi_s, \theta_r)}{\mu_r \mu_0} g(\phi_s - \theta_r) \quad (2.20)$$

or

$$B_r(\phi_s, \theta_r) = \mu_r \mu_0 \frac{\text{MMF}(\phi_s)}{g(\phi_s - \theta_r)} \quad (2.21)$$

Substituting (2.7) and (2.16) into (2.21) we can get the airgap flux density due to current in phase A of stator winding with all other currents are set to zero.

$$B_r(\phi_s, \theta_r) = \mu_r \mu_0 \frac{N_s}{2} i_{as} \cos \phi_s [\alpha_1 - \alpha_2 \cos 2(\phi_s - \theta_r)] \quad (2.22)$$

Similarly for a 3-phase system where the currents are displaced by $2\pi/3$ radian apart, the flux density due to current in phase B winding with all other currents zero,

$$B_r(\phi_s, \theta_r) = \mu_r \mu_0 \frac{N_s}{2} i_{bs} \cos \left(\phi_s - \frac{2\pi}{3} \right) [\alpha_1 - \alpha_2 \cos 2(\phi_s - \theta_r)] \quad (2.23)$$

And flux density due to phase C with all the other currents zero,

$$B_r(\phi_s, \theta_r) = \mu_r \mu_0 \frac{N_s}{2} i_{cs} \cos \left(\phi_s + \frac{2\pi}{3} \right) [\alpha_1 - \alpha_2 \cos 2(\phi_s - \theta_r)] \quad (2.24)$$

Assuming that the field winding is sinusoidally distributed with N_f equivalent turns, for the field current i_f , air gap MMF is expressed as

$$\text{MMF}_f = -\frac{N_f l}{2} i_f \sin \phi_r \quad (2.25)$$

Using the similar calculation in (2.19) and (2.20), the airgap flux due to i_f with all other currents zero may be expressed as,

$$B_r(\theta_r) = \mu_r \mu_0 \frac{N_f}{2} i_f \sin \phi_r [\alpha_1 - \alpha_2 \cos 2\phi_r] \quad (2.26)$$

As inductance is expressed in terms of flux linkage and current, determination of self and mutual inductance is imperative on computation of flux linking due to its own current (for self-inductance) and due to current in another winding (for mutual inductance). The flux linkages of a single turn of the stator winding located at ϕ_s angle and whose span is π radian, is given by,

$$\Phi(\phi_s, \theta_r) = \int_{\phi_s}^{\phi_s + \pi} B_r(\xi, \theta_r) r l d\xi \quad (2.27)$$

where Φ is the flux linkage for a single turn, l is the stack length, r is the mean radius of the airgap and ξ is a dummy variable for integration. For the flux linkage of a full winding, the flux linked by each turn have to be summed up which is the integration over all coil sides. The total flux linkage for the current flowing only in phase A of stator winding becomes,

$$\lambda_{\text{as}} = L_{ls} i_{\text{as}} + \int N_{\text{as}}(\phi_s) \Phi(\phi_s, \theta_r) d\phi_s \quad (2.28)$$

or

$$\lambda_{\text{as}} = L_{ls} i_{\text{as}} + \int N_{\text{as}}(\phi_s) \int_{\phi_s}^{\phi_s + \pi} B_r(\xi, \theta_r) r l d\xi d\phi_s \quad (2.29)$$

where L_{ls} is the stator leakage inductance due to leakage flux at ending ring, N_{as} is the number of stator winding for phase A located at ϕ_s angle. As we know from eqns. (2.6) and (2.3), $N_p=N_s/2$ and substituting $B_r(\xi, \theta)$ from eqn (2.23) into eqn. (2.29) we get

$$\lambda_{ass} = L_{ls} i_{as} - \int_{\pi}^{2\pi} \frac{N_s}{2} \sin \phi_s \int_{\phi_s}^{\phi_s + \pi} i_{as} \mu_0 \mu_r \frac{N_s}{2} \cos \xi \left[\alpha_1 - \alpha_2 \cos 2(\xi - \theta_r) \right] r l d\xi d\phi_s \quad (2.30)$$

$$\text{or} \quad \lambda_{ass} = L_{ls} i_{as} + \left(\frac{N_s}{2} \right)^2 \pi \mu_0 \mu_r r l i_{as} \left[\alpha_1 - \frac{\alpha_2}{2} \cos 2\theta_r \right] \quad (2.31)$$

As stated earlier, inductance can be expressed in terms of the ratio of flux linkage and winding current. For self-inductance in phase A it should be only the current flowing in the winding of phase A, while keeping all other winding currents zero

$$L_{ass} = \frac{\lambda_{ass}}{i_{as}} \quad (2.32)$$

$$\text{So,} \quad L_{ass} = L_{ls} + \left(\frac{N_s}{2} \right)^2 \pi \mu_0 \mu_r r l \left[\alpha_1 - \frac{\alpha_2}{2} \cos 2\theta_r \right] \quad (2.33)$$

The self-inductance for other two phases can be similarly found,

$$L_{abs} = L_{ls} + \left(\frac{N_s}{2} \right)^2 \pi \mu_0 \mu_r r l \left[\alpha_1 - \frac{\alpha_2}{2} \cos 2 \left(\theta_r - \frac{2\pi}{3} \right) \right] \quad (2.34)$$

$$\text{and} \quad L_{acs} = L_{ls} + \left(\frac{N_s}{2} \right)^2 \pi \mu_0 \mu_r r l \left[\alpha_1 - \frac{\alpha_2}{2} \cos 2 \left(\theta_r + \frac{2\pi}{3} \right) \right] \quad (2.35)$$

The flux density in phase A of stator winding due to current i_{bs} in phase B of stator winding is given as

$$\lambda_{abs} = \int_{\phi_s}^{ \phi_s + \pi} N_m(\phi_s) \int_{\phi_r} B_r(\xi, \theta_r) r l d\xi d\phi_s \quad (2.36)$$

Substituting eqns. (2.3), (2.6) and (2.23) into eqn. (2.36) we get the mutual inductance in phase A of stator winding due to current of phase B of stator winding as

$$\lambda_{abs} = - \int_{\pi/2}^{\pi} \frac{N_s}{2} \sin \phi_s \int_{\phi_r}^{\phi_r + \pi} i_{br} \mu_0 \mu_r \frac{N_r}{2} \cos \xi \left[\alpha_1 - \alpha_2 \cos 2 \left(\xi - \theta_r + \frac{\pi}{3} \right) \right] r l d\xi d\phi_s \quad (2.37)$$

or

$$\lambda_{abs} = - \left(\frac{N_s}{2} \right)^2 \frac{\pi}{2} \mu_0 \mu_r r l i_{br} \left[\alpha_1 - \frac{\alpha_2}{2} \cos 2 \left(\theta - \frac{\pi}{3} \right) \right] \quad (2.38)$$

Therefore the mutual inductance between phase A and phase B will be

$$M_{abs} = - \left(\frac{N_s}{2} \right)^2 \frac{\pi}{2} \mu_0 \mu_r r l \left[\alpha_1 - \frac{\alpha_2}{2} \cos 2 \left(\theta - \frac{\pi}{3} \right) \right] \quad (2.39)$$

The self-inductance for field current i_f may be obtained as

$$\lambda_f = L_{ff} i_f + \int_{\pi/2}^{3\pi/2} \frac{N_f}{2} \cos \phi_r \int_{\phi_r}^{\phi_r + \pi} \mu_0 \mu_r \frac{N_f}{2} i_f \sin \xi \left[\alpha_1 - \alpha_2 \cos 2\xi \right] r l d\xi d\phi_r \quad (2.40)$$

Then,

$$\lambda_f = L_{ff} i_f + \left(\frac{N_f}{2} \right)^2 \pi \mu_0 \mu_r r l i_f \left[\alpha_1 + \frac{\alpha_2}{2} \right] \quad (2.41)$$

where L_{ff} is the leakage inductance for field current and self-inductance follows as

$$L_f = L_{ff} + \left(\frac{N_f}{2} \right)^2 \pi \mu_0 \mu_r r l \left[\alpha_1 + \frac{\alpha_2}{2} \right] \quad (2.42)$$

Similarly other mutual inductances can be found as

$$M_{acs} = -\left(\frac{N_s}{2}\right)^2 \frac{\pi}{2} \mu_0 \mu_r r l \left[\alpha_1 + \frac{\alpha_2}{2} \cos 2\left(\theta + \frac{\pi}{3}\right) \right] \quad (2.43)$$

$$M_{bcs} = -\left(\frac{N_s}{2}\right)^2 \frac{\pi}{2} \mu_0 \mu_r r l \left[\alpha_1 + \frac{\alpha_2}{2} \cos 2(\theta + \pi) \right] \quad (2.44)$$

For mutual flux linkage between stator winding of phase A, i_{as} and field winding is determined by substituting $B_r(\theta_r)$ from eqn. (2.26) into eqn. (2.36) for a rotor position ϕ_s from the fixed frame.

$$\lambda_{fas} = -\frac{N_s N_f}{4} \pi \mu_0 \mu_r r l \left(\alpha_1 + \frac{\alpha_2}{2} \right) \sin \theta_r i_f \quad (2.45)$$

Dividing by field current i_f we get the mutual inductance between rotor field and stator phase A,

$$M_{fas} = -\frac{N_s N_f}{4} \pi \mu_0 \mu_r r l \left(\alpha_1 + \frac{\alpha_2}{2} \right) \sin \theta_r \quad (2.46)$$

Similarly for phase B and phase C it will be

$$M_{fbs} = -\frac{N_s N_f}{4} \pi \mu_0 \mu_r r l \left[\left(\alpha_1 + \frac{\alpha_2}{2} \right) \sin \left(\theta_r - \frac{2\pi}{3} \right) \right] \quad (2.47)$$

$$M_{fcs} = -\frac{N_s N_f}{4} \pi \mu_0 \mu_r r l \left[\left(\alpha_1 + \frac{\alpha_2}{2} \right) \sin \left(\theta_r + \frac{2\pi}{3} \right) \right] \quad (2.48)$$

If we replace these equations with the following expressions,

$$L_s = \left(\frac{N_s}{2} \right)^2 \pi \mu_0 \mu_r r l \alpha_1 \quad (2.49)$$

$$L_B = \frac{1}{2} \left(\frac{N_s}{2} \right)^2 \pi \mu_0 \mu_r r l \alpha_2 \quad (2.50)$$

$$L_F = \left(\frac{N_f}{2} \right)^2 \pi \mu_0 \mu_r r l \left(\alpha_1 + \frac{\alpha_2}{2} \right) \quad (2.51)$$

$$L_{sf} = \left(\frac{N_s}{2}\right)\left(\frac{N_f}{2}\right)\pi\mu_0\mu_r l \left(\alpha_1 + \frac{\alpha_2}{2}\right) \quad (2.52)$$

then the machine inductances can be written in shortened form as

$$L_{as} = L_{ls} + L_A - L_B \cos 2\theta_r \quad (2.53)$$

$$L_{bs} = L_{ls} + L_A - L_B \cos 2\left(\theta_r - \frac{2\pi}{3}\right) \quad (2.54)$$

$$L_{cs} = L_{ls} + L_A - L_B \cos 2\left(\theta_r + \frac{2\pi}{3}\right) \quad (2.55)$$

$$L_f = L_{ff} + L_F \quad (2.56)$$

$$M_{abs} = -\frac{1}{2}L_A + \frac{L_B}{2} \cos 2\left(\theta_r - \frac{\pi}{3}\right) \quad (2.57)$$

$$M_{acs} = -\frac{1}{2}L_A + \frac{L_B}{2} \cos 2\left(\theta_r + \frac{\pi}{3}\right) \quad (2.58)$$

$$M_{bcs} = -\frac{1}{2}L_A + \frac{L_B}{2} \cos 2(\theta_r - \pi) \quad (2.59)$$

$$M_{fas} = L_{sf} \sin \theta_r \quad (2.60)$$

$$M_{fbs} = L_{sf} \sin\left(\theta_r - \frac{2\pi}{3}\right) \quad (2.61)$$

$$M_{fcs} = L_{sf} \sin\left(\theta_r + \frac{2\pi}{3}\right) \quad (2.62)$$

Thus the flux linkages with armature phases A, B, C and field winding f in terms of inductances and currents can be expressed in matrix form,

$$[\lambda] = [L] \times [i] \quad (2.63)$$

$$\begin{bmatrix} \lambda_{as} \\ \lambda_{bs} \\ \lambda_{cs} \\ \lambda_{fs} \end{bmatrix} = \begin{bmatrix} L_{as} & M_{abs} & M_{acs} & M_{fas} \\ M_{bas} & L_{bs} & M_{bcs} & M_{fbs} \\ M_{cas} & M_{cbs} & L_{cs} & M_{fcs} \\ M_{fas} & M_{fbs} & M_{fcs} & L_f \end{bmatrix} \begin{bmatrix} i_{as} \\ i_{bs} \\ i_{cs} \\ i_f \end{bmatrix} \quad (2.64)$$

2.2 Modeling of Interior Permanent Magnet Synchronous Motor

The novelty of permanent magnet synchronous machines rest with the addition of a permanent magnet in rotor structure. Hence we can dispense with field winding from the standard wire-wound synchronous motor. This permanent magnet provides the excitation instead of field winding. A mathematical model of the IPMSM can be derived from the standard model of synchronous motors by removing the components related to field current and adding an extra term for the flux linkages provided by the permanent magnets.

The permanent magnet provides a constant flux λ_m . The flux linkage in the stator winding for phase A, B, C due to permanent magnet rotor is given as

$$\begin{bmatrix} \lambda_{fas} \\ \lambda_{fbs} \\ \lambda_{fcs} \end{bmatrix} = \begin{bmatrix} \lambda_m \sin \theta_r \\ \lambda_m \sin \left(\theta_r - \frac{2\pi}{3} \right) \\ \lambda_m \sin \left(\theta_r + \frac{2\pi}{3} \right) \end{bmatrix} \quad (2.65)$$

So we can rewrite the equations from (2.11) to (2.13)

$$\lambda_{as} = L_{aas}i_{as} + M_{abs}i_{bs} + M_{acs}i_{cs} + \lambda_m \sin \theta_r \quad (2.66)$$

$$\lambda_{bs} = M_{bas}i_{as} + L_{bbs}i_{bs} + M_{bcs}i_{cs} + \lambda_m \sin \left(\theta_r - \frac{2\pi}{3} \right) \quad (2.67)$$

$$\lambda_{cs} = M_{cas}i_{as} + M_{cbs}i_{bs} + L_{ccs}i_{cs} + \lambda_m \sin \left(\theta_r + \frac{2\pi}{3} \right) \quad (2.68)$$

or in matrix form

$$\begin{bmatrix} \lambda_{as} \\ \lambda_{bs} \\ \lambda_{cs} \end{bmatrix} = \begin{bmatrix} L_{aas} & M_{abs} & M_{acs} \\ M_{bas} & L_{bbs} & M_{bcs} \\ M_{cas} & M_{cbs} & L_{ccs} \end{bmatrix} \begin{bmatrix} i_{as} \\ i_{bs} \\ i_{cs} \end{bmatrix} + \lambda_m \begin{bmatrix} \sin \theta_r \\ \sin \left(\theta_r - \frac{2\pi}{3} \right) \\ \sin \left(\theta_r + \frac{2\pi}{3} \right) \end{bmatrix} \quad (2.69)$$

Here L with two like subscripts denote a self-inductance and M with two different subscripts denote mutual inductances.

The phase terminal voltage is the sum of armature resistance voltage drop $r_{as}i_{as}$ and the voltage induced by the field winding flux. The voltage e_{af} induced by the field winding flux can be found by setting armature current i_a equal to zero. With dc excitation in i_f in the field winding, this is given as [70],

$$e_{af} = \frac{d}{dt}(L_f i_f) = -\omega_e L_f i_f \sin(\omega_e t + \delta_{e0}) \quad (2.70)$$

ω_e is the angular electrical frequency of the motor and is defined as $\omega_e = (\text{poles}/2)\omega_s$ where ω_s is the angular synchronous frequency of the rotor, δ_{e0} is the electrical angle of the rotor at time $t=0$. So the terminal voltage can be expressed as

$$\begin{aligned} v_{as} &= r_{as} i_{as} + \frac{d\lambda_{as}}{dt} \\ &= r_{as} i_{as} + L_{aas} \frac{di_{as}}{dt} + e_{af} \end{aligned} \quad (2.71)$$

From eqn. (2.70), the generated voltage e_{af} is a function of frequency ω_e which in turn depends on the rotor frequency. As for IPMSM, without any damper winding and field current dynamics the voltage equations for phase A, B and C simplify to

$$v_{as} = r_{as} i_{as} + \frac{d\lambda_{as}}{dt} \quad (2.72)$$

$$v_{bs} = r_{bs} i_{bs} + \frac{d\lambda_{bs}}{dt} \quad (2.73)$$

$$v_{cs} = r_{cs} i_{cs} + \frac{d\lambda_{cs}}{dt} \quad (2.74)$$

or in matrix form

$$\begin{bmatrix} v_{as} \\ v_{bs} \\ v_{cs} \end{bmatrix} = \begin{bmatrix} r_{as} & 0 & 0 \\ 0 & r_{bs} & 0 \\ 0 & 0 & r_{cs} \end{bmatrix} \begin{bmatrix} i_{as} \\ i_{bs} \\ i_{cs} \end{bmatrix} + p \begin{bmatrix} \lambda_{as} \\ \lambda_{bs} \\ \lambda_{cs} \end{bmatrix} \quad (2.75)$$

where p is the differential operator $\frac{d}{dt}$. Under synchronous operation all machine quantities (current and flux linkage) will also vary sinusoidally in time at frequency ω_e . Thus the inductances in eqn. (2.69) are functions of the rotor position θ , and therefore functions of the rotor speed ω_r . Hence from the eqn. (2.71) the co-efficient of the voltage equations are time varying. These make the solution of the voltage equations all the more difficult unless the reference frame is changed to a synchronously rotating one.

The usefulness of this concept stems from the fact that although each of the stator phases sees a time-varying inductance due to the virtual saliency of the rotor, the transformed quantities rotate with the rotor and hence see constant magnetic paths. Additional saliency effects are present under transient conditions, due to the different conducting paths in the rotor, rendering the concept of this transformation all the more useful.

Similarly, this transformation is useful from the point of view of analyzing the interaction of the rotor and stator flux and MMF-waves, independent of whether or not saliency effects are present. By transforming the stator quantities into equivalent quantities which rotate in synchronism with the rotor, under steady-state conditions these interactions become those of constant MMF- and flux-waves separated by a constant spatial angle. This is the point of view which corresponds to that of an observer in the rotor reference frame [70].

R. H. Park in the 1920s, proposed a new theory of electric machine analysis to solve this problem. He formulated a change of variables which, in effect replaced the variables phases (voltages, currents, flux linkages) associated with the stator windings of a synchronous machine with variables associated with

fictitious windings rotating with the rotor at synchronous speed. Essentially, he transformed or referred, the stator variables to a synchronously rotating reference frame fixed in the rotor. This is commonly referred to as Park's transformation.

2.3 Park's Transformation

Park's transformation is obtained in two stages. First the a-b-c reference frame is transformed to the d-q-0 frame. If the initial angle is set to zero, so that the q-axis is aligned with the as-axis, we can eliminate the zero sequence component. Secondly the variables in the stationary d-q frame can be converted to the synchronously rotating rotor d^r-q^r frame. The superscript r denotes the rotor reference frame.

We make the following assumptions:

- 1- No squirrel cage winding in the rotor.
- 2- No field current in the absence of field winding.
- 3- Eddy currents and hysteresis effects are deemed negligible.
- 4- Induced voltage is sinusoidal shy of any high order harmonics.
- 5- Saturation effect on rotor materials is neglected.

Assuming d-q axes are oriented at θ angle the 3-phase variables in any reference frame can be transformed to the orthogonal components by the following relationship,

$$[\chi_{qd0}] = [c_1][\chi_{abc}] \quad (2.76)$$

where χ may represent any variable such as voltage, current or flux linkage. c_1 is the coefficient matrix of transformation and is given as

$$[c_1] = \frac{2}{3} \begin{bmatrix} \cos \theta & \cos \left(\theta - \frac{2\pi}{3} \right) & \cos \left(\theta + \frac{2\pi}{3} \right) \\ \sin \theta & \sin \left(\theta - \frac{2\pi}{3} \right) & \sin \left(\theta + \frac{2\pi}{3} \right) \\ \frac{1}{2} & \frac{1}{2} & \frac{1}{2} \end{bmatrix} \quad (2.77)$$

the inverse of which is given as

$$[c_1]^{-1} = \begin{bmatrix} \cos \theta & \sin \theta & 1 \\ \cos \left(\theta - \frac{2\pi}{3} \right) & \sin \left(\theta - \frac{2\pi}{3} \right) & 1 \\ \cos \left(\theta + \frac{2\pi}{3} \right) & \sin \left(\theta + \frac{2\pi}{3} \right) & 1 \end{bmatrix} \quad (2.78)$$

From eqn. (2.76), the voltage equations in the machine can be transformed to the orthogonal components of a rotating reference as

$$[V_{qd0}] = [c_1][V_{abc}] \quad (2.79)$$

From eqn. (2.75) this can be expanded as.

$$[V_{qd0}] = [c_1] \{ [r_{abc}] [i_{abc}] + p [\lambda_{abc}] \} \quad (2.80)$$

This eqn. (2.80) can be simplified further for a fixed rotor frame as,

$$[V_{qd0}]^T = [c_1] \{ [r_{abc}] [c_1]^{-1} [i_{dq0}]^T + p [c_1]^{-1} [\lambda_{dq0}]^T \} \quad (2.81)$$

$$\text{or} \quad [V_{qd0}]^T = [c_1][c_1]^{-1} [r_{abc}] [i_{dq0}]^T + [c_1] p [c_1]^{-1} [\lambda_{dq0}]^T + [c_1][c_1]^{-1} p [\lambda_{dq0}]^T \quad (2.82)$$

Substituting this eqn. (2.82) by value of $[r_{abc}]$ (as given in pages 140-143 of [67])

$$\begin{bmatrix} V_{qd0} \end{bmatrix}^T = \begin{bmatrix} r_{abc} \end{bmatrix} \begin{bmatrix} i_{dq0} \end{bmatrix}^T + P\omega_r \begin{bmatrix} \lambda_{dq} \end{bmatrix}^T + p \begin{bmatrix} \lambda_{dq0} \end{bmatrix}^T \quad (2.83)$$

If $r_s=r_b=r_c=r_r$, then the former equation can be rewritten as

$$\begin{bmatrix} v_q^r \\ v_d^r \\ v_0^r \end{bmatrix} = \begin{bmatrix} r_s & 0 & 0 \\ 0 & r_s & 0 \\ 0 & 0 & r_s \end{bmatrix} \begin{bmatrix} i_q^r \\ i_d^r \\ i_0^r \end{bmatrix} + P\omega_r \begin{bmatrix} \lambda_d^r \\ -\lambda_q^r \\ 0 \end{bmatrix} + p \begin{bmatrix} \lambda_q^r \\ \lambda_d^r \\ \lambda_0^r \end{bmatrix} \quad (2.84)$$

or in voltage equation form

$$v_q^r = r_s i_q^r + P\omega_r \lambda_d^r + p\lambda_q^r \quad (2.85)$$

$$v_d^r = r_s i_d^r - P\omega_r \lambda_q^r + p\lambda_d^r \quad (2.86)$$

$$v_0^r = r_s i_0^r + p\lambda_0^r \quad (2.87)$$

For determining flux linkages in these equations (2.85-2.87), we write them as

$$\begin{bmatrix} \lambda_{qd0} \end{bmatrix}^T = [c_1] [\lambda_{abc}] \quad (2.88)$$

$$\begin{bmatrix} \lambda_{q0} \end{bmatrix}^T = [c_1] \{ [L] [i_{abc}] + [\lambda_r] \} \quad (2.89)$$

$$\begin{bmatrix} \lambda_{qd0} \end{bmatrix}^T = [c_1] [c_1]^{-1} [L] [i_{dq0}]^T + [c_1] [\lambda_r] \quad (2.90)$$

By putting the value of $[c_1]$, $[c_1]^{-1}$, $[L]$ from eqn. (2.64) and $[\lambda_r]$ from eqn. (2.65) and shortening them using eqns. (2.46) and (2.51) we get [67]

$$\begin{bmatrix} \lambda_q^r \\ \lambda_d^r \\ \lambda_0^r \end{bmatrix} = \begin{bmatrix} L_{ls} + \frac{3}{2}(L_A - L_B) & 0 & 0 \\ 0 & L_{ls} + \frac{3}{2}(L_A + L_B) & 0 \\ 0 & 0 & L_{ls} \end{bmatrix} \begin{bmatrix} i_q^r \\ i_d^r \\ i_0^r \end{bmatrix} + \lambda_m \begin{bmatrix} 0 \\ 1 \\ 0 \end{bmatrix} \quad (2.91)$$

For general case, from eqn. (2.91) we can define d-q axis magnetizing inductances as

$$L_{mq} = \frac{3}{2}(L_A - L_B) \quad (2.92)$$

$$L_{md} = \frac{3}{2}(L_A + L_B) \quad (2.93)$$

Putting $L_q = L_{ls} + L_{mq}$ and $L_d = L_{ls} + L_{md}$ we can rewrite the eqn. (2.91) as

$$\begin{bmatrix} \lambda_q^r \\ \lambda_d^r \\ \lambda_0^r \end{bmatrix} = \begin{bmatrix} L_q & 0 & 0 \\ 0 & L_d & 0 \\ 0 & 0 & L_{ls} \end{bmatrix} \begin{bmatrix} i_q^r \\ i_d^r \\ i_0^r \end{bmatrix} + \lambda_m \begin{bmatrix} 0 \\ 1 \\ 0 \end{bmatrix} \quad (2.94)$$

where L_{ls} is the leakage inductance, L_{md} and L_{mq} are the d-q axis magnetizing inductance respectively.

It is normally assumed that $L_{mq} = L_{md}$.

$$\lambda_q^r = L_q i_q^r \quad (2.95)$$

$$\lambda_d^r = L_d i_d^r + \lambda_m \quad (2.96)$$

In the rotor zero sequence reference frame $\lambda_0^r = L_{ls} i_0^r$

Ignoring the zero sequence components eqn. (2.85) and (2.86) become,

$$v_q^r = (r_s + pL_q)i_q^r + P\omega_r L_d i_d^r + P\omega_r \lambda_m \quad (2.97)$$

$$v_d^r = (r_s + pL_d)i_d^r - P\omega_r L_q i_q^r \quad (2.98)$$

where the mutual flux λ_m for the d -axis is zero. Eqn. (2.97) and (2.98) can be explained in matrix form

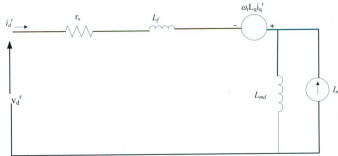
$$\begin{bmatrix} v_q^r \\ v_d^r \end{bmatrix} = \begin{bmatrix} r_s + pL_q & P\omega_r L_d \\ -P\omega_r L_q & r_s + pL_d \end{bmatrix} \begin{bmatrix} i_q^r \\ i_d^r \end{bmatrix} + \begin{bmatrix} P\omega_r \lambda_m \\ 0 \end{bmatrix} \quad (2.99)$$

From eqn. (2.99) we can get the d and q axis rotor currents as

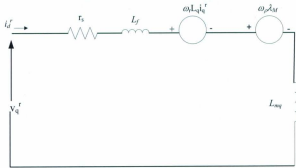
$$pi_q^r = \frac{(v_q^r - r_s i_q^r - P\omega_r L_d i_d^r - P\omega_r \lambda_m)}{L_q} \quad (2.100)$$

$$pi_d^r = \frac{(v_d^r - r_s i_d^r + P\omega_r L_q i_q^r)}{L_q} \quad (2.101)$$

Fig. 2.2 shows the d^r and q^r dynamic model equivalent circuits that satisfy the equations (2.100) and (2.101)



(a)



(b)

Fig 2.2: Park's model of PMSM (a) d-axis, (b) q-axis

2.4 Relationship between a-b-c axis and d-q axis quantities in stationary and synchronous reference form

For a stationary reference frame 3-phase axis transformation in eqn. (2.76) can be rewritten as

$$\begin{bmatrix} x_a \\ x_b \\ x_c \end{bmatrix} = \begin{bmatrix} \cos \theta & \sin \theta & 1 \\ \cos \left(\theta - \frac{2\pi}{3} \right) & \sin \left(\theta - \frac{2\pi}{3} \right) & 1 \\ \cos \left(\theta + \frac{2\pi}{3} \right) & \sin \left(\theta + \frac{2\pi}{3} \right) & 1 \end{bmatrix} \begin{bmatrix} x_q^s \\ x_d^s \\ x_o^s \end{bmatrix} \quad (2.102)$$

If the q-axis is coincident with the a-phase, we can set $\theta=0$, where eqn. (2.102) can be rewritten as

$$\begin{bmatrix} x_a \\ x_b \\ x_c \end{bmatrix} = \begin{bmatrix} 1 & 0 \\ -\frac{1}{2} & \frac{\sqrt{3}}{2} \\ -\frac{1}{2} & -\frac{\sqrt{3}}{2} \end{bmatrix} \begin{bmatrix} x_d^s \\ x_d^s \end{bmatrix} \quad (2.103)$$

or

$$v_a = v_q^s \quad (2.104)$$

$$v_b = -\frac{1}{2}v_q^s - \frac{\sqrt{3}}{2}v_d^s \quad (2.105)$$

$$v_c = -\frac{1}{2}v_q^s + \frac{\sqrt{3}}{2}v_d^s \quad (2.106)$$

For the stationary reference frame eqn. (2.76) can be rewritten as

$$\begin{bmatrix} v_q^s \\ v_d^s \\ v_0^s \end{bmatrix} = \frac{2}{3} \begin{bmatrix} \cos \theta & \cos \left(\theta - \frac{2\pi}{3} \right) & \cos \left(\theta + \frac{2\pi}{3} \right) \\ \sin \theta & \sin \left(\theta - \frac{2\pi}{3} \right) & \sin \left(\theta + \frac{2\pi}{3} \right) \\ \frac{1}{2} & \frac{1}{2} & \frac{1}{2} \end{bmatrix} \begin{bmatrix} v_a \\ v_b \\ v_c \end{bmatrix} \quad (2.107)$$

Which can be simplified at $\theta=0$ as

$$\begin{bmatrix} v_q^s \\ v_d^s \\ v_0^s \end{bmatrix} = \frac{2}{3} \begin{bmatrix} 1 & -\frac{1}{2} & -\frac{1}{2} \\ 0 & -\frac{\sqrt{3}}{2} & \frac{\sqrt{3}}{2} \\ \frac{1}{2} & \frac{1}{2} & \frac{1}{2} \end{bmatrix} \begin{bmatrix} v_a \\ v_b \\ v_c \end{bmatrix} \quad (2.108)$$

From there v_q^s and v_d^s can be written as

$$v_q^s = \frac{2}{3} v_a - \frac{1}{3} v_b - \frac{1}{3} v_c \quad (2.109)$$

$$v_d^s = -\frac{\sqrt{3}}{2} v_b + \frac{\sqrt{3}}{2} v_c \quad (2.110)$$

For a balanced system $v_a + v_b + v_c = 0$ or $v_a = -v_b - v_c$, therefore

$$v_q^s = v_a \quad (2.111)$$

$$v_d^s = -\frac{1}{\sqrt{3}} v_b + \frac{1}{\sqrt{3}} v_c \quad (2.112)$$

For a stationary rotating frame of eqn. (2.104) can be converted to synchronously rotating d-q frame using the Fig.2.3 as

$$\begin{bmatrix} v_q^r \\ v_d^r \end{bmatrix} = \begin{bmatrix} \cos \theta_r & -\sin \theta_r \\ \sin \theta_r & \cos \theta_r \end{bmatrix} \begin{bmatrix} v_q^s \\ v_d^s \end{bmatrix} \quad (2.113)$$

or in an inverted form,

$$\begin{bmatrix} v_q^s \\ v_d^s \end{bmatrix} = \begin{bmatrix} \cos\theta_r & \sin\theta_r \\ -\sin\theta_r & \cos\theta_r \end{bmatrix} \begin{bmatrix} v_q^r \\ v_d^r \end{bmatrix} \quad (2.114)$$

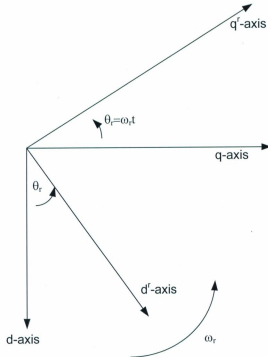


Fig 2.3: Stationary d-q axis to synchronously rotating d^r-q^r axis transformation

2.5 Torque expression of PMSM

In an electromechanical system torque is measured as proportional to two electric signals. In one example it is determined through the ratio of developed power, as the product of voltage and current, and speed.

The total input power in a electric machine is given by,

$$P_m = v_s i_s \quad (2.115a)$$

or for a three phase system,

$$P_m = v_a i_a + v_b i_b + v_c i_c \quad (2.115b)$$

This power transferred across the air gap and with the losses incorporated becomes the developed power.

When the stator phase a-b-c quantities are transformed to the rotor d-q-0 reference frame that rated at

constant speed $\omega_r = \frac{d\theta_r}{dt}$, substituting the voltages from (2.108) to (2.110) and (2.111) as well as currents

in eqn. (2.118) we get [67],

$$P_m = \frac{3}{2} \left(v_q^r i_q^r + v_d^r i_d^r \right) + 3v_0^r i_0^r \quad (2.116)$$

Using eqns. (2.97) and (2.98), eqn. (2.116) can be written as [67]

$$P_m = \frac{3}{2} \left\{ r_s \left(i_q^2 + i_d^2 \right)^r + i_q^r \frac{d\lambda_q^r}{dt} + i_d^r \frac{d\lambda_d^r}{dt} + \omega_r \left(\lambda_d^r i_q^r - \lambda_q^r i_d^r \right) \right\} + 3i_0^2 r_0 \quad (2.117)$$

Discarding the terms for copper, windage and frictional losses rate of change in speed therefore the change in magnetic energy, the above equation of the electromechanical developed power P_d becomes

$$P_d = \frac{3}{2} \omega_r \left(\lambda_d^r i_q^r - \lambda_q^r i_d^r \right) \quad (2.118)$$

For a P-pole pair, the rotor speed ω_r is given as $\omega_r = \frac{P}{2} \omega_m$ where ω_m being the rotor mechanical speed in radians per second. Thus eqn. (2.121) becomes

$$P_d = \frac{3P}{2} \omega_m (\lambda_d^r i_q^r - \lambda_q^r i_d^r) \quad (2.119)$$

By dividing the developed power by the mechanical speed of the rotor, we get the expression for electromechanical torque,

$$T_m = \frac{3P}{2} (\lambda_d^r i_q^r - \lambda_q^r i_d^r) \quad (2.120)$$

By substituting equations (2.95-2.96) in eqn. (2.120) we get

$$T_m = \frac{3P}{2} (L_d i_d^r i_q^r + \lambda_m i_q^r - L_q i_q^r i_d^r) \quad (2.121)$$

Chapter 3

3.1 Finite Element Approach

The magnetic equivalent circuit approach shown in the previous chapter can approximately calculate magnetic fields in motors with simple geometry. For more accurate and efficient calculation we use any numerical method like Finite Element Method. Nowadays the finite element is widely used in the field of Ocean and Mechanical Engineering for stress and force calculation.

In the equivalent magnetic circuit method we need a presumption of magnetic flux lines and the paths of them for any cross-sectional area. This presumption is inaccurate given that we consider them to be straight lines which in some extents are erroneous. For calculation of the effects of flux fringing, saturation and leakage flux we use practical factors rather than derived equations. These practical factors are well known as the motors are in vogue for many years or newer designs are only a subtle change from the closest ones. But for new motor concepts there is a great need to accurately determine the effects of geometric changes and saturation on the motor efficiency and other parameters related to the magnetic field.

For simulation purposes we used Maxwell® 2D which employs a finite element method to solve two-dimensional electrostatic, magnetostatic, eddy current, and transient problems. This software requires no assumption of flux paths or related empirical factors and can be used to calculate:

- Static electric fields, forces, torques, and capacitances caused by voltage distributions and charges.
- Static magnetic fields, forces, torques, and inductances caused by DC currents, static external magnetic fields, and permanent magnets.

- Time-varying magnetic fields, forces, torques, and impedances caused by AC currents and oscillating external magnetic fields.
- Transient magnetic fields caused by electrical sources and permanent magnets.

3.1.1. Equations for magnetic field windings

The magnetic field in an electrical machine is governed by Maxwell's equations:

$$\nabla \times \mathbf{H} = \mathbf{J} \quad (3.1)$$

$$\nabla \times \mathbf{E} = -\frac{\partial \mathbf{B}}{\partial t} \quad (3.2)$$

where,

\mathbf{H} is the magnetic field strength

\mathbf{J} is the current density

\mathbf{E} is the electric field strength

\mathbf{B} is the magnetic flux density

The law of conservation of energy can be derived from Maxwell's equations where input active power is [73]

$$P_a = \int_V \sigma E^2 dV = \int_V \mathbf{E} \cdot \mathbf{J} dV = \int_V \int_S (\mathbf{J} \cdot d\mathbf{S}) \mathbf{E} \cdot d\mathbf{l} \quad (3.3)$$

The EMF from Faraday's law

$$e = \int_l \mathbf{E} \cdot d\mathbf{l} = -\frac{\partial}{\partial t} \int_S \mathbf{B} \cdot d\mathbf{S} \quad (3.4)$$

From Ampere's enclosed circuital law is

$$I_{en} = \int_s \mathbf{J} \cdot d\mathbf{S} = \oint_l \mathbf{H} \cdot d\mathbf{l} \quad (3.5)$$

where I_{en} is the current enclosed in a loop. From above three equations we get the net input electrical power

$$P_a = \oint_l \mathbf{H} \cdot d\mathbf{l} \left[-\frac{\partial}{\partial t} \int_s \mathbf{B} \cdot d\mathbf{s} \right] = - \int_v \mathbf{H} \cdot \frac{\partial \mathbf{B}}{\partial t} dV \quad (3.6)$$

or

$$P_a = \int_v \mathbf{E} \cdot \mathbf{J} dV = -\frac{\partial}{\partial t} \int_v \left[\int_0^B \mathbf{H} \cdot d\mathbf{B} \right] dV \quad (3.7)$$

The right-most term is the stored magnetic energy W_m

$$W_m = \int_v \left[\int_0^B \mathbf{H} \cdot d\mathbf{B} \right] dV \quad (3.8)$$

The input power can also be expressed in terms of magnetic vector potential \mathbf{A} rather than \mathbf{E} by using definition of \mathbf{A} :

$$\mathbf{B} = \nabla \times \mathbf{A} \quad (3.9)$$

From Faraday's law:

$$\nabla \times \mathbf{E} = -\frac{\partial \mathbf{B}}{\partial t} \quad (3.10)$$

Hence

$$\bar{\nabla} \times \mathbf{E} = -\frac{\partial}{\partial t}(\bar{\nabla} \times \mathbf{A}) \quad (3.11)$$

When there is no power loss $\mathbf{E} = -\frac{\partial}{\partial t} \mathbf{A}$

Substituting the expression for \mathbf{E} in (3.3) gives

$$P_a = \int_v \mathbf{J} \cdot \frac{\partial \mathbf{A}}{\partial t} dV = -\frac{\partial}{\partial t} \int_v \left[\int_0^A \mathbf{J} \cdot d\mathbf{A} \right] dV \quad (3.12)$$

So, from (3.12)

$$\int_v \left[\int_0^B \mathbf{H} \cdot d\mathbf{B} \right] dV = \int_v \left[\int_0^A \mathbf{J} \cdot d\mathbf{A} \right] dV \quad (3.13)$$

which demonstrates that magnetic energy stored in a lossless device is equal to input electrical energy.

Variational techniques like finite element or finite difference are used to obtain a solution by minimizing the difference between the stored energy and input energy. The energy functional F can be formulated as:

$$F = \int_v \left[\int_0^B \mathbf{H} \cdot d\mathbf{B} - \int_0^A \mathbf{J} \cdot d\mathbf{A} \right] dV \quad (3.14)$$

F is minimized for:

$$\frac{\partial F}{\partial \mathbf{A}} = 0 \quad (3.15)$$

Thus

$$\int_v \left[\frac{\partial}{\partial \mathbf{A}} \int_0^B \mathbf{H} \cdot d\mathbf{B} - \mathbf{J} \right] dV = 0 \quad (3.16)$$

However, the energy functional F in (3.14) changes when we consider losses from induced current, then F becomes,

$$F = \int_V \left[\frac{B^2}{2\mu} - \mathbf{J} \cdot \mathbf{A} + j\omega \frac{1}{2} \sigma \mathbf{A}^2 \right] dV \quad (3.17)$$

where \mathbf{J} is the applied current density of angular frequency ω , μ is magnetic permeability, σ is electric conductivity.

3.2 Finite Element Formulation

A proper application of the Finite Element Method must involve the following major steps [71]:

- Discretization of the 2-D domain.
- Formulation of governing differential equation.
- Choosing an interpolation function or shape function or basis function.
- Derivation of the element matrices and vectors.
- Assembly of the global matrix system.
- Imposition of boundary conditions.
- Solution of the global matrix system.

3.2.1 Discretization of the 2-D domain

The cross-section of a permanent magnet machine is irregular with curves on edges. The first step is to accurately represent the physical domain of the permanent magnet motor by a set of basic shapes called the finite elements. These finite elements can be triangular or quadrilateral. For a triangular mesh, the shape of triangles must be close to equilateral whereas the shape of quadrilaterals must be close to square. Whichever element is chosen it must accurately represent the geometrical shape, minimizing the discretization error. The elements mustn't have a large variation in size therefore keeping a uniform aspect ratio among them. The element boundaries cannot overlap and adjacent elements must have a common edge.

3.2.2 Choosing an Interpolation Function

An approximate solution obtained over the discretized domain is represented inside an element by a set of functions called interpolation functions. These differential functions are second or third order complete polynomial and guarantee continuity of unknown value across the whole domain. For a linear triangular element the interpolation function is given by

$$N(x, y) = c_1 + c_2x + c_3y \quad (3.18)$$

where x and y are two nodes for a triangular element. If u is a primary unknown quantity inside an element, it can be expressed as

$$u = u_1^e N_1 + u_2^e N_2 + u_3^e N_3 \dots \dots \dots = \sum_{j=1}^n u_j^e N_j \quad (3.19)$$

u_1^e, u_2^e and u_3^e are nodal values for primary unknown quantity.

3.2.3 Derivation of the element matrices and vectors

3.2.3.1 Weighted Residual Method

A generic solution for 2-D problem is given by 2nd order differential equation:

$$\frac{\partial}{\partial x} \left(\alpha_x \frac{\partial u}{\partial x} \right) + \frac{\partial}{\partial y} \left(\alpha_y \frac{\partial u}{\partial y} \right) + \beta u = g_1 \quad (3.20)$$

$\alpha_x, \alpha_y, \beta, g$ are constants. Residual is given by

$$r^e = \frac{\partial}{\partial x} \left(\alpha_x \frac{\partial u}{\partial x} \right) + \frac{\partial}{\partial y} \left(\alpha_y \frac{\partial u}{\partial y} \right) + \beta u - g_1 \quad (3.21)$$

Our main goal is to minimize this element residual. To achieve this we must multiply r^e with a weight function ω_d , then integrate the result over the area of the element and finally set the integral to zero.

$$\int_{\Omega^e} \omega_d \left[\frac{\partial}{\partial x} \left(\alpha_x \frac{\partial u}{\partial x} \right) + \frac{\partial}{\partial y} \left(\alpha_y \frac{\partial u}{\partial y} \right) + \beta u - g_1 \right] dx dy = 0 \quad (3.22)$$

where Ω^e is the domain area for an element. From the Green's theorem [71] this could be solved as

$$\int_{\Omega^e} \left[\frac{\partial}{\partial x} \left(\omega_d \alpha_x \frac{\partial u}{\partial x} \right) + \frac{\partial}{\partial y} \left(\omega_d \alpha_y \frac{\partial u}{\partial y} \right) \right] dx dy = \oint_{\Gamma_e} \left(\alpha_x A_x n_x + \alpha_y A_y n_y \right) dl \quad (3.23)$$

where n_x, n_y are two scalars, Γ_e is the contour bounding the area under the triangle. According to the Galerkin approach [51] ω_d must belong to the same set of shape functions that are used to interpolate primary unknown value u . Setting $\omega_d = N_i$ for $i=1,2,3,\dots,n$ and using u from (3.19),

$$\begin{aligned}
& - \int_{\Omega^e} \left[\alpha_x \left(\frac{\partial N_i}{\partial x} \right) \left(\sum_{j=1}^n u_j^e \frac{\partial N_j}{\partial x} \right) + \alpha_y \frac{\partial N_i}{\partial y} \left(\sum_{j=1}^n u_j^e \frac{\partial N_j}{\partial y} \right) \right] dx dy + \int_{\Omega^e} \beta N_i \left(\sum_{j=1}^n u_j^e N_j \right) dx dy = \\
& \int_{\Omega^e} N_i g dx dy - \oint_{\Gamma_e} N_i \left(\alpha_x \frac{\partial u}{\partial x} n_x + \alpha_y \frac{\partial u}{\partial y} n_y \right) dl
\end{aligned} \tag{3.24}$$

which can be expressed in Matrix form as

$$[M_{ij}^e][u_i^e] + [T_{ij}^e][u_i^e] = [f_i^e] + [p_i^e] \tag{3.25}$$

$$\text{or} \quad [K_{ij}^e][u_i^e] = [b_i^e] \tag{3.26}$$

where $K_{ij}^e = M_{ij}^e + T_{ij}^e$ and $b_i^e = f_i^e + p_i^e$

3.2.4 Assembly of Global Matrix

For each element in the domain there exist a coefficient matrix K^e , from (3.26) and a right hand side vector b^e that must be mapped added to global coefficient matrix K and the global right hand side vector b according to the connectivity information. This process of mapping and adding is called "Assembly Process". The dimension of the element co-efficient matrix K^e is the same with the number of nodes in each element and the global matrix is the number of nodes in all elements in a domain.

The assembly process begins by forming element connectivity array which bears the connectivity information. The array is of the form $n(e,i) = n_i$ for $i=1,2,3,4,...,n$ where e denotes the element number and n_i denotes the global node number that corresponds to the i th local node number. After forming the array, global coefficient matrix K is formed using the following algorithm:

for $e=1$: no. of elements in the domain

for $i=1$: no. of local nodes for element e

for $j=1$: no. of local nodes for element e

$K(n(e,i),n(e,j)) = K(n(e,i),n(e,j)) + ke(i,j)$; % ke is the element coefficient matrix.

Similarly global matrix for right hand side vector \mathbf{b} is also formed.

3.2.5 Imposition of Boundary Condition

Boundary conditions are imposed to simplify the finite element model and approximate a solution for unknown at node points. Two widely used boundary conditions are Dirichlet Boundary Condition and Mixed boundary condition.

3.2.5.1 Dirichlet Boundary Conditions

In Dirichlet Boundary Condition, the unknown quantity u is made constant at a particular point like $u_i^e = m$ where m is a specified value corresponding to node 1 of element 1. If this $m=0$ then the corresponding row will be zero limiting the progression of differential equation for the element.

3.2.5.2 Mixed Boundary Conditions

In mixed Mixed Boundary Conditions we need an unknown quantity and its derivative which can be shown of the following form,

$$\varepsilon \frac{du_i^e}{dx} + \alpha u_i^e = \beta \quad (3.27)$$

where α and β are constants and ε is the permittivity of the medium [71].

3.2.6 Solution of the global matrix system

In professional commercial finite element softwares, the resulting linear system of equations is solved using iterative techniques. This type of techniques can take the advantage of sparsity of the matrix, where the matrix grows along the diagonal elements thus minimizes memory usage. This technique includes conjugate gradient (CG) and biconjugate gradient (BiCG) methods in combination with a variety of preconditioners and accelerators. Other popular iterative methods are generalized minimal residual (GMRES) method and the quasi minimal residual (QMR) method [73-76].

3.3 Finite Element Formulation of Electromagnetic Field

Using the same approach discussed in the previous section, the magnetic energy functional for F in (3.17) over a set of elements can be minimized to a matrix equation that can be solved to determine magnetic vector potential \mathbf{A} .

Fig 3.1 shows the coordinate system for a set of triangular element or mesh. The entire planar mesh may represent the stator, rotor, airgap between them and lamination for stator windings etc. Fig 3.2 shows a mesh generated for 2-D analysis of a permanent magnet synchronous motor. As for triangular elements, for each node a shape function or interpolation function of any order can be declared. For the sake of simplicity and finite element analysis assuming a linear shape function for the magnetic vector potential \mathbf{A} within an element, the scalar A inside each element can be stated as [77]

$$A = c_1 + c_2x + c_3y \quad (3.28)$$

where x and y are the Cartesian co-ordinate positions of the node, for which the magnetic vector potential is calculated.

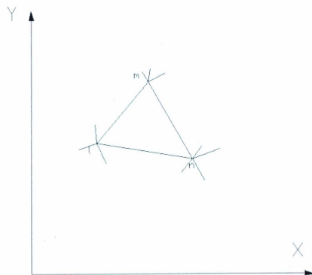


Fig 3.1: Typical triangular element connected to other elements

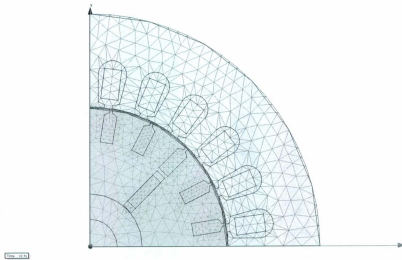


Fig 3.2: Mesh generated by Maxwell® for one-quarter of cross-section of a motor.

For each node in Fig 3.1 the values are

$$\begin{aligned} A_l &= c_1 + c_2 x_l + c_3 y_l \\ A_m &= c_1 + c_2 x_m + c_3 y_m \\ A_n &= c_1 + c_2 x_n + c_3 y_n \end{aligned} \quad (3.29)$$

where $A_l = A(x_l, y_l)$, $A_m = A(x_m, y_m)$, $A_n = A(x_n, y_n)$ in matrix form

$$\begin{bmatrix} A_l \\ A_m \\ A_n \end{bmatrix} = \begin{bmatrix} 1 & x_l & y_l \\ 1 & x_m & y_m \\ 1 & x_n & y_n \end{bmatrix} \begin{bmatrix} c_1 \\ c_2 \\ c_3 \end{bmatrix} \quad (3.30)$$

The solution is

$$A = \frac{1}{2\Delta} \sum_{k=l,m,n} [a_k + b_k x + c_k y] A_k \quad (3.31)$$

where a_k , b_k , c_k are scalars, x and y are the co-ordinates thereby scalars and Δ is the surface area of the triangular element. From Maxwell's fourth equation $\text{div} \mathbf{B} = 0$, the magnetic field in a triangle is:

$$\mathbf{B} = \bar{\nabla} \times \mathbf{A} = \bar{\nabla} \times A \hat{u}_z \quad (3.32)$$

$$\mathbf{B}(x, y) = -\frac{\partial A}{\partial y} \hat{u}_x + \frac{\partial A}{\partial x} \hat{u}_y \quad (3.33)$$

\hat{u}_x, \hat{u}_y and \hat{u}_z are unit vectors in x, y, z co-ordinates, substituting (3.32) into (3.33) gives

$$\mathbf{B}(x, y) = \frac{1}{2\Delta} \sum_{k=i, m, n} [c_k A_k \hat{u}_x - b_k A_k \hat{u}_y] \quad (3.34)$$

Thus it can be shown magnetic field is constant within a particular finite element. The grid point potential A_k can be found by minimizing energy functional F from (3.17)

$$\int_i \left[\frac{1}{2\mu} \frac{\partial}{\partial A_k} \left[\left(\frac{\partial A}{\partial x} \right)^2 + \left(\frac{\partial A}{\partial y} \right)^2 \right] - \frac{\partial}{\partial A_k} (\mathbf{J} \cdot \mathbf{A}) \right] dx dy + j \int_i \left[\omega \frac{1}{2} \sigma \frac{\partial}{\partial A_k} (\mathbf{A})^2 \right] dx dy = 0 \quad (3.35)$$

where $dS = dx dy$. (3.35) can further be written in matrix form

$$[\mathbf{R}][\mathbf{A}] + j[\mathbf{M}][\mathbf{A}] = [\mathbf{C}] \quad (3.36)$$

where

$$[\mathbf{R}] = \frac{1}{4\mu\Delta} \begin{bmatrix} b_i b_i + c_i c_i & b_i b_m + c_i c_m & b_i b_n + c_i c_n \\ b_m b_i + c_m c_i & b_m b_m + c_m c_m & b_m b_n + c_m c_n \\ b_n b_i + c_n c_i & b_n b_m + c_n c_m & b_n b_n + c_n c_n \end{bmatrix} \quad (3.37)$$

$$[\mathbf{M}] = \frac{\omega\sigma}{12} \begin{bmatrix} 2 & 1 & 1 \\ 1 & 2 & 1 \\ 1 & 1 & 2 \end{bmatrix} \quad (3.38)$$

and

$$[C] = \frac{J\Delta}{3} \begin{bmatrix} 1 \\ 1 \\ 1 \end{bmatrix} \quad (3.39)$$

Equations (3.36) through (3.39) provide the solution for the magnetic potential A for a region of only one triangle, for N nodes the above process is repeated iteratively for each element.

3.4 Boundary Conditions

For a 2-D problem there is no boundary condition for the elements inside a domain but for edges, elements are constrained according to the boundary conditions at the exterior of the domain analyzed. For analysis of permanent magnet machine, flux lines for constant magnetic vector potential are assumed to be confined within the rotor outer boundary. Enforcing this boundary condition, $A=0$, flux lines are constrained to follow the boundary.

The flux lines inside any domain can be shown to be perpendicular to elements within the mesh as there is no constraint for them in the interior of the domain. For any electrical machine with the identical pole shape, has periodic boundary condition for each pole. This boundary conditions for a rotating machine can be expressed as [77]:

$$A(e, \theta_0 + q) = -A(r, \theta_0) \quad (3.40)$$

where θ_0 is the angle of radial boundary and q is the pole pitch angle.

3.5 Forces and Torque Calculation in an Electromagnetic Field

One of the prime objectives of FEM in an Electromagnetic Field is to compute force and torque. The most appropriate method is problem dependent, although five basic methods are well in vogue.

3.5.1 Maxwell Stress Tensor

The Maxwell stress tensor is the simplest of all methods considering the computational complexity involved since it requires only local flux density distribution along a specific line or contour. Using the Maxwell stress tensor, for a planar problem total force can be calculated as

$$\mathbf{F} = \iint \frac{1}{\mu_0} \left[\mathbf{B}(\mathbf{B} \cdot \mathbf{n}) - \frac{B^2 \mathbf{n}}{2} \right] dS \quad (3.41)$$

From where torque can be calculated using the following relationship [78],

$$\mathbf{T} = L_i \int_s \left\{ r_i \cdot \frac{1}{\mu_0} \left[(\mathbf{B} \cdot \mathbf{n}) \mathbf{B} - \frac{B^2 \mathbf{n}}{2} \right] \right\} dS \quad (3.42)$$

where r_i is the radius of the circumference, L_i is the length for the surface S .

3.5.2 Arkkio's Method

This is a variant of Maxwell stress tensor and derived from integration of the torque given by (3.42) in the whole volume of the airgap comprised between the layers of radii r_i and r_s . This method has been presented by Arkkio [79]

$$\mathbf{T} = \left(\frac{L_i}{[\mu_0(r_s - r_i)]} \right) \int_s r \mathbf{B}_r \mathbf{B}_t dS \quad (3.43)$$

3.5.3 Method of Magnetic Coenergy Derivation

Torque can be calculated by deriving the magnetic coenergy W by maintaining the current constant.

$$\mathbf{T} = L_i \frac{dW}{d\alpha} = \frac{d}{d\alpha} \left\{ \int_0^H \mathbf{B} \cdot d\mathbf{H} dv \right\} \quad (3.44)$$

Using the finite difference approximation, the torque derivation of (3.44) is approximated taking the difference between two successive calculations [80, 81],

$$\mathbf{T} = L_i (W_{\alpha+\delta\alpha} - W_{\alpha}) / \delta\alpha \quad (3.45)$$

where L_i is the length and $\delta\alpha$ represents the displacement.

3.5.4 Coulomb's Virtual Work

Using the principle of virtual works [82], we derive the following expression for the torque:

$$\mathbf{T} = \int_{\Omega} L_i \left[-\mathbf{B}^t G^{-1} \left(\frac{dG}{d\phi} \right) \mathbf{H} + \int_0^H \mathbf{B} d\mathbf{H} |G|^{-1} \left(\frac{d|G|}{d\phi} \right) \right] d\Omega^e \quad (3.46)$$

where the integration is carried out over the elements situated between the $\frac{dG}{d\phi}$ fixed and moving parts. Here L_i is the length, G denotes the jacobian matrix, is the element deformation during the displacement $d\phi$.

3.5.5 Magnetizing Current Method

This method is based on the calculation of the magnetizing current and the flux density over the element edges for the boundary between the boundary between the iron or permanent magnet and the air [83],

$$\mathbf{T} = \frac{L_g}{\mu_0} \int_{\Gamma_e} \left\{ \mathbf{r} \times \left[\left(\mathbf{B}_{t1}^2 - \mathbf{B}_{t2}^2 \right)_n - \left(\mathbf{B}_{t1} \mathbf{B}_{t2} - \mathbf{B}_{n2}^2 \right)_t \right] \right\} d\Gamma_e \quad (3.47)$$

Γ_e denotes all the interfaces between the iron or permanent magnet and airgap and $d\Gamma_e$ is the length of the element edge located at the boundary, \mathbf{r} is the vector to connect origin to midpoint of $d\Gamma_e$. B_{t1} , B_{n1} is the tangent and normal flux density in respect to $d\Gamma_e$, the subscript n and t refers to the normal and tangential components, respectively of the flux density.

3.6 Inductance and Reactance Calculation in a Electromagnetic Field

The calculation of steady-state or linear inductance is straight-forward for permanent magnet machines, dividing the flux linkages of the coil by the current in the coil or dividing the energy stored in the coil by half of the current squared. But these methods are not valid for calculation of dynamic inductance as the inductance changes with the change of rotor position. Various methods are used to make an accurate approximation of inductance for a time varying magnetic field.

3.6.1 Dynamic Inductance Calculation

Energy or winding current perturbations are the basis of a method for calculating saturated and apparent inductances of permanent magnet machine. This method is general because it can be used for high-powered machines and it uses numerical field calculation technique like Finite Element for obtaining stored energy in the magnetic circuit of such machines [58]

The terminal voltage v_f for an n winding rotating machine can be modeled as

$$v_j = R_j i_j + \frac{d\lambda_j}{dt} \quad (3.48)$$

where i_j is the current λ_j is the flux linkage for j -th winding. Due to the magnetic saturation, the total flux linkage of the j -th coil becomes a nonlinear function of the n -winding current at a given rotor angle θ . So for j -th coil, (3.48) can be written as

$$v_j = R_j i_j + \frac{\partial \lambda_j}{\partial i_1} \frac{di_1}{dt} + \frac{\partial \lambda_j}{\partial i_2} \frac{di_2}{dt} + \dots + \frac{\partial \lambda_j}{\partial i_j} \frac{di_j}{dt} + \dots + \frac{\partial \lambda_j}{\partial i_n} \frac{di_n}{dt} + \frac{\partial \lambda_j}{\partial \theta} \frac{d\theta}{dt} \quad (3.49)$$

For a fixed rotor position the last term in (3.49) is zero as $\frac{d\theta}{dt} = 0$. Also in (3.49) $\frac{\lambda_j}{i_k}$ is defined as L_{jk}^{inc} . So the instantaneous terminal power P_j is given as,

$$P_j = R_j i_j^2 + i_j L_{j1}^{inc} \frac{di_1}{dt} + i_j L_{j2}^{inc} \frac{di_2}{dt} + \dots \quad (3.50)$$

The first term in (3.50) represent the instantaneous power loss for j -th coil, whereas the rest of the terms combined are the magnetic stored energy. So total stored magnetic energy can be given as,

$$W = \sum_{j=1}^n \left\{ \sum_{k=1}^n \int_{i_k(0)}^{i_k(t)} (i_j L_{jk}^{inc}) di_k \right\} \quad (3.51)$$

In large machine the inductance is given in a matrix form

$$\begin{pmatrix} L_{11} & \dots & L_{j1} \\ \vdots & \ddots & \vdots \\ L_{kj} & \dots & L_{nn} \end{pmatrix} \quad (3.52)$$

where L_{jj} is the self inductance and L_{jk} is the mutual inductance. For l windings these inductances are expressed as the partial derivative of global stored energy with respect to small perturbation in winding current Δi_j and Δi_k which is further expanded around a “quiescent” magnetic field [58, 84]. For a machine where $L_{jk}=L_{kj}$, the inductances are.

$$L_{jj} = \frac{\partial^2 w}{\partial (\Delta i_j)^2} \approx \frac{[w(i_j - \Delta i_j) - 2w + w(i_j + \Delta i_j)]}{(\Delta i_j)^2} \quad (3.53)$$

$$L_{jk} = \frac{\partial^2 w}{\partial (\Delta i_j) \partial (\Delta i_k)} \approx \frac{\begin{bmatrix} w(i_j + \Delta i_j, i_k + \Delta i_k) - w(i_j - \Delta i_j, i_k + \Delta i_k) \\ -w(i_j + \Delta i_j, i_k - \Delta i_k) + w(i_j - \Delta i_j, i_k - \Delta i_k) \end{bmatrix}}{4\Delta i_j \Delta i_k} \quad (3.54)$$

3.6.2 Steady-state Inductance Calculation

As stated earlier for steady-state inductance calculation we divide flux linkages λ by current,

$$L = \frac{\lambda}{I} \quad (3.55)$$

3.6.3 Synchronous Reactance Calculation

For an interior permanent magnet synchronous machine saliency is created inside the rotor by magnets arrangement though it has a smooth airgap. So IPMSM is basically a salient pole synchronous machine [57]. For a salient pole synchronous motor the d-axis and q-axis synchronous reactances are given by

$$X_d = X_l + X_{md} \quad (3.56)$$

$$X_{sq} = X_l + X_{mq} \quad (3.57)$$

X_d and X_q are the d and q axis synchronous reactances, X_{md} and X_{mq} are the d and q axis magnetizing reactances, respectively and X_l is the leakage reactance.

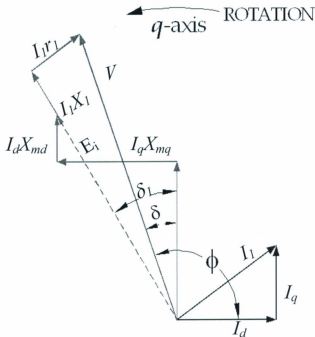


Fig 3.3: Phasor Diagram of a PM Motor

From the phasor diagram of Fig 3.3 for a permanent magnet d-q axis currents I_d and I_q can be obtained as [85],

$$I_d = \frac{V(X_q \cos \delta - r_l \sin \delta) - E_0 X_q}{r_l^2 + X_d X_q} \quad (3.58)$$

$$I_q = \frac{V(r_l \cos \delta + X_d \sin \delta) - E_0 r_l}{r_l^2 + X_d X_q} \quad (3.59)$$

where V is the terminal voltage, E_0 is the excitation voltage due to permanent magnet flux alone, r_f is the stator resistance, δ is the torque angle shown in the phasor diagram of Fig 3.3. From the same phasor diagram of Fig 3.3, the voltage equation can be expressed as

$$E_0 + I_d X_{md} + j I_q X_{mq} = E_i \angle \delta_i \quad (3.60)$$

where δ_i is the interior torque angle of the rotor position at time i . For the two-dimensional planar case, the lines of constant vector potential represent flux lines, E_i is the back-EMF at any time i . Hence, both d-axis and q-axis fundamental components of flux in the airgap can be derived by performing a Fourier analysis on the vector potentials \mathbf{A} around the inner surface of the stator. The cosine term a_1 represents the quantity of half the q-axis flux per pole (per unit depth) with respect to the analytical model of pm motor. The sine term coefficient b_1 represents the quantity of half the d-axis flux per pole (per unit depth). So the value of the resultant flux per pole is given by [86]

$$\phi_m = 2l_i \sqrt{a_1^2 + b_1^2} \quad (3.61)$$

$$\text{and} \quad \delta_i = \arctan\left(\frac{b_1}{a_1}\right) \quad (3.62)$$

where l_i is the length of the airgap. This flux induces a voltage E_i in each stator phase winding as

$$E_i = 4.44 f \phi_m N_s K_w \quad (3.63)$$

where N_s is the number of series turns per phase and K_w is the product of stator winding distribution and pitch factors. Further equating voltage components in d-axis and q-axis we have

$$E_i \cos \delta_i = E_0 + I_d X_{md} \text{ or } X_{md} = \frac{E_i \cos \delta_i - E_0}{I_d} \quad (3.64)$$

$$E_i \sin \delta_i = I_q X_{mq} \text{ or } X_{mq} = \frac{E_i \sin \delta_i}{I_q} \quad (3.65)$$

3.6.4 Leakage Reactance Calculation

The armature leakage reactance is calculated from numerical evaluation of the energy stored in the slots and the ending rings or end connection [87]. This method includes the magnetic saturation effect and end connection leakage reactance. The scheme is performed for each slot and each tooth as they are defined as volume in which the local contribution to the leakage energy can be calculated. The calculation of end connection leakage reactance calculation is difficult in 2-D FEM program where 3-D FEM is a better fit [88].

3.7 Time-Stepping Finite Element Analysis

To take into account the time variation of flux density and induced currents during a time cycle, a time-stepping method is introduced. In this method a new mesh is created in each time step and pertinent values are calculated using methods described in this chapter.

Assuming $\frac{\partial A}{\partial t} = 0$ at $t=0$ as though there is no induced voltage and no induced current we make a first estimate of stator winding current.

Using the estimation of $\frac{\partial A}{\partial t}$ or A_i , we derive the next $A_{i+\Delta t}$ using the following formulation [72],

$$A_{i+\Delta t} = A_i + \Delta t \cdot \frac{\partial A}{\partial t} \quad (3.66)$$

where A is the magnetic vector potential, Δt is the time-step. This process continues until changes in element permeability and node potentials are below a specific level.

Chapter 4

Design Case Studies

As an integral part of research, efforts have been made to make some extensive simulation on various rotor structures with different magnet shape. In this chapter, a Computer Aided Design tool is introduced to better address various design intricacies of line-start permanent magnet synchronous motors. Meticulous information is given on each step of various design aspects.

4.1 Analytical vs. Finite Element Analysis

As a result of a tremendous increase in the complexities and widespread applications of solid-state controlled permanent magnet motor drives, computer models and simulations have become extremely useful tools in the design as well as performance prediction and analysis of such systems and their associated electronic circuits. This includes their interaction with the various electric machines with which they are interfaced. Accordingly, the resulting synergistic effects between the time harmonics, produced by the cyclic and sequential switching in the electronic circuits, and the intrinsic space harmonics, resulting from the specific magnet circuit configurations and winding layouts, can be rigorously investigated and quantified.

Meanwhile, previous efforts toward modeling machine-drive systems using variation of linear transformations of the $dq0$ frame of reference type are gradually falling out of favor in recent modeling efforts. This is because these models are inherently formulated in terms of transformed “synthetic” direct and quadrature axes currents and voltages, which are based on the assumptions of flux distributions around the air gaps and armature circumferences of such machines that are purely sinusoidal in nature. This precludes a sufficiently rigorous account of the effects of space harmonics resulting from winding

layouts and rotor excitation effects as well as stator and rotor magnetic circuit saturation and geometrics. This is unlike the typical *abc* frame of reference approach which is formulated in terms of the natural "physical" *a*, *b*, and *c* armature currents and their corresponding winding inductances as well as flux linkages. [89]

4.2 Computer Aided Design

The design of machines is the important stage before developing them. Over the years engineers have accumulated much experience in the design process. Much deliberation and research time went on to pursue an efficient design process. With the advent of new computers and their application in engineering design, the manual labor in machine design has been cut short decisively. Computer Aided Design (CAD) packages have been widely used and will play a more important role in near future.

The application of numerical methods in electromagnetic fields began the revolutionary stage of CAD. The approximate machine model with magnetic circuits was replaced by much more accurate finite difference and finite element analysis. These numerical methods in association with Galerkin approach and Newton- Raphson (N-R) method helped the machine designers greatly. He/she can even take a particular section of machine and predict the performance discreetly with the results obtained by numerical method.

Design is an art, an empirical and scientific work. The rules, formulae and information used in the design process are not in general, as precise as in numerical computation. A given design problem may have more than one solution. The specifications of electric machines usually cover such items as output power, speed, voltage, torque, efficiency etc. The final results of the design process must satisfy these requirements without exceeding certain limit of cost, heating, error in calculation, converging threshold (for numerical calculation) etc. For these designers, there are many factors to account and also the

extensive pool of knowledge involved in the design process [90]. Normally the specific criterion facilitated by the designers for a successful design of permanent magnet motor can be compiled as:

- ✓ Power rating: the output mechanical power for motors.
- ✓ Voltage rating.
- ✓ Number of phases of the power supply and the connection of phases.
- ✓ Speed rating or synchronous speed.
- ✓ Power factor.
- ✓ Selection and calculation of the electromagnetic parameters in the machine.
- ✓ Armature winding design which includes the selection of the type of winding connection and the wire gauge, determination of turns (both serial and parallel), layers and calculation of resistance of these windings.
- ✓ Ending ring and stacking factor design. Though the ending ring is considered as an extension of rotor bars, it is computed with lower conductivity from the materials used in rotor and winding. Rotor length includes the stacking length and stacking factor dictates the interleaving among the sheets used for rotor structure which is computed according to sturdiness of motor and lamination of conductors [91, 92].
- ✓ Design of mechanical components of the machine. We must decide the dimensions of stator, rotor, poles, interpoles, slots, teeth, shaft etc.
- ✓ Calculation of various losses, temperature changes and if possible tweaking the motor to better accommodate the cooling system.
- ✓ Define the insulators and lamination of conductors (thickness, coating etc.) used in the machine.
- ✓ Usage of materials and possible cost of these materials.

4.3 Maxwell® Software Package for Analysis of Electric Motor

The two-dimensional and three-dimensional simulation software for electromagnetic analysis, Maxwell® from Ansoft Corp. can carry out simulation in both frequency and time domain electromagnetic fields in complex 2D and 3D structures. In this thesis it is employed to simulate and evaluate the performance of the 3-phase line-start permanent magnet synchronous motor.

4.3.1 Maxwell 2D

Maxwell 2D is a software package for two-dimensional simulation of electromagnetic fields.

Using Maxwell 2D one can easily predict the transient and magnetostatic performance of electromagnetic and electromechanical component designs in virtual environment thereby giving a cheap and ready design prototype. The software provides the ability to simulate electromagnetic fields both in the time and frequency domains, as well as parametric modeling and optimization. Maxwell 2D is part of Ansoft's complete electromechanical design solution. The following are the type of solutions provided by Maxwell 3D®.

4.3.2 Two Dimensional (2D) AC Magnetic

Maxwell 3D's AC Magnetic solver analyzes systems that have significant eddy currents, displacement currents, and skin and proximity effects. The software can simulate the full range of eddy-current behavior in bus bars, transformers, coils, sensors. It automatically calculates quantities, including but not limited to power and core loss, impedance at a given frequency, force, torque, inductance, and stored energy. The power and core loss may be directly exported to ePhysics™ for coupled thermal and stress analysis. Additionally, plots of flux lines, \vec{B} and \vec{H} fields, and energy densities over the entire phase cycle are available. Using the material and airgap boundary condition with this solver, designers can simulate fields radiating from a device or within a electromagnetic device.

4.3.3 Two Dimensional (2D) DC Magnetic

The electric conduction field simulator computes steady-state 2D or 3D electric fields in conductors due to current excitation or applied electric potential. As a source of electric field, one consider following

- The voltage difference between surfaces and objects.
- The current excitation, total current flowing through a surface or a 2D object.
- The sink excitation, a collection of surfaces or 2D objects are called sink. One can apply sink excitations when only current excitations are defined in a conduction path and there is no voltage excitation.

The quantity for which the electric conduction field simulator solves is the electric potential, ϕ ; the electric field (\vec{E} -field) and the current density (\vec{J} -field) are automatically calculated from the potential using Maxwell's law. The resistance matrix, a derived quantity, may be calculated from these basic field quantities. As an additional option, perfect insulators, that is, non-conduction regions, surrounding the conductors can also be added to the simulation domain allowing calculation of the electric field everywhere including the insulators.

4.3.4 Electrostatic field calculation

Maxwell 2D electrostatic field solver has a particular usefulness for the design of high voltage insulator, bushings and electrostatic discharge devices. This solver enumerates static electric fields due to stationary charge distributions and applied potentials. Thus the simulator automatically calculates the electric field strength and electric flux fields lines which in effect can be useful to derive force, torque, energy and capacitance from these basic field quantities.

4.3.5 Magnetostatic Field Solution

The magnetostatic field simulator computes static magnetic fields both in 2D and 3D analysis. This source of magnetic field can be either DC current in conductors or static external magnetic fields represented by boundary conditions or for our case permanent magnets. These applications are included in the simulation of motors, actuators, sensors, and permanent magnets. This feature, which directly computes current distribution and the corresponding magnetic field (\vec{H}), derives the magnetic flux density (\vec{B}) from the H field and the nonlinear BH characteristics. For a specific magnetic material, we can also define 10 points in its BH curve based on empirical values ultimately which can lead to a successful establishment of a new material. Magnetization can also be specified in Cartesian, cylindrical, or spherical material coordinate systems. It automatically calculates forces, torques, inductances, and saturation in devices containing linear, nonlinear, and anisotropic materials. Even if not in standard machine parameters, a calculator expression can be used to conveniently calculate frequently used quantities. An advanced nonlinear option allows for a second-pass analysis by the use of distributed "frozen" permeability or magnetization. Thus, the analysis of devices containing nonlinear permanent magnets benefits from the increased accuracy of the simulation. The post-processor provides plots of flux lines for magnetostatic analysis, B and H fields, energy densities, saturation, and more.

4.3.6 Eddy Current Analysis

The eddy current (AC magnetics) field simulator or harmonic solver computes electromagnetic fields in the frequency domain both in 2D or 3D simulation. It is based on the assumption that all electromagnetic fields pulsate with the same frequency and have magnitudes and initial phase angles calculated by Maxwell equation. There are no moving objects. As all materials are

assumed to be linear, permanent magnets cannot be part of the model. Simulation also includes electromagnetic radiation. Magnetic field tangent is the boundary condition applied in regular eddy current problems unless differently specified. The eddy current field simulator solves the magnetic field, \vec{H} , from which magnetic flux density, \vec{B} , is automatically calculated. Optionally, the eddy current solver can incorporate displacement currents into the solution even in non-conducting domains, thereby allowing the solution of the full system of Maxwell's equations and the recovery of the electric field \vec{E} everywhere including the non-conducting regions. Quantities such as forces, torques, energy, losses, and impedances may be calculated from these basic field quantities for solution in frequency domain.

4.3.7 Transient Analysis

The transient field simulator calculates magnetic fields in time-domain both in 2D or 3D analysis. This magnetic field can come from

- Moving or non-moving time varying currents and voltages.
- Moving or non-moving permanent magnets and/or coils.
- Moving or non-moving external circuit coupling.

This application can resolve the machine quantities for both translational and cylindrical rotation. Two of the basic quantities solved by the transient field simulator are the magnetic field, \vec{H} , and the current distribution, \vec{J} and the magnetic flux density, \vec{B} , is automatically calculated from the \vec{H} -field. Eddy current effects (such as skin and proximity effects) are ignored for voltage driven stranded conductors whereas they are included for voltage driven solid state conductors. Maxwell 2D[®] uses the fixed coordinate system for the Maxwell's equations in the moving and the stationary part of the model. Each component in a model has to be declared according to a

specific coordinate system or a different coordinate system in case a different rotational direction. The automatic output includes current, induced voltage, and flux linkage at every time step. Available outputs also include the dynamic force or torque response, loss, and core loss, including eddy, excess, and hysteresis loss, including minor loops. Maxwell 3D allows users to set up a variable, user-specified time-step profile. Thus, the time step can follow any arbitrary function of time, position, or speed, providing increased flexibility of the time-stepping solution process and leading to significant reduction in computational resources. Users can easily determine core loss with Maxwell®. Core-loss coefficients can be automatically extracted from a user specified core-loss characteristic.

4.4 Design Components in Maxwell® package

For designing a model Maxwell® uses different software modules for different design challenges. Drawing a simple induction generator can first invoke the RMxpert™ which cares for the cylindrical design of stators and rotors. An induction of an external circuit can be carried out by a circuit editor; PExprt™ and PMxpert™ are used for power electronic component (converter, transformers etc.) design. Finally for simulation purposes we have Maxwell 2D and Maxwell 3D. The pertinent software modules which are necessary for successful design of permanent magnet synchronous motor are described.

4.4.1 RMxpert

Rotational Machine Expert (RMxpert™) is an interactive software package used for designing and analyzing rotating electrical machines. It has some commonly used electric-machine templates.

RMxpert™ can simulate and analyze the following types of machines:

- Three-phase and single-phase induction motors.
- Three-phase synchronous machines.
- Brushless permanent-magnet DC motors.

- Adjust-speed synchronous motors and generators.
- Permanent-magnet DC motors.
- Switched reluctance motors.
- Line-start permanent-magnet synchronous motors.
- Universal motors.
- General DC machines.
- Claw-pole alternators.
- Three-Phase Non-Salient Synchronous Machine.
- Generic Rotating Machine.

Each machine-specific template includes basic rotor and stator configurations, running strategies, and drive circuits. The templates have auto-design compensating features that automatically determine minimum slot geometry to obtain the optimum flux density value, select the correct wire diameter for the slot, calculate starting capacitance, and select winding arrangements. Any design anomaly is correctly indicated before any lengthy simulation takes place. RMxprt™ can automatically arrange almost all commonly used single- or double-layer poly-phase ac windings provided all coils have the same number of turns. Users do not need to define coils one by one. It also provides a very flexible tool, the Winding Editor, to allow users to design a variety of special winding types according to their own needs, such as compound single- and double-layer winding, big- and small-phase-spread variable-pole multiple-speed distributed winding, sinusoidal three-phase winding, concentratic winding and so forth.

Specialized templates like those for PM, BLDC, SRM allows the introduction of specific motor geometry which is normally not used in generic motor design and the use of accurate magnetic circuit algorithms to make sizing decisions and performance estimates during the initial stage of the design process. These templates are handy because of ready availability of some established

design features which are not usually tweaked for further performance improvement. The template-based interface is a convenient tool for calculation of critical design parameters, such as torque versus speed, power loss, flux in the air gap, and efficiency.

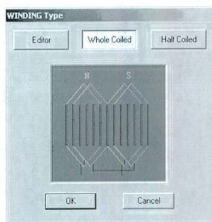


Fig 4.1: Winding Type for RMxpert™

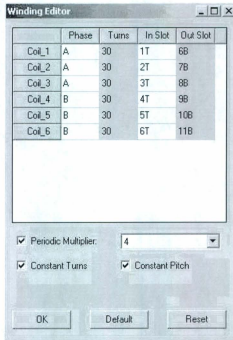


Fig 4.2: Winding Editor for RMxpri™

RMxpri™ can be used as a stand-alone design tool or as part of a complete design solution. It is normally trailed by Maxwell®2D or Maxwell®3D for detailed electromagnetic field modeling.

4.4.2 External Circuit Editor

Transient solver includes an external circuit coupling feature, complete with schematic to support arbitrary topology of power-electronic drive circuits and winding connections. Maxwell circuit editor graphically represents and captures the electrical structure and characteristics of a circuit. Such a circuit is designed by the schematic editor by placing components, such as linear and nonlinear resistances, capacitances, inductances, diodes, controlled switches, independent sources, and voltage and current probes and wires into a default empty schematic.

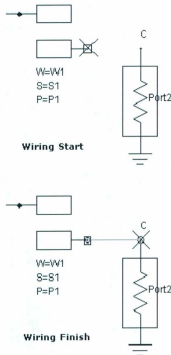


Fig 4.3: Few components used in Maxwell Circuit Editor Schematic

4.4.3 PExprt™

PExprt™ is a software unit that specializes in design, analysis and optimization of transformers and inductors found in power electronic applications. Using analytical expression, PExprt™ allows designers to instantly calculate all possible combinations of core size, core material, wire gauge, turns, and gap length that satisfy user-supplied electrical specifications. Traditionally, these cycles of design-build-test methodologies are trusted upon engineers with years of experience from trial and error. In conjunction with Finite Element Analysis package like Maxwell® these designs are further streamlined and optimized to predict quantities such as magnetizing and leakage inductance, interwinding capacitance, peak flux density, AC winding

resistance, eddy current effects, core loss and temperature rise. Equivalent circuit generation is another feature that takes into account magnetic and thermal properties. The basic features of PExprt™ can be given as:

- Design inductors, multi-winding transformers, coupled inductors, and flyback type components.
- Both sinusoidal and square input wave can be used.
- Design of boost, buck, buck-boost, forward, push-pull, half-bridge, full-bridge and flyback converters.
- Construction parameters like core shapes, size, material, gap, wire type and gauge, and winding strategies are also considered to optimize the magnetic design.
- Analysis takes into account complex effects, such as skin and proximity effects, fringing flux near the air-gap for energy calculations, and incremental permeability as a function of the field strength as well as winding position and stacking, including interleaving, intra-winding capacitance, temperature, losses, gap effect and end effect, parallel connection etc.
- These can be modelled seamlessly by importing Simplorer®, which is a powerful multi-domain system analysis software program.

which the model is imported on a Maxwell 2D or 3D panel to perform further magnetic analysis. The whole procedure can be explained in a simple flow-chart:

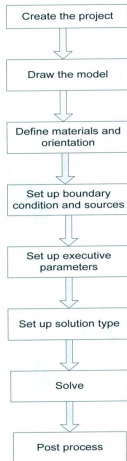


Fig 4.5 Flow chart for Maxwell® 2D

4.5.1 Creating a project for Maxwell 2D

When the project window is opened in Maxwell® a default blank project is opened

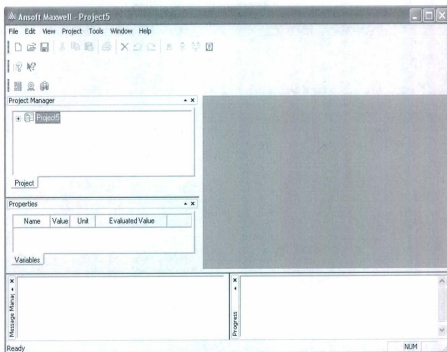


Fig 4.6: Project window of Maxwell® 2D

Maxwell® analyzes the 2D geometry as a cross-section of the 3D model, and then generates a solution for that cross-section of the model. This axi-symmetric model takes advantage of 3D geometry that exhibit rotational symmetry about an axis. To kick-start a project we can insert a RMxpert design.

We can select any of the six options from the number of solution type for the type simulation from the same model. These six options include Magnetostatic, Eddy Current and Transient in magnetic simulation and Electrostatic, AC conduction and DC conduction in electric simulations. All these options are explained briefly in the earlier part of this chapter.

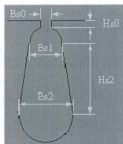
4.5.2 Drawing the Project

As I stated in paragraphs before, we can select from a palette of built-in designs as a base for our new model. Although building a model should literally mean a variegated posse of new parameters but these are not radically changed from the machines already in vogue. Like for line-start permanent magnet synchronous motors, the stator structure is almost same as induction motor but the rotor has extra space for permanent magnets. Our design changes mostly revolve around the shape, size and allocation of magnetic materials.

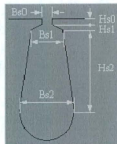
For the twelve options given as a basis for new motor design, we select the line-start permanent magnet synchronous motor as having the closest resemblance to our model. This gives us three separate part stator, rotor and shaft design to fiddle with the parameters.

4.5.2.1 Stator Slot Design

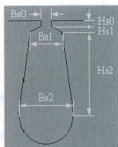
There are six User Defined Primitives (UDP's)



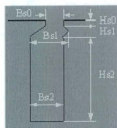
(a)



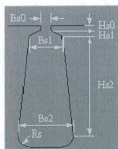
(b)



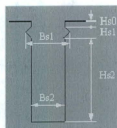
(c)



(d)



(e)



(f)

Fig 4.7 (a, b, c, d, e, f): Six separate structure for stator slot

For our model we selected 4.7(c). Every single length (Bs_0 , Bs_1 , Bs_2 , Hs_0 , Hs_1 , Hs_2) is customizable through user input.

Now Maxwell supports three type winding half-coiled, full coiled and user-defined. One can also select number of layers, number of parallel branches and number of serial branches, number of conductors per slot, number of strands, wire size and wire wrap.

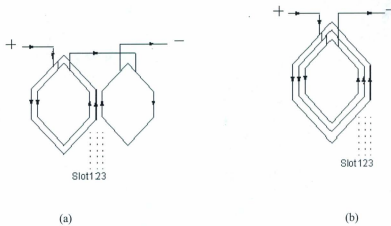


Fig 4.8 (a): Whole-coiled concentric stator winding arrangement

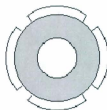
Fig 4.8 (b) half-coiled concentric stator winding arrangement

4.5.2.2 Rotor Slot Design

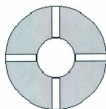
For rotor bars, similarly dimensions can be selected from a pool of four designs. Permanent magnet machines do not have an external connection to the rotor, so bar conductor types, ending length, ending ring width, ending ring height and ending ring material can be selected under rotor designs.

4.5.2.3 Rotor Pole Geometries

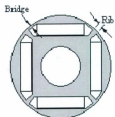
Depending on the arrangement of magnets numerous rotor geometries are possible. Maxwell provides some basic templates in their design pool.



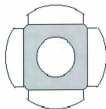
(a)



(b)



(c)



(d)

Fig 4.9 (a,b,c,d): Various rotor pole structure.

After successfully designing stator, rotor and shaft, we can either convert this RMXprt design to Maxwell 2D design or we can import a completely new Maxwell 2D template. Maxwell® gives us a wide range of tools like line, polyline, spline, rectangle, sphere, box, core etc. to draw a new object.

Maxwell 2D modeler gives us the flexibility of using standard tools like cutting, sweeping, moving and rotating etc, where axi-symmetric object can be replicated around a definitive axis or an external shape can be brought to make necessary changes to the original shape.

For better design flexibility, an external CAD software Autocad® is used. This software has a broad acceptance among engineers for concise and conspicuously placed tool icons. The 2D models are exported to an external Autocad® window through the file extension .dxf. After necessary modifications the model is brought back to Maxwell® window for simulation purposes. Figure 4.10 shows the drawing window of Autocad®.

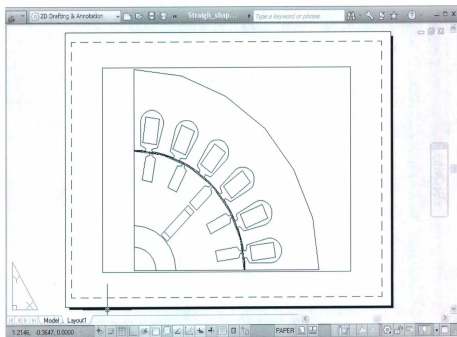


Fig 4.10: Drawing window of Autocad®

4.5.3 Setting up the problem

Analyzing a permanent magnet synchronous machine involves three steps.

4.5.3.1 Assign materials to objects

We can assign to each object in the model a separate material. Maxwell in itself has a library of predefined attributes for commonly used materials in Maxwell 2D. These definitions are locked, so that they cannot be changed or altered.

For a material not in the list, users can define a new material and add it to the library. For such, they have to define 10 points in the BH curve (permittivity-permeability) or conductivity.

Maxwell® lets users set the polarization of each magnetic object. In our case the polarization was circumferential for each magnetic object. Moreover Maxwell® lets users validate if the range of values specified for each material property is reasonable.

4.5.3.2 Setting up boundary condition

Maxwell 3D automatically assigns boundaries to the objects in the model based on the material properties assigned to it. Boundaries specify the action of an electric or magnetic field within the edges of objects. Boundary conditions can also be used to simulated magnetically isolated, electrically insulated structure. It is especially helpful in simulating a field pattern that is replicated throughout the whole region but drawn only a part of it or the patterns produced by tiny layers (like eddy current). There are six types of boundary conditions depending on the solver used,

- Vector Potential
- Symmetry

- Balloon
- Impedance
- Resistance
- Master/Slave

For our models in Maxwell® 2D, we used Master/slave condition. The mathematical boundary conditions used in Maxwell® is both the Neumann and natural boundary condition. A brief description of these boundary conditions is given in chapter 3.

4.5.3.3 Assigning voltage and current source excitation

Depending on the solver we have to define three basic types of sources, voltage, current or electric or magnetic field. At least one object or edge is either a source or value boundary.

Voltage sources are available for the Electrostatic, DC Conduction, AC Conduction and Transient solver types. Voltage sources specify the total DC voltage (electric potential), or the magnitude and phase of the AC voltage on a conductor.

Current sources are available in the Magnetostatic, Eddy Current, and Transient solver types. The current value cannot be assigned directly in a coil. Normally a terminal is used as a cutaway of the coil. Direction of current source is also defined when a current source is added.

We can also add eddy effects or core losses in this phase.

4.5.4 Defining forces, torques and related values

We can assign force or torque parameters for all Magnetostatic, Electrostatic, Eddy Current and transient solver. Assigning a force or torque for an object must be followed by declaring a reference frame for the object.

For any magnetostatic problem, capacitance, inductance, or impedance are declared in matrix form. A matrix calculation, where the elements are defined based on excitations, may include coil terminals, outer terminals etc. In case of inductance matrix, the source is a current excitation.

4.5.5 Setting up the analysis

In finite element analysis, mesh operation is run when subdividing the motor cross-section into smaller elements. In Maxwell, mesh operations are optional. Mesh refinement settings provide Maxwell with mesh construction guidance. We can use both tetrahedral and triangular elements for meshing operation. The length of these tetrahedral elements can be refined within a surface or volume until they are below a certain threshold or they are within a specified value. In our case we used triangular elements for our simulation. Fig 4.11 shows a mesh plot for a concentrated stator winding permanent magnet machine.

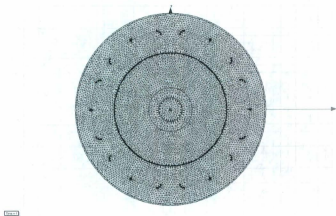


Fig 4.11: Mesh plot for concentrated winding permanent magnet machine

Once the model is set-up, a solution setup must be added for analysis in any solver. The options for solution setup includes

- Range and increments of any data input to the solver
- Precision of result
- Number of times solution will be repeated.
- Simulation run time
- Time step also defined as the function of time, speed, and position.

4.5.6 Solving the problem

“Time should be set to zero” after every aborted simulation. If we want to run simulation more than one simulation at a time, we should go with “Analyze option”. We can use other PC on the network for running the operation from a remote place. “Distributed Analysis” can be used to share the resources from other PC.

4.5.7 Post processor

After the simulation is run, we can either display the data or analyze them. View data give us the option of viewing the information like convergence information, computing resources used, output variables and parameters available and matrix data. Or we can analyze these data by creating reports of RLC matrices and basic and derived field quantities. Derived field quantities are user defined calculator expression. These reports can be plotted on a cross section plane, in three dimension plane or at a specific point.

The Maxwell® gives us usability to perform the complex finite element analysis without writing the complicated codes but through a Graphic User Interface (GUI) and complicated tools. Information shared in this chapter is based on Ansoft website [40], user manual and design experiences. All steps to perform

the operation in this chapter are further explained in Appendix A. In the next chapter, I will explain some models for experimental studies and difficulties faced during the construction of those models.

Chapter 5

Simulation and Results

As part of our study, we built 3 models based on basic rotor structures using Maxwell® and AutoCad®. Simulations are run on these models to make a comparison among the already established results and the results found from Maxwell®. In this chapter, the models are presented along with simulation results presented to provide a full comparison among these models.

5.1 Working Model

The motor models built in this chapter are established and used for higher efficiency line-start interior permanent magnet synchronous machines (IPMSM). The specifications of pertinent design data of these PM motors are given in tables. The standard aluminum rotor cage is used to provide the capability of line frequency starting and synchronization. The permanent magnet materials used in the rotor are NdFeB (Neodymium Boron Iron) or NEOREC- 38SH. The NEOREC magnet is a new product, surpassing the Rare Earth Cobalt (REC) magnet. The main raw materials are neodymium, a rare-earth element, common iron and boron. Its magnetic characteristics at the mass production level reach 49MGOe in maximum energy product(BH), achieving 50 to 80% high performance with 10% reduction in specific gravity compared with samarium-cobalt magnets [93].

Since finite element analysis is limited to 2D, the end effects due to the end shorting ring resistance are treated by a modification of the rotor bar conductivity and the stator end winding leakage flux has been accounted.

5.2 Straight shape line-start IPMSM

The first model to be designed is the interior permanent magnet synchronous motor (IPMSM) with straight shape motor arrangement. Here permanent magnets are buried below the rotor surface and below the stator slotted surface and the smooth rotor surface. Fig. 5.1 shows the cross section of IPMSM with straight magnet arrangement. Necessary flux barrier of PM exist at end of the magnets to direct the magnet flux north-south across the airgap. This is one of the first configuration arrangements in IPMSM design.

Fig 5.1 shows only one-fourth cross-section of a 4-pole line-start interior permanent magnet synchronous motor with straight-shape magnet arrangement. The specification for this motor is given in Table 5.1.

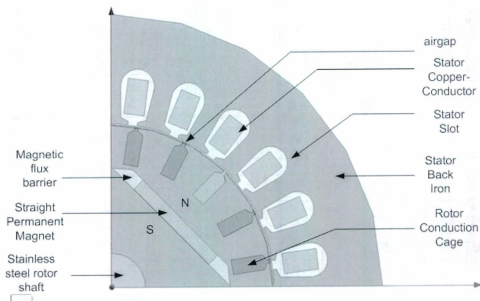


Fig 5.1: Cross-section of line-start IPMSM with straight-shape magnet arrangement

Table 5.1: Specification of straight-shape permanent magnet synchronous motor

Power Rating	687 kW
Line Voltage	195V (P-P)
Rated Current	3A
Base speed	1500 rpm
No. of Phases	3
No. of Poles	4
No. stator slots	24
No. of cage slots	24
Conductors	56
Connection	Y
Winding Layout	Single layer
Stator Outer Diameter	128mm
Stator Inner Diameter	77mm
Rotor Outer Diameter	76.2mm
Rotor Inner Diameter	16mm
Rotor Length	70mm
End Connection Resistance	2.86601e-006 ohm
End Connection Inductance	1.62855e-009H

As stated before the stator of a permanent magnet synchronous motor is essentially identical with that of AC induction motor of comparable rating. A three phase distributed winding is used to produce a near sinusoidal spatial distribution of rotating magnetomotive force in the airgap. Stator has a single layer, whole coiled winding with only one parallel branch. Only two strands of wires with a diameter of

"50www470" whose B-H curve is given as

Ansoft LLC

50www470



Fig 5.2: BH curve for the material “50www470”

of motor.

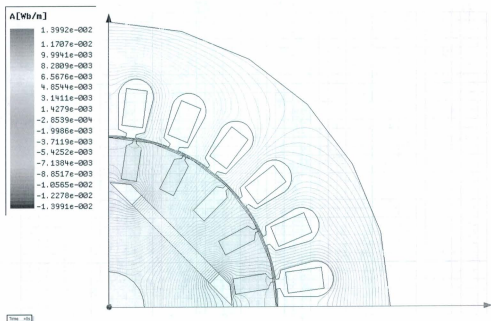


Fig 5.3(a): Flux lines for line-start IPMSM with straight magnet arrangement

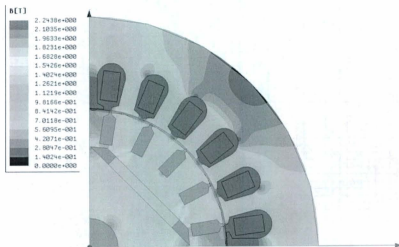


Fig 5.3(b): Flux density of line-start IPMSM with straight shape magnet arrangement.

5.2.1 Performance Investigation of Straight Shape line-start IPMSM

The Backward Euler time integration method has been used for simulation. Initially the simulation was run for 4 seconds with a time step of 0.02 ms. The simulation results are not satisfactory and simulation hits a snag mid-way through the simulation period of 4 sec. The speed-time response does not reach to the synchronous value (at 1500 rpm for 4- pole 50 Hz motor) if we choose a time-stepping of 0.02 ms. We increased the time step from 0.02 ms to 0.1 ms within a time span of 50 ms for the expected performance results. Even at 0.1 ms the simulations failed to achieve synchronous speed. We investigated and found that the losses at asynchronous speed are responsible for these unsatisfactory results not reaching synchronism. The IPMSM rotor is highly non-linear. The Ansoft FEA simulation package (Maxwell 2D, version 12.0) has problem with the IPMSM due to saturation and changes of relative permeability.

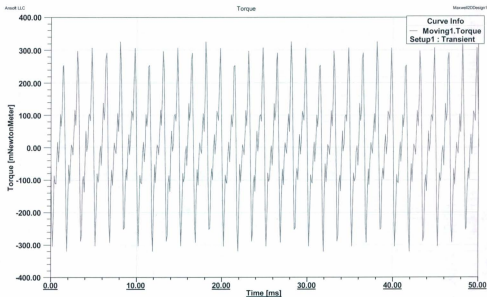


Fig 5.4: Torque –time response for line-start IPMSM

Fig 5.4 shows the simulated torque versus time response. It is to be noted from the torque time response of Fig 5.4 that the rotor torque shows significant hunting, and failed to attain successful synchronization. When the bigger time-step of 0.1 ms is used, the torque response shows normal operation considering the iron losses due to high-frequency harmonics. Fig. 5.5 shows simulated induced voltage versus time waveform of the straight shape IPM motor. When the time-step of 0.02ms is used the induced waveform shows significant harmonics. However when a step of 0.1ms used including the core losses, the induced voltage waveform is normal, following the expected pattern. It is found that unsatisfactory torque and induced voltage response are subjected to higher core and solid losses. The core loss and solid loss phenomena of this IPM motor has been

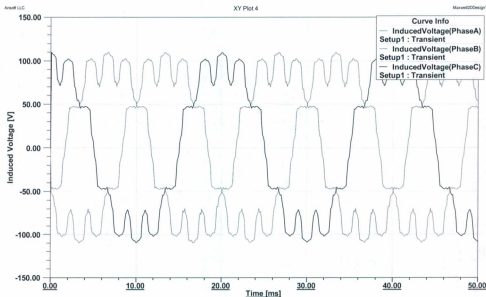


Fig 5.5: Induced voltage –time response for straight shape line-start IPMSM

investigated. Fig 5.6 shows the core loss versus time curve during the run-up and near synchronous for straight shape IPM motor. The core loss variation of 5W to 8.5W occurs during the asynchronous period.

It stabilizes at 8.5W; Fig 5.7 shows the solid loss versus time curve for straight shape IPM motor. The abnormality of torque response at asynchronous speed is due to core loss and solid losses in the IPM motor. The details of core loss and solid loss are briefly provided in sub-section of 5.4.1 of this chapter.

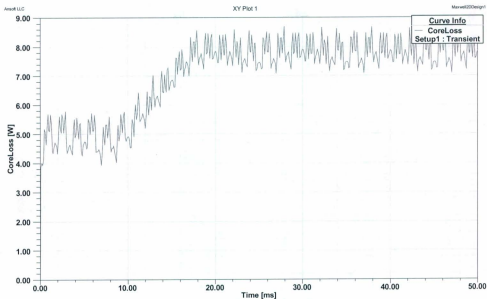


Fig 5.6: Core loss-time response for straight shape line-start IPMSM

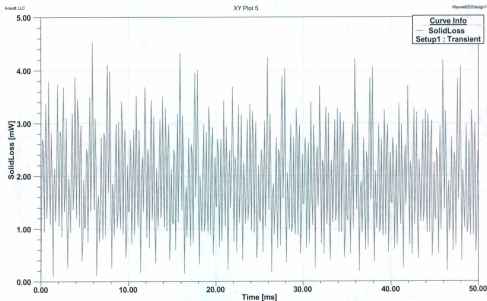


Fig 5.7: Solid Loss-time response for straight shape line-start IPMSM

5.3 V- Shape line-start IPMSM

The design of a V-shape permanent magnet rotor pole has many geometric degrees of freedom [94]. With single-layer design of the pole magnet it is possible to have a high percentage of reluctance torque to the total developed torque [95]. Changes to the electromagnetic design like introduction of V-shaped magnet arrangement provide the needed mechanical robustness of the rotor geometry at maximum speed plus the required safety factor but the mechanical robustness of the rotor often contrasts the needs of the electromagnetic design in terms of leakage flux etc. A mechanically optimized design could result in a low utilization of the PM flux and therefore leads to higher costs for the IPM motor [96].

Fig 5.8 shows a cross section of V-shaped line-start IPMSM where the permanent magnets are placed vertically with the shaft of the rotor instead of horizontally in the rotor. In this arrangement, necessary flux barrier was created in the rotor at the top and bottom of permanent magnet location to guide the flux lines through the rotor to the air gap of the IPM motor. Conducting materials like aluminum were used in

the rotor cage bar to make the flux as perpendicular as possible through the airgap. The magnetic material used here is the NdFeB magnets and has circumferential magnetization. So magnetic flux lines starting from North side of the magnet goes through the airgap, stator tooth, stator back iron and returns back on the South side of magnet. Fig 5.9 shows the flux lines and figure 5.10 shows the flux density for V-shaped line-start IPMSM. The major problem in the simulation of this magnet arrangement is the magnetic flux saturation in the rotor iron material. This saturation is highlighted by red shade in Fig 5.10 which shows that high flux density around the top of the NdFeB magnetic material. This problem is overcome by introducing a conducting material bar at the top of the magnet, which is explained in the next model.

The specifications for the motor are given at Table 5.2. The stator windings arrangement is the same as in the previous model, but in place of “50www470” we used laminated steel in stator core. The stator has a single layer, whole coiled distributed windings with only two parallel branches. There are only two strands of wires with a diameter of 0.511mm, and they are inserted in the stator slots in AACBBB arrangement to produce a near sinusoidal spatial distribution of the magnetomotive force (MMF) in the airgap.

Table 5.2: Specification of V-shaped permanent magnet synchronous motor

Power Rating	687 kW
Line Voltage	114.31V (P-P)
Rated Current	3A
Base speed	1500 rpm
No. of Phases	3
No. of Poles	4
No. stator slots	24

No. of cage slots	24
Conductors	56
Connection	Y
Winding Layout	Single layer
Stator Outer Diameter	128mm
Stator Inner Diameter	77mm
Rotor Outer Diameter	76.2mm
Rotor Inner Diameter	16mm
Rotor Length	70mm
End Connection Resistance	3.43715e-006ohm
End Connection Inductance	1.95246e-009H
Moment of inertia	0.0273 kgm ²
Load Torque	7 Nm

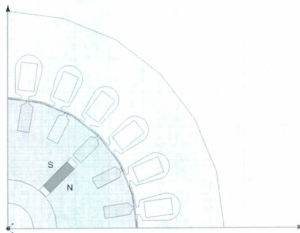


Fig 5.8: Cross-section of line-start IPMSM with V-shaped magnet arrangement

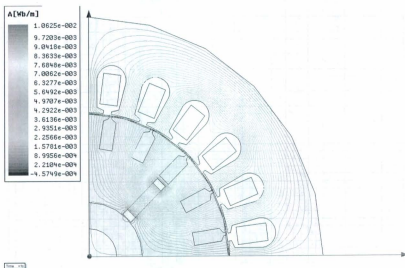


Fig 5.9: Flux lines for line-start IPMSM with V-shaped magnet arrangement

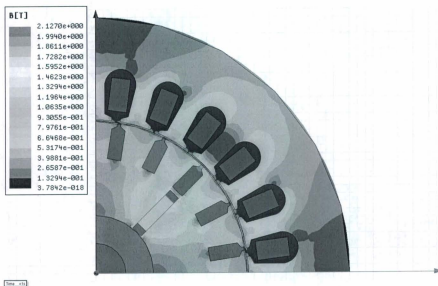


Fig 5.10: Flux density distribution for line-start IPMSM with V-shaped magnet arrangement

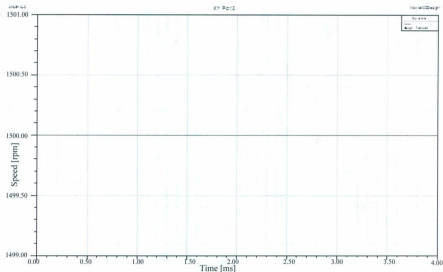


Fig 5.11: Speed – time response for V-shaped line-start IPMSM

5.3.1 Performance Investigation

The results shown here are not from physical experiments of a motor but from simulations of IPM synchronous motors where a commercial software package is used. The software is heavily dependent on the user inputs like changing relative permeability and magnets arrangement and may show an absurd result if everything does not fall in the right groove.

The novelty of the IPM synchronous motor is its usage of permanent magnets to replace the dc excitation which also create an extra MMF thereby magnetic flux to connect the stator winding. The performance of the IPM synchronous motor depends heavily on the magnet choice, their energy product, relative permeability and direction of the flux lines travelling in the airgap.

Fig 5.11 shows the simulated speed versus time response for a V- shaped IPM synchronous motor with NdBF_e magnets. It is to be noted that Fig 5.11 shows a flat line instead of the typical run-up response curve for an IPM motor having V- shape magnets arrangement. So we proposed to change the magnetic

material from NdBF_e to NEOREC-SH as well as the orientation of the material location as shown in Fig 5.13. The second quadrant of the B-H curve with H of 950kA/m and B_r= 1.28T of NEOREC-SH is shown in Fig 5.12. Its relative permeability (μ_r) is close to 1.1. The new simulation is run for 4 seconds with a time-step of 0.02 milliseconds. Fig 5.14 shows the run-up speed response illustrating the typical speed curve of an IPM synchronous motor. The run-up time is quite fast with typical overshoots and settles in smooth synchronization at 1500 rpm (for 4-pole 50 Hz IPM motor).

When the motor is connected to a balanced 3-phase 50 Hz system, it runs-up toward synchronous speed, using its rotor cage winding. This run-up torque is comprised of a steady time averaged accelerating torque and a pulsating torque. The resultant accelerating torque is responsible for propelling the rotor forward while the pulsating torque produces noise and vibration during starting period. The resultant motor torque is comprised of two components one is called the induced cage torque and the other one is magnet torque. The cage torque depends highly on stator winding reactance and rotor resistance, and the magnet torque depends on air gap excitation reactance and back-electromotive force (EMF) [32]. Fig 5.15 shows the torque versus time response of V-shape line-start IPM synchronous motor. The torque response is quite normal for the line-start IPM synchronous motor with minor dip for a very short period.

Fig 5.16 shows the induced voltage-time response of V-shape line-start IPM synchronous motor. Fig 5.17 shows the current-time response of the V-shape IPM synchronous motor with the same loading conditions.

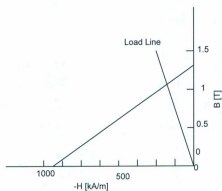


Fig 5.12: Demagnetization curve of NEOREC Magnet

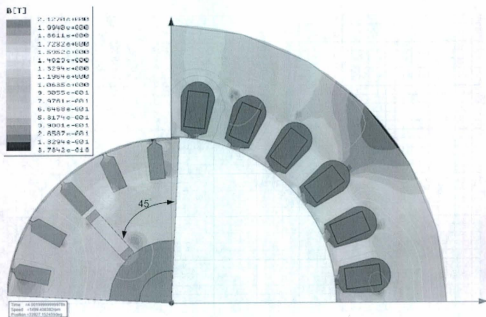


Fig 5.13: Flux density for V-shaped line-start IPMSM with an initial angle of -45°

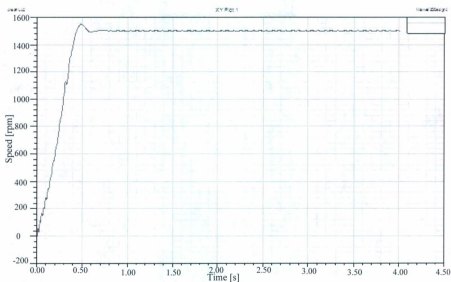


Fig 5.14: Speed-time response of V-shaped line-start IPMSM

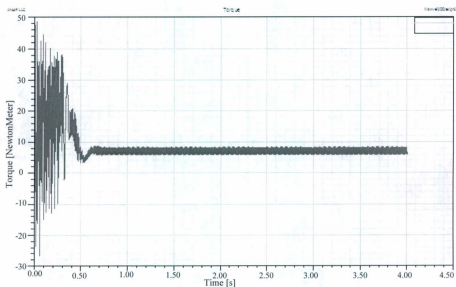


Fig 5.15: Torque-time response of V-shaped line-start IPMSM

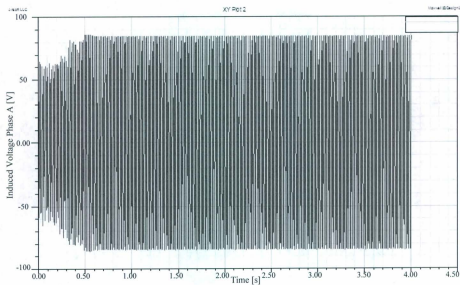


Fig 5.16: Induced voltage- time response of V- shaped line-start IPMSM

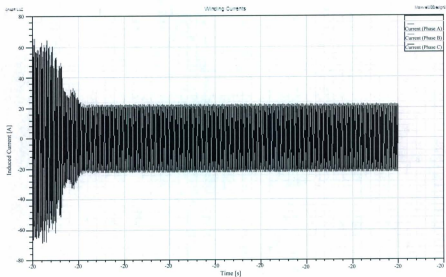


Fig 5.17: Induced current-time response of V-shaped line-start IPMSM

5.4 Partial V-shape line-start IPMSM

Fig 5.18 shows the cross-section of one quarter of a partial V-shape IPM synchronous motor. For this motor the four-pole magnets arrangement in the rotor is oriented in partial V-shape for a high-field-type IPM synchronous motor. The model rotor has the following distinctive design features.

- 1) The fluxes from both sides of the magnet are concentrated effectively in the middle of the magnetic poles of the rotor.
- 2) The reluctance of the d -axis is larger than that of the q -axis, because the d -axis flux passes across the magnet with high reluctance. Large reluctance torque can be obtained [100].
- 3) The large pull-in torque can be obtained due to deep conduction cage bars in the rotor.
- 4) The conducting material between the magnet and the rotor core is made from aluminum and has both functions of the flux barrier and conduction cage bar.

In particular, the conducting material on the magnet near the air gap decreases the magnet leakage flux in the rotor iron core and causes large reluctance torque. These features are different compared to the configurations of the V-shaped line-start PM synchronous motors in the previous model.

Furthermore, the number and configuration of rotor slots have been successfully designed so that the waveform of the induced electromotive force (EMF) due to the PMs is close to the sine waveform and the cogging torque is low [97]. The magnetic material used here is NEOREC-SH which is circumferentially magnetized, so that it shows almost the same magnetic flux lines (contours). Fig 5.19 shows the finite element grids of one quarter of the partial V-shape IPM synchronous motor. Fig 5.20 shows magnet flux lines (contours) of partial V-shape IPM synchronous motor. Fig 5.21 shows the magnet flux density characteristics of the partial V-shape IPM synchronous motor.

Table 5.3: Specification of partial V-shaped permanent magnet synchronous motor

Power Rating	687 kW
Line Voltage	140.31V (P-P)
Rated Current	3A
Base speed	1500 rpm
No. of Phases	3
No. of Poles	4
No. stator slots	24
No. of cage slots	24
Conductors	56
Connection	Y
Winding Layout	Single layer
Stator Outer Diameter	128mm
Stator Inner Diameter	77mm
Rotor Outer Diameter	76.2mm
Rotor Inner Diameter	16mm
Rotor Length	70mm
End Connection Resistance	3.43715e-006ohm
End Connection Inductance	1.95246e-009H
Moment of inertia	0.0278 kgm ⁻²
Load Torque	3.82 Nm

The pertinent design information is included in Table 5.3. The calculated value of inductance for stator winding is 0.0028509H and resistance is 5.09 Ω . The voltage in stator winding was set at 130 volt first for

the experimental motor, because the power factor at no load is low at this voltage from V-curve as the experimental result shows. But the simulated motor could not start or synchronize with the large load inertia at 130V. Therefore we chose the rated voltage at 140V L-L considering the requirement of sufficient line-start capability and the efficiency-power-factor product. Fig 5.22 shows the simulated speed-time responses with 3.82Nm load when the motor is supplied with balanced three phase voltages at a rated frequency of 60 Hz and rated voltage of 140V. The inertia of the rotor is 0.0278kgm^{-2} . The results showed in Fig 5.22 are during the run-up and synchronizing period when time-steps are set at 0.02 milliseconds and initial angle was set to -45° . Fig 5.23 shows the torque-time response for this model.

Fig 5.24 shows the input current (phase A) vs. time response for this model. As the motor is connected to a balanced three phase system of voltages so the input current for other two phases should be the same and mutually displaced by 120° . The induced current has a number of harmonics until the motor reaches the synchronization speed of 1800 rpm. This time is almost 2.5 seconds for higher stator inductance and a large load. Fig 5.25 shows the induced voltage vs. time curve. Fig 5.26 shows the magnetic flux lines changes against a normalized distance of rotor.

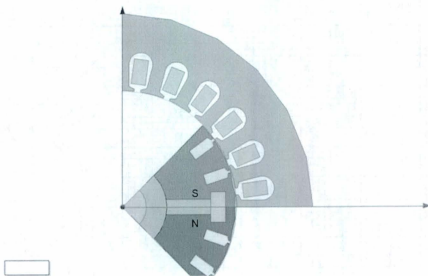


Fig 5.18: Cross-section of line-start IPMSM with partially V-shaped magnet arrangement

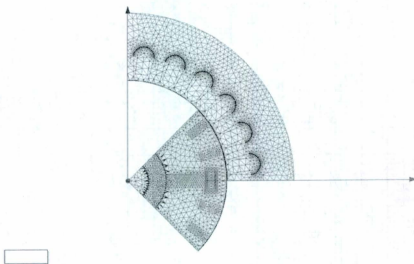


Fig 5.19: Finite Elements (grid) for partial V-shaped IPMSM for magnetic flux distribution in the motor

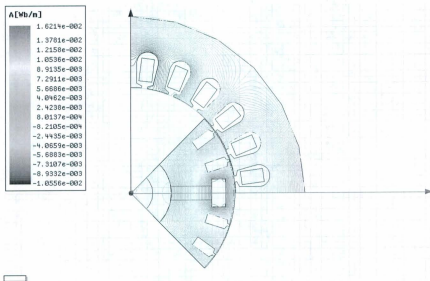


Fig 5.20: Magnetic flux lines (contours) for partially V-shaped line-start IPMSM

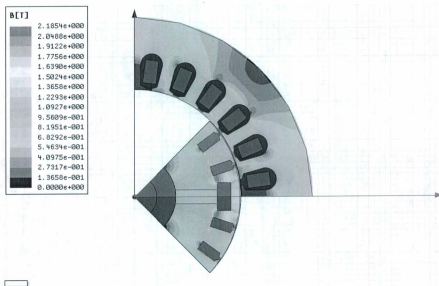


Fig 5.21: Flux density for partially V-shaped line-start IPMSM

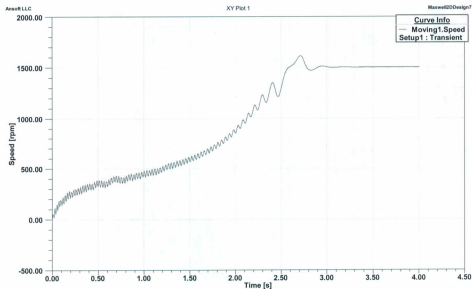


Fig 5.22: Speed-time response of line-start partial V-shaped IPMSM

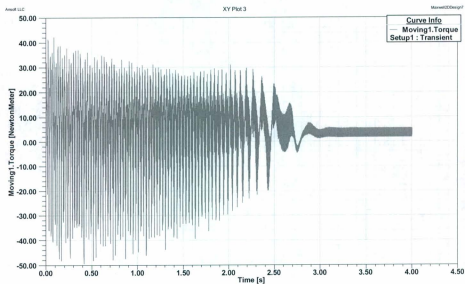


Fig 5.23: Torque-time response of partial V-shaped line-start IPMSM

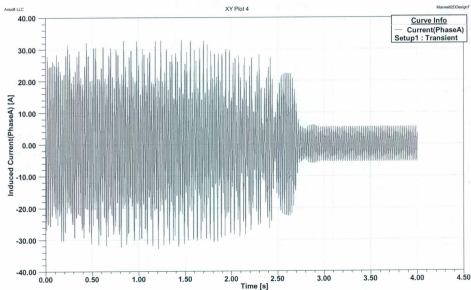


Fig 5.24: Motor current-time response partial V-shaped line-start IPMSM (Phase A)

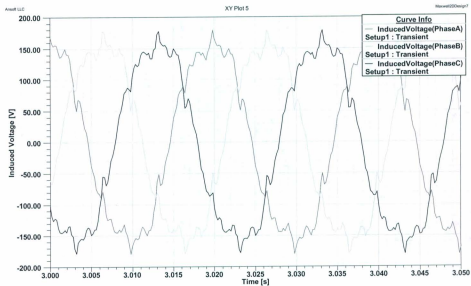


Fig 5.25: Simulated voltage versus time waveforms of line-start IPMSM

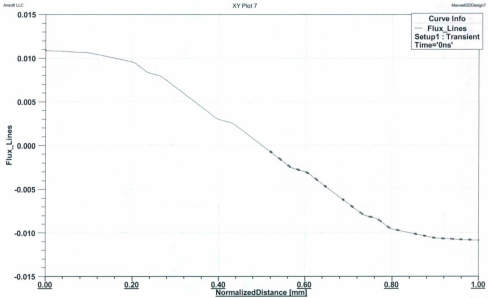


Fig 5.26: Flux lines vs. Normalized distance for partial V-shaped IPMSM

5.4.1 Loss Calculation

Iron losses are caused by eddy currents and hysteresis losses in the iron path. Iron losses occur in the stator back structure (yoke) and stator iron teeth and stator iron bridges and losses due to saturation. These losses are defined as stator iron loss. Also iron losses occur in the rotor iron core of an IPM synchronous motor. This is called rotor iron loss. These two stator iron losses and rotor iron losses are defined as core loss in the transient finite element analysis used in this thesis [99]. Fig 3.27 shows Core loss versus time curve of partial V shape IPM synchronous motor.

Copper loss consists of stator i^2R loss in stator iron and rotor conduction cage. These two copper losses are defined as solid loss in transient FEM analysis in the context of this thesis.

Stray load loss consists of mechanical losses like friction and windage loss, stator tooth losses, losses arising due to saturation in stator and rotor iron lamination and stranded steady-state and transient losses.

This is usually called standard (constant) loss. Fig 3.28 shows Standard loss versus time curve of the partial V- shape IPM synchronous motor. Fig 3.29 shows all the losses vs. time curve of the partial V- shape IPM synchronous motor. It is to be noted that transient losses are high but the steady-state losses only 5-8% of the partial V-shape IPM synchronous motor.

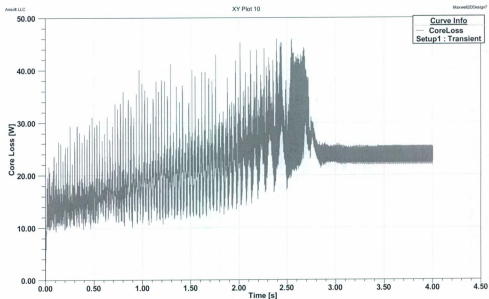


Fig 5.27: Core Loss- time response for partial V-shaped line-start IPMSM

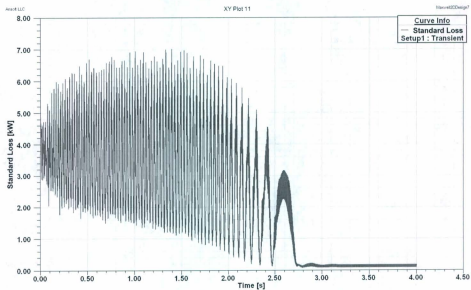


Fig 5.28: Standard Loss- time response of partial V-shaped line-start IPMSM

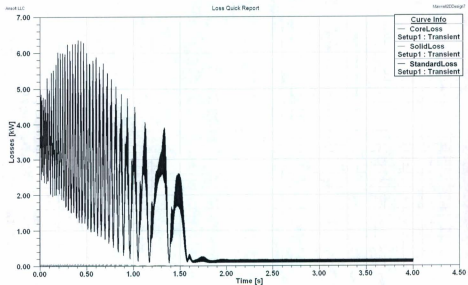


Fig 5.29: Loss-time report on partial V-shaped line-start IPMSM

5.4.2 Airgap Flux Distribution calculation

The length of the air gap influences the shape in the air gap flux density distribution. The leakage flux around the end of the magnet is mainly behind this shape change. The flux crossing the airgap funnels into stator teeth which is almost half the space in stator periphery at a radius halfway down the slot. So the airgap length increases with each stator slot. Given the magnet type, the increase of air gap length will result in the distortion of the maximum flux density. Fig 5.30 plots the airgap flux density against normalized rotor distance.

For this analysis we had to carry magnetostatic field simulation on this model. The procedure is carried out for maximum 10 passes with a limit of 10% error on each pass. Permanent magnet is the sole source of excitation in this case and the maximum length of each element in FEA is set to 3mm.

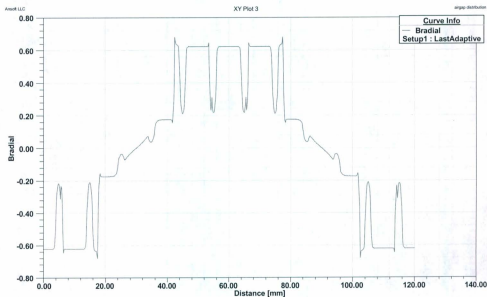


Fig 5.30: Flux distribution vs. normalized distance curve.

5.4.3 Back-EMF Calculation

Maxwell® commercial package does not offer the options of directly calculating back-EMF for 2D analysis of an IPM motor model. So we used the concept of “blocked rotor test” where the rotor is blocked so that it cannot rotate. Hence slip is equal to unity and balanced three phase voltages are applied to stator terminal. The blocked rotor test should be performed under certain voltage and frequency for which the performance is already known. This test demands a prior knowledge of leakage impedance. So we set the stator winding leakage resistance and inductance to the lowest value.

We artificially set the output torque to zero, the motor was running at rated speed 1500 rpm, and set the winding current to 0A. The simulation was run for 50 ms with a time step of 0.1 ms and from the induced voltage in the air gap, the back-EMF is computed. Fig 5.31 shows the back-EMF waveforms. It is to be noted that the back-EMF waveforms of partial V-shape IPM synchronous motor contain significant harmonics. The harmonic contents are expressed by the total harmonic distortion factor (THD). The orientation and shape of rotor permanent magnets influence the THD of this section. The minimization of the THD factor for IPMSM is attempted in this thesis.

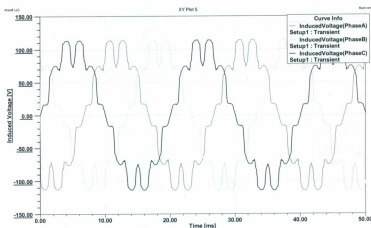


Fig 5.31: Back EMF- waveforms for partial V-shaped IPMSM

5.4.4 Cogging Torque Calculation

Cogging torque is the result of the interaction between the permanent magnets and stator slot opening in the air gap. Cogging torque adds a ripple component to the desired constant output torque from the machine. This can produce vibration and noise which in effect, reduces the performance of IPM motor. The cogging torque characteristics are susceptible to minor loop excursion caused by magnet shape and size, magnet flux barrier angle or even stator slot depth [98].

In Finite Element Analysis, the cogging torque is computed from magnetic energy variation. For an open circuit analysis, no electrical energy exchange is permitted through the motor terminals; we set the input current to 0 Amp. A rigorous constant speed of 1800 rpm (synchronous speed) was imposed to avoid any other inertial torque contribution. Cogging torque was calculated from output torque. Simulation was run for 60 ms with a time step of 0.12 ms. Fig 5.32 shows the cogging torque versus time curve for partial V-shaped line-start IPM synchronous motor.

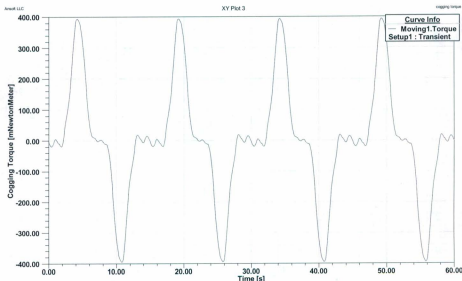


Fig 5.32: Cogging torque vs. time curve for partial V-shaped line-start IPMSM

5.5 Partial V-shape with concentrated winding

Stator concentrated winding is becoming popular to be used in place of the distributed winding in cases of many electric appliances. However, their usage is mainly limited to low speed operation where motor size is not an issue. The issues of concentrated windings are not dealt with vividly in this thesis.

However few models are established to show some promising results. Fig 5.33 shows the cross section of partial V-shaped line-start IPMSM with concentrated winding in two dimensional views. Fig 5.34 shows the flux line contour for the same motor and Fig 5.35 shows the flux density distribution of a typical line-start IPM synchronous motor with concentrated stator windings.

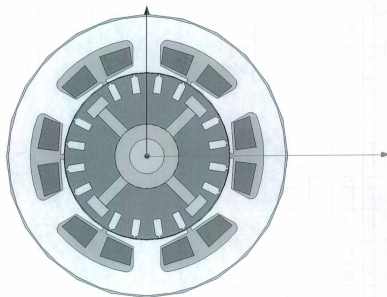


Fig 5.33: Partial V-shaped line-start IPMSM with concentrated winding

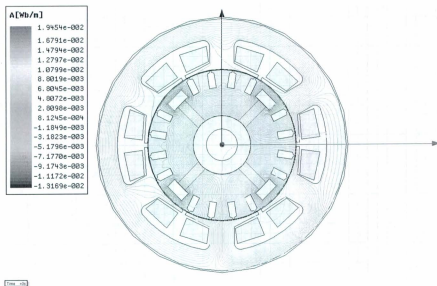


Fig 5.34: Flux lines in partial V-shaped line-start IPMSM with concentrated winding

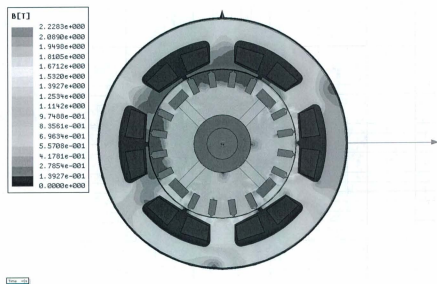


Fig 5.35: Flux density distribution in partial V-shaped line-start IPMSM with concentrated winding

Simulation results shown in this chapter show a good agreement with already published result of Dr. Kazumi Kurihara and Dr. M. A. Rahman during their work on high-efficiency line-start interior permanent magnet synchronous motors [39]. The established results from their experiments are attached in Appendix B.

Chapter 6

Conclusion and Future Work

The design of line-start interior permanent magnet synchronous motors depends on accurate calculation of starting and synchronous performances. Traditional equivalent circuits and lumped parameter model fail to take into account saturation, complex shapes and arrangements of permanent magnet, flux barriers induced eddy currents etc. Finite Element Analysis is of great help as it formulates a variational expression called energy functional. For electromagnetic field problems, this energy functional is the energy stored in the field. Using this method the field region is subdivided into smaller units and from energy functional formulations, unknown quantities are calculated for each element. For precise electric machine performance evaluations, a combination of finite element analysis and coupled circuit analysis is required for a minimum computational effort. On this line, the first stage is the analytical procedure to develop a unified lumped parameter circuit model. The second stage should follow the extraction of lumped parameters using finite element analysis.

The first chapter of this thesis is an overview of early history on the development of permanent magnets and their application in modern motor technology. The chapter summarizes the inclusion of finite element methods for the analysis of permanent magnet machines and recent advances made in recent years in the field of finite element analysis of permanent magnet synchronous motors.

The second chapter gives a generalized lumped parameter model for line-start interior permanent magnet synchronous motors. A per-phase equivalent circuit is proposed taking into account the saliency of a PM motor and the influence of core losses. Park's transformation is used to transform the motor quantities

from traditional abc coordinates to $dq0$ coordinates. Finally based on these a torque expression is developed based on coupled circuit method.

In the third chapter, a Finite Element approach is explained for analysis of interior permanent magnet synchronous motors. This chapter explains the major steps in solving a finite element problem. Based on Maxwell's theory first energy functional is developed. From these energy functional formulations, pertinent motor parameters like inductances and performances like torque can be calculated. These are explained in the later part of the chapter. Maxwell® 2D as a software package to employ the finite element method is also introduced in this chapter.

The advent of modern computing power, computer aided design technique makes possible the employment of numerical methods like Newton- Raphson (N-R) method, Jacobi's method for solving traditional motor problems. In the fourth chapter, how computer aided design tools can better address various design complicacies of line-start permanent magnet synchronous motors is explained. A step-by-step procedure is given to make a model in Maxwell® 2D and to solve various design parameters of a line-start IPM synchronous motor.

In chapter 5, simulation models and results for various line-start interior permanent magnet synchronous motors are presented. As part of this study, we built 3 models based on basic rotor structures using Maxwell® and AutoCad®. Simulations were run on these models to make a comparison among the already established results and the results found using Maxwell®. Although the straight shape magnet model of line-start IPMSM shows some starting performance lapse for higher core loss and standard loss, the V-shape and partial V-shape rotor permanent magnets show good starting and synchronous performances. It is to be noted that, performance of partial V-shape IPMSM is in good agreement with already published results.

The main objective for this thesis was to develop a unified approach for design and modeling of line-start synchronous motors. This objective has been achieved. In that process three basic models were analyzed and a comparison was made among the models with performance graphs and results found from simulation results.

The work presented in this thesis is the first phase of design and development of an Interior Permanent Magnet Wind Generator under the NSERC strategic grant. Although in motoring application usage of permanent magnets is very wide, in power generation they have not gained that strong a foothold. As in the later part of this research, a "Double-Layered Interior Permanent Magnet Generator" with straight and pi shape rotor structure is already developed. The optimization of the PMs is established based on the induced electromotive force (EMF), harmonic contents of the stator current and torque ripples at low speeds. The optimization shows that the π -shape double-layered permanent magnets geometry is capable of inducing an EMF with the high magnitude and low harmonic contents, along with producing stator currents with the low harmonic contents and minimum torque ripples [101]. The finding from this research is accepted and awaiting publication at International Electric Machines and Drives Conference 2011 (IEMDC 2011).

In future, the research will be extended to work on IPM wind generator based on various rotor structures. The main objective will be proposing rotor layouts to increase the air gap flux to ensure high induced terminal voltage at low operating speeds of typical IPM wind generators.

References

- [1] F. W. Merrill, "Permanent magnet excited synchronous motors," AIEE Transaction, vol. 74, pp. 1754-1760, 1955.
- [2] C. G. Veinott, "Theory and design of small induction motors," New York: McGraw-Hill, 1959.
- [3] M. A. Copeland and G. R. Slemon, "An analysis of the hysteresis motor: II-the circumferential-flux machine," IEEE Transactions on Power Apparatus and System, vol. 83, pp. 619-625, June 1964.
- [4] A. Moraru, "Starting and operation of asynchronous single-phase micro-motor", Review R. Sci. Tech. Electrotech, 12, pp. 549-562, 1967.
- [5] M. A. Rahman, M. A. Copeland and G. R. Slemon, "An analysis of the hysteresis motor: III-parasitic losses," IEEE Transactions on Power Apparatus and System, vol. 88, no. 6, pp. 954-961, June 1969.
- [6] D. O'Kelly, "Equivalent circuits for single phase induction and hysteresis motors," IEEE Transactions on Power Apparatus and System, vol. PAS-90, no. 1, pp. 279-288, January/February 1971.
- [7] K. J. Binns, W. R. Barnard and M. A. Jabbar, "Hybrid permanent magnet synchronous motors," IEE Proc., part B, vol.125, no.3, pp. 203-208, 1978.
- [8] B. Adkins and R.G. Harley, "The general theory of alternating current machines", Chapman & Hall, London, 1978.
- [9] R. Steen, "Direct axis aiding permanent magnets for a laminated synchronous motor rotor," U. S. Patent 4,139,790, February 13, 1979.

- [10] M.A. Rahman and D.B. Patton, "Single-phase Balanced Operation of Polyphase Hysteresis Motors," Proc. of IEEE International Electrical and Electronics Conference and Exposition, Toronto, October 2-4, 1979, pp. 136-137.
- [11] K. Miyashita, H. Okuda, S. Yamashita and S. Tanabe, "Stress protection for permanent magnet type synchronous motor," U. S. Patent 4,144,469, March 13, 1979.
- [12] M. A. Rahman, " Permanent magnet synchronous motor-a review of the design art," in Proc. of Int. Conf. of Electrical Machines-ICEM'80, Athens, Greece, September 15-17, 1980, pp. 312-319.
- [13] M.A. Rahman, "Combination hysteresis, reluctance, permanent magnet motor", US Patent No. 5,187,401, February 16, 1993.
- [14] P. Zhou, M.A. Rahman and M.A. Jabbar, "Field circuit analysis of permanent magnet machines," IEEE Transactions on Magnetics, vol. 30, no. 4, pp. 1350-1359, July 1994.
- [15] M. A. Rahman and P. Zhou, "Analysis of brushless permanent-magnet synchronous motors," IEEE Transactions on Industrial Electronics, vol. 43, no. 2, pp. 256-267, April 1996.
- [16] George J. Wey, "The Shielding of Permanent Magnets From Transient Magnetic Fields", American Institute of Electrical Engineers, Transactions of the Volume: 60, Issue: 9, Publication Year: 1941, Page(s): 875 – 877.
- [17] S. Evershed, "Permanent magnets in theory and practice", Journal of the Institution of Electrical Engineers, Volume: 58, Issue: 295 Publication Year: 1920 , Page(s): 780 – 825.
- [18] Robert M.Saunders and Robert H. Weakley, "Transactions of the American Institute of Electrical Engineers", Volume: 70, Issue: 2 Publication Year: 1951, Page(s): 1578 – 1581.
- [19] Maurice W.Brainard, "Synchronous Machines with Rotating Permanent-Magnet Fields; Part I. Characteristics and Mechanical Construction", Transactions of the American Institute of Electrical Engineers Power Apparatus and Systems, Part III. Volume: 71, Issue: 1 , Part: III Publication Year: 1952 , Page(s): 670 – 676.

- [20] M. W. Brainard, "Dry Plate Type Rectifier", U.S. patent no. 2665334, 9 Apr 1951.
- [21] David Ginsberg and Leo J. Misenheimer, "Design Calculations for Permanent-Magnet Generators", Transactions of the American Institute of Electrical Engineers, Power Apparatus and Systems, Volume: 72, Issue: 2, Part: III Publication Year: 1953, Page(s): 96 – 103.
- [22] Nicola Bianchi and Thomas Jahns, "Design, Analysis and control of Interior PM Synchronous machines", IEEE IAS tutorial course 2004 on Permanent-Magnet Excited Synchronous Motors.
- [23] D. D. Hershberger, "Design Considerations of Fractional Horsepower Size Permanent-Magnet Motors and Generators", Transactions of the American Institute of Electrical Engineers Power Apparatus and Systems, Volume: 72, Issue: 2, Part: III Publication Year: 1953, Page(s): 581 – 585.
- [24] D. J. Hanrahan and D. S. Toffolo, "Permanent Magnet Generators Part I - Theory", Transactions of the American Institute of Electrical Engineers Power Apparatus and Systems, Volume: 76, Issue: 3, Publication Year: 1957, Page(s): 1098 – 1103.
- [25] P. Gozzoli, "Contributo Al Calcolo Degli Alternatori A Magneti Permanenti", Elettrotecnica, Milan, Italy, vol. 40, no. 10, 40, 1953 pp. 537-52.
- [26] J.F. Bell, "Permanent magnet materials", IEE Colloquium on Permanent Magnet Machines and Drives, Publication Year: 1993 , Page(s): 1/1 - 1/4.
- [27] M. A. Rahman, Akira Chiba, Kai Wang, and H. M. Zubayer, "Advances on Single Phase Line-start High Efficiency Interior Permanent Magnet Motors", IEEE transactions on Industrial Electronics 2010 (accepted not published).
- [28] C. G. Veinott, "Theory and design of small induction motors," New York: McGraw-Hill, 1959.

- [29] H. M. Zubayer, Dr. Karim Shaarbafi and Dr. M. A. Rahman, "Comparative study on line-start permanent magnet synchronous machines with different rotor structures", The Eighteenth Annual Newfoundland Electrical and Computer Engineering Conference, 2010.
- [30] M. Rahman, A. Osheiba and T. Radwan, "Synchronization process of line-start permanent magnet synchronous motor," *Electric Machines and Power Systems*, vol. 25, 1997, pp 577-592.
- [31] J. Salo, T. Heikkila, J. Pyrhonen, "New low-speed high-torque permanent magnet synchronous machine with buried magnets," *Proc. ICEM 2000*, 28-30 August, 2000, Espoo, Finland, vol.2, pp.1246-1250.
- [32] V.B. Honsinger, "Permanent Magnet Machines: Asynchronous Operation," *IEEE Trans. Power Apparatus and Systems*, Vol. PAS-99, No. 4 July/Aug.
- [33] K. Kurihara and M.A. Rahman, "Transient performance analysis for permanent-magnet hysteresis synchronous motor", *IEEE Transactions on Industry Applications*, Volume: 40 , Issue: 1 Publication Year: 2004 , Page(s): 135 – 142.
- [34] A.C. Smith, E. Peralta-Sanchez and S. Purbrook, "Line-start permanent magnet motors for pump applications", *The 3rd IET International Conference on Power Electronics, Machines and Drives*, 2006. PEMD 2006. Publication Year: 2006, Page(s): 526 – 530.
- [35] K.J. Binns, M.S.N. Al-Din and P.J.G. Lisboa, "Use of canned rotors in high-field permanent magnet machines", *IEE Proceedings B Electric Power Applications*, Volume: 139, Issue: 5 Publication Year: 1992, Page(s): 471 – 477.
- [36] J. Qian and M.A Rahman, "Analysis of field oriented control for permanent magnet hysteresis synchronous motors" *IEEE Transactions on Industry Applications*, Volume: 29 , Issue: 6 Publication Year: 1993 , Page(s): 1156 – 1163.

- [37] F. Libert and J. Soulard, "Manufacturing Methods of Stator Cores with Concentrated Windings", The 3rd IET International Conference on Power Electronics, Machines and Drives, 2006. Publication Year: 2006, Page(s): 676 – 680.
- [38] K.J. Binns, F.B. Chaaban and A.A.K. Hameed, "Major design parameters of a solid canned permanent magnet motor with skewed magnets", IEE Proceedings B Electric Power Applications, Volume: 140, Issue: 3 Publication Year: 1993, Page(s): 161 – 165.
- [39] K. Kurihara and M. Azizur Rahman, "High efficiency line-start interior permanent magnet synchronous motors", IEEE Transactions on Industry Applications, Volume: 40, Issue: 3 Publication Year: 2004, Page(s): 789 – 796.
- [40] Maxwell, Electrical Engineering Simulation Software, Copyright 1984-2003, Ansoft Corporation, Four Station Square, Suite 200, Pittsburgh, PA 15219.
- [41] M. Popescu, T. J. E. Miller, Malcolm I. McGilp, G. Strappazzon, N. Trivillin, and R. Santarossa, "Line-Start Permanent-Magnet Motor: Single- Starting Performance Analysis", IEEE Transactions on Industry Appl., Vol. 39, No. 4, July/August 2003, pp 1021-1030.
- [42] T. J. E. Miller, "Synchronization of line-start permanent-magnet ac motors", IEEE Trans. Power Apparatus Systems 1984; PAS-103:1822–8.
- [43] M. A. Rahman and A. M. Osheiba, "Parameter sensitivity analysis for line-start permanent magnet motors." In: Electric machine and power systems, vol. 14; 1988. pp. 195–212.
- [44] S. Ruoho, E. Dlalal, and A. Arkio, "Comparison of Demagnetization Models for Finite-Element of Permanent-Magnet Synchronous Machines", IEEE Trans. on Magnetics, Vol. 43, No. 11, pp. 3964–3968, Aug. 2006.
- [45] N. Bianchi and S. Bologniani, "Design techniques for reducing cogging torque in surface mounted PM motors," IEEE Trans. Ind. Applicat., vol. 38, no. 5, pp. 1259–1265, Oct. 2002.

- [46] P. Zhu, S. Ruangsinnchaiwanich, D. Isahak, and D. Howe, "Analysis of cogging torque in brushless machines having no uniformly distributed stator slots and stepped rotor magnets", IEEE Trans. on Magnetics., vol. 41, no. 10, pp. 3910–3912, Oct. 2005.
- [47] T. Ding, N. Takorabet, F. M. Sargos, and X. Wang, "Design and Analysis of Different Line-Start PM Synchronous Motors for Oil-Pump Applications", IEEE Trans. on Magnetics, Vol. 45, No. 3, March 2009.
- [48] R. W. Clough, "The Finite Element in Plane Stress Analysis", Proc. 2nd conf Electronic Computation, ASCE, Pittsburg, Pa Publication Year: 1960.
- [49] P. Silvester and M. V. K. Chari, "Finite Element Solution of Saturable Magnetic Field Problem", IEEE trans. on PAS, PAS-89, 1642-1651.
- [50] M. V. K. Chari and Z. J. Csendes, "Finite Element Solution Of Saturable Magnetic Field Problem", IEEE trans. on Magnetics, Vol. MAG-13, No. 5 pp 1125-27, 1977.
- [51] P. Silvester and R. L. Ferrari, "Finite Elements for Electrical Engineers", Cambridge University Press, 1990.
- [52] P. Silvester, H. S. Cabayan and B. T. Browne, "Efficient Techniques for Finite Element Analysis of Electrical Machines", IEEE trans. on Power Apparatus and Systems, Vol. PAS-92, No. 4, pp-1274-81, 1973.
- [53] F. A. Fouad, T. W. Nehl, and N. A. Demerdash, "Magnetic field modeling of permanent magnet type electrically operated synchronous machines using finite element", IEEE trans. on Power Apparatus and System, Vol. PAS-100, No. 9, pp. 4125-35, 1981.
- [54] D. Shen, G. Meunier and J. L. Coloumb, "Solution of Magnetic fields and electrical circuits combined problems", IEEE trans. on Magnetics, Vol. MAG-21, No. 6, pp. 2288-91, 1985.
- [55] Thomas W. Nehl, Fakhry A. Fouad and Nabeel A. Demerdash, "Dynamic Simulation of Radially Oriented Permanent Magnet-Type Electronically Operated Synchronous Machines

- with Parameters Obtained from Finite Element Field Solutions", IEEE Transactions on Industry Applications, Volume: IA-18 , Issue: 2 Publication Year: 1982 , Page(s): 172 – 182.
- [56] B.J. Chalmers, S.A. Hamed and G.D. Baines, "Parameters and performance of a high-field permanent-magnet synchronous motor for variable-frequency operation", IEE Proceedings on Electric Power Applications, Volume: 132, Issue: 3 Publication Year: 1985, Page(s): 117 – 124.
- [57] M.A. Rahman, P. Zhou, D. Lin and M.F. Rahman, "Measurement of parameters for interior permanent magnet motors", IEEE Power & Energy Society General Meeting, 2009. PES '09.
- [58] T. W. Nehl, F. A. Fouad and N. A. Demerdash, "Determination of Saturated Values of Rotating Machinery Incremental and Apparent Inductances by an Energy Perturbation Method", IEEE Transactions on Power Apparatus and Systems, Vol. PAS-101, No. 12 December 1982.
- [59] N. Bianchi and S. Bolognani, "Magnetic models of saturated interior permanent magnet motors based on finite element analysis", The 1998 IEEE Industry Applications Conference, 1998. Thirty-Third IAS Annual Meeting, Volume: 1 Publication Year: 1998 vol.1, Page(s): 27 - 34.
- [60] J. Mizia, K. Adamiak, A.R. Eastham and G.E. Dawson, "Finite element force calculation: comparison of methods for electric machines", IEEE Transactions on Magnetics, Volume: 24 , Issue: 1 Publication Year: 1988 , Page(s): 447 – 450.
- [61] K. Binns, C. Riley and M. Wong, "The efficient evaluation of torque and field gradient in permanent-magnet machines with small air-gap", IEEE Transactions on Magnetics, Volume: 21, Issue: 6 Publication Year: 1985, Page(s): 2435 – 2438.

- [62] J. Coulomb and G. Meunier, "Finite element implementation of virtual work principle for magnetic or electric force and torque computation", IEEE Transactions on Magnetics, Volume: 20, Issue: 5 Publication Year: 1984, Page(s): 1894 – 1896.
- [63] M. Marinescu and N. Marinescu, "Numerical computation of torques in permanent magnet motors by Maxwell stresses and energy method", IEEE Transactions on Magnetics, Volume: 24, Issue: 1 Publication Year: 1988, Page(s): 463 – 466.
- [64] L. Chang, A.R. Eastham and G.E. Dawson, "Permanent magnet synchronous motor: finite element torque calculations", IEEE Industry Applications Society Annual Meeting, 1989, Conference Record of the 1989 Publication Year: 1989, Page(s): 69 - 73 vol.1.
- [65] Andrew M. Knight and Catherine I. McClay, "The Design of High-Efficiency Line-Start Motors", IEEE transactions on industry applications, vol. 36, no. 6, November/December 2000.
- [66] R. H. Park, "Two-reaction theory of synchronous machines generalized method of analysis-part I", Transactions of the American Institute of Electrical Engineers, Volume: 48, Issue: 3 Publication Year: 1929, Page(s): 716 – 727.
- [67] Paul C. Krause, "Analysis of electric machinery", McGraw Hill, 1986, Page(s) 140-143.
- [68] T. J. E. Miller, "Design of Brushless Permanent-Magnet Motors", Oxford Science Publications 1994.
- [69] D. M. Triesenberg, "Electric Power Systems", Purdue University, 1978.
- [70] A. E. Fitzgerald, Charles Kingsley Jr. "Electric Machinery", McGraw Hill, 1990.
- [71] Anastasis C. Polycarpou, "Introduction to the Finite Element Method in Electromagnetics", Morgan & Claypool Publishers, 2006.
- [72] A. B. J. Reece and T. W. Preston, "Finite Element Methods in Electrical Power Engineering", Oxford University Press, 2000.

- [73] R. S.Varga, "Matrix Iterative Analysis", Prentice-Hall, Englewood Cliffs, New Jersey, 1962.
- [74] D. M. Young, "Iterative Solution of Large Linear Systems". New York: Dover Publications, 2003.
- [75] Y. Saads, "Iterative Methods for Sparse Linear Systems". Boston: PWS Publishing, 1996.
- [76] A. M. Bruaset, "A Survey of Preconditioned Iterative Methods. London", UK: Chapman & Hall, 1995.
- [77] Peyman Niazi, "Permanent Magnet Assisted Synchronous Reluctance Motor Design and Performance Improvement", Ph. D thesis, Texas A&M University, December, 2005.
- [78] N. Sadowski and Y. Lefevre, "Finite Element Calculation in Electrical machines while considering the movement", IEEE Transactions on Magnetics, March 1992.
- [79] A. Arkkio, "Time-stepping finite element analysis of induction motors", ICEM -1988, pp. 275-282.
- [80] John R Brauer, "What Every Engineer Should Know about Finite Element Analysis", New York, Marcel Dekker, 1988.
- [81] DA Lowther and PP Silvester, "Computer Aided Design in Magnetics", Berlin, Springer Verlag, 1986.
- [82] J.L. Coulomb, "A Methodology the determination of global electromechanical quantities from a finite element analysis and its application to the evaluation of magnetic forces, torques and stiffness", IEEE Trans.Magn.19, No.6, November 1983, pp.2514- 2519.
- [83] T.Kabashimal, A.Kawahara and T.Goto, "Force calculation using magnetizing currents", IEEE Trans.Magn.24, No.1, January 1988, pp.451-454.
- [84] N. A. Demerdash and T. M. Hijazi, "Computation of Winding Inductances of Permanent Magnet Brushless De Motors With Damper Windings By Energy Perturbation", IEEE Transactions on Energy Conversion, Vol. 3, No. 3, September 1988.

- [85] Alfio Consoli and Alfonso Abela, "Transient performance of permanent magnet AC motor drives", IEEE Trans. on Industry Applications, Vol. IA-22, No.1, pp 32-41, 1986.
- [86] M. Azizur Rahman and Ping Zhou, Determination of Saturated Parameters of PM Motors Using Loading Magnetic Fields, IEEE Transactions on Magnetics, vol. 27, no. 5, September 1991.
- [87] B. Mellara, E. Santini, "FEM Computation And Optimization Of L_d And L_q In Disc PM Machines", 2nd Int Workshop on Electr and Magn Fields, Leuven, Belgium, 1994, Paper No. 89.
- [88] R Wang, NA Demerdash, "Comparison of load performance and other parameters of extra high speed modified Lundell alternators". IEEE Trans on EC, 1992.
- [89] Ling Qin, "A Permanent-Magnet Switched-Flux Generator", Ph. D thesis, University of Nevada, Reno, August 2005.
- [90] Zonhfanzhu, "An intelligent CAD System for DC machines", Master's thesis, McGill University, July 1991.
- [91] Ralph E. Tarter, "Solid-state power conversion handbook", Wiley Science, 1993.
- [92] S. A. Nasar, "Schaum's Outline of Theory and Problems of Electric Machines and Electromechanics", McGraw Hill, 1997.
- [93] Tomy Sebastian, "Steady-state Performance of Variable Speed Permanent Magnet Synchronous Motor", Ph. D. thesis, University of Toronto, 1986.
- [94] M. A. Rahman, G. R. Slemon, "Analytical Models For Interior-Type Permanent Magnet Synchronous Motors" IEEE Transactions on Magnetics, vol. mag-21, no. 5, September 1985.
- [95] W. L. Soong, "Design and Modelling of Axially-Laminated Interior Permanent Magnet Motor Drives for Field Weakening Applications", Doctoral Thesis, University of Glasgow, September 1993.

- [96] Steffen Hahlbeck and D. Gerling, "Design Considerations for Rotors with Embedded V-Shape Permanent Magnets", Conference proceedings of International Conference on Electrical Machines, 2008.
- [97] Chao-hui Zhao, Shui-liang Li and Yang-guang Yan, "Influence Factor Analysis of PMSM Air Gap Flux Density", IEEE ICEMS 2005.
- [98] A. Keyhani, T. Sebastian et al, T. Sebastian and S.K. Murthy, "Study of Cogging Torque in Permanent Magnet Machines", IEEE IAS general meeting 1997.
- [99] Gordon R. Slemon and X. Liu, "Core Losses in Permanent Magnet Motors" IEEE Transactions on Magnetics, vol. 26, no. 5, September 1990.
- [100] G.Wakui, K. Kurihara, and T. Kubota, "Hybrid permanent-magnet synchronous motor," Trans. Inst. Elect. Eng. Jpn., vol. 110-D, no. 7, pp. 841–847, 1990.
- [101] Saleh A. Saleh, H. M. Zubayer, T. Iqbal, M. A. S. K. Khan, M. A. Rahman, "Design and Performance of a Double-Layered Interior Permanent Magnet Generator", International Electric Machines and Drives Conference 2011, Niagara Falls, May 15-18, 2011

Appendix A

Setting Up a Maxwell Design for IPM motors

The steps given in this Appendix are obtained from Ansoft Manual [40]. After inserting a design, one does not need to perform the basic steps sequentially, but they all must be completed before a solution can be generated.

To set up a Maxwell design, follow this general procedure:

- 1) Insert a Maxwell design into a project. After you insert the design, you can then set the model's units of measurement and the background material.
- 2) Draw the model geometry.
- 3) Specify the solver type.
- 4) Assign material characteristics to objects.
- 5) Assign boundaries and excitations.
- 6) (For Transient Solutions Only) Set up motion.
- 7) Add parameters for which you want to solve.
- 8) Specify mesh settings.
- 9) Specify how Maxwell will compute the solution.
- 10) (Optional) Set up any optimetrics you want to run.
- 11) Run the simulation.
- 12) View solution results, post-process results, view reports, and create field overlays.
- 13) (Optional) Export the circuit to generate a circuit equivalent of the model.

For simplicity the steps are tucked down to bare nominal as explained below.

1) Inserting a Maxwell Design

The first step in setting up a Maxwell Project is to add a design to the active project.

To insert a design:

1. Click Project and select one of the following:
 - Insert Maxwell 3D Design
 - Insert Maxwell 2D Design
 - Insert RMXprt Design
2. The new design is listed in the project tree. It is named Maxwell3DDesign n , Maxwell2DDesign n , or RMXprt Design n by default, where n is a number signifying the order in which the design was added to the project.

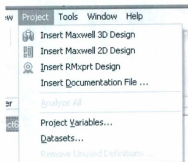


Fig A.1: Menu for inserting a project

The Modeler window appears to the right of the Project Manager. You can now create the model geometry.

Note:

Click the plus sign to the left of the design icon in the project tree to expand the project tree and view specific data about the model.

2) Drawing a Model

After you insert a design into the current project, you can draw a model of the electromagnetic structure. The general strategy is to build the model as a collection of 3D objects. You can assign any single material to each 3D object.

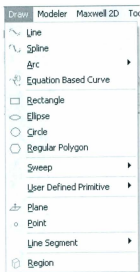


Fig A.2: Drawing Menu for Maxwell 2D

You can create 3D objects by using the modeler's Draw commands or you can draw 1D and 2D objects, and then manipulate them to create 3D objects. Objects are drawn in the 3D Modeler window. You can also import objects from other systems.

To open a new 3D Modeler window, do one of the following:

- Insert a new design into the current project.

- Double-click a design in the project tree.

The model you draw is saved with the current project when you click File>Save.

Note

If you access your machine via Remote Desktop, if Maxwell is running and one or more modeler windows are open, those modeler windows automatically close. The message manager window displays a message indicating that Maxwell closed the modeler windows.

Note

If the menu command is unavailable, then the selected design is already in the modeler window.

3) Specifying the Solver Type

Before you begin to draw the models in your project, choose which field solver to use for it. Each solver requires a different type of problem setup. If you later change the solver, all problem setups become invalid, and all solutions are deleted. Because of this, it is a good idea to decide on a solver before starting.

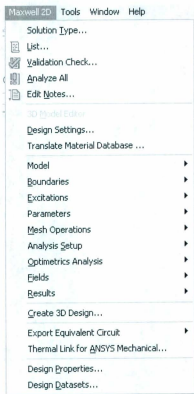


Fig A.3: Menu for specifying a solver

To specify a solver:

1. Click Maxwell 2D>Solution Type or Maxwell 3D>Solution Type.

The Solution Type window appears with the solvers generally split between Magnetic and Electric solver types.

1. For Maxwell2D designs, select one of the following solver types:
 - Magnetostatic
 - Eddy Current

- Transient
- Electrostatic
- AC Conduction
- DC Conduction

4) Assigning Materials

You can add, remove, and edit materials in two main ways:

- Using the **Tools>Edit Configured Libraries>Materials** menu command.
- Right-clicking **Materials** in the project tree and selecting **Edit All Libraries**.

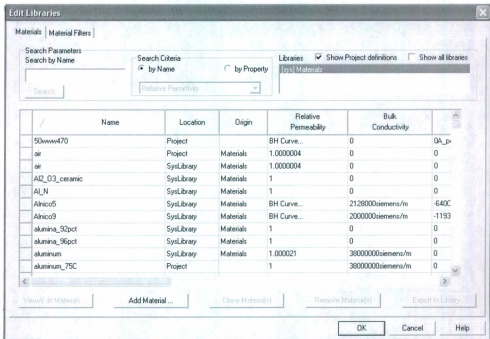


Fig A.4: Menu window for editing a material

Editing definitions from the project window does not modify the configured libraries for any particular design. To consider the current design, use the **Tools>Edit Configured Libraries** option. Doing so ensures that new libraries are added to the configured list for the current design. If you edit materials from this command for the current and then export them, they will also be available to assign to objects in other designs.

To assign a material to an object, follow the general procedure:

1. Select the object to which you want to assign a material.

2. Click **Modeler>Assign Material**  .

The **Select Definition** dialog box appears. When the **Show all libraries** checkbox is selected, the window lists all of the materials in Ansoft's global material library as well as the project's local material library.

You can also open the **Select Definition** window in one of the following ways:

- In the **Properties** dialog box for the object, click the material name under the **Attributes** tab. A drop-down menu shows an **Edit...** button that opens the **Select Definition** window. The menu also lists materials included in the current project. Selecting one of these materials provides another way to assign materials to an object.
- Right-click **Model** in the project tree, and then click **Assign Material** on the shortcut menu.
- Right-click the object in the history tree, and then click **Assign Material** on the shortcut menu.

3. Select a material from the list.

Note:

You can search the listed materials by name or property value.

If the material you want to assign is not listed, add a new material to the global or local material library, and then select it.

4. Click **OK**.

The material you chose is assigned to the object.

Note:

In the history tree, by default, Maxwell groups objects by material. To change the default, select the object icon and right-click to display the Group Objects by Material checkbox.

5) Assigning Boundaries and Excitations for 3D Designs

For every project, you need to assign boundaries and excitations. For 3D designs, you can use the Maxwell3D menu or the project tree to do the following:

- Define boundary conditions that control how the electric or magnetic field behaves at object faces, planes of symmetry and periodicity, and edges of the problem region.
- Define excitations of voltage, charge, coil, and current.
- Identify conductors in which eddy currents are induced.
- For magnetic transient projects, set up a winding and an external circuit connection.

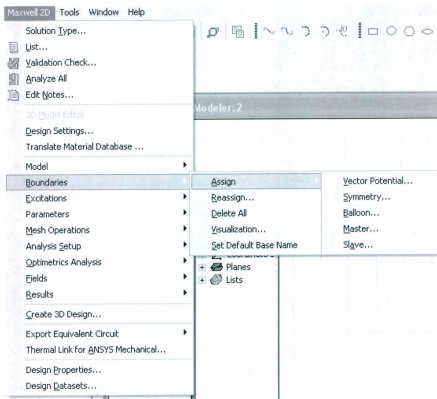


Fig A.5: Menu for assigning boundary conditions

Each field solver requires you to specify excitations of electric or magnetic fields and references for computing these fields.

- Magnetostatic Boundaries and Excitations
- Electrostatic Boundaries and Excitations
- DC Conduction Boundaries and Excitations
- Eddy Current Boundaries and Excitations
- Transient Boundaries and Excitations

- Electric Transient Boundaries and Excitations

One must specify at least one of the boundary conditions or excitations listed in these sections, so that the simulator can compute accurate values for fields and parameters.

6) Setting Up Motion for Transient Projects

For transient projects (where you selected transient as the solution type), you need to define how the model components move in relation to one another. This is accomplished by assigning a **Motion Setup** to a Band object.

For Maxwell2D designs, two bands may be assigned with independent motion characteristics. Multiple motion bands are primarily for certain types of motors where multiple rotors may rotate about a common central axis; however, other applications are possible. For example, the project shown below is comprised of two rectangular magnets, each surrounded by a band object with a Motion-Setup assigned to it. When one magnet moves, the other magnet realigns itself. Also note that the solution context display shows the position and speed for both motion setups.

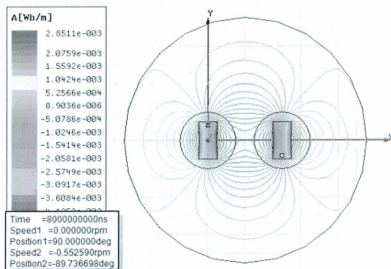


Fig A.6: Motion band Maxwell® design

7) Adding Solution Parameters

When you assign a solution parameter, the solver calculates the parameter value as part of the solution process. The table shows the solution parameters that may be calculated based upon the solver type.

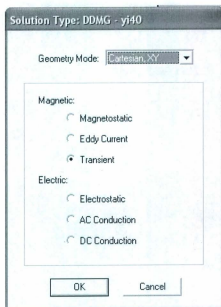


Fig A.7: Menu for specifying a solution

Table A.1: Solution parameters for Maxwell Design

Parameter	3D Solvers	2D Solvers
Force/Torque	Magnetostatic	Magnetostatic
	Electrostatic	Electrostatic
	Eddy Current	Eddy Current
	Transient	Transient
Matrix	Magnetostatic	Magnetostatic
	Electrostatic	Electrostatic Eddy Current

	Eddy Current	AC Conduction
--	--------------	---------------

8) Specify mesh settings.

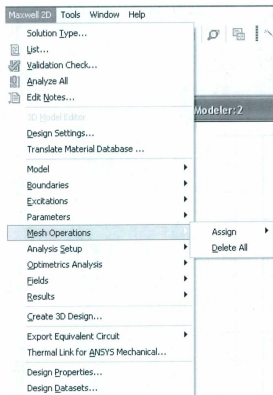


Fig A.8: Menu for specifying mesh operation

9) Specifying Solution Settings

Specify how Maxwell computes a solution by adding a solution setup to the design. You can define more than one solution setup per design. Each solution setup includes:

- General data about the solution's generation.

- Adaptive mesh refinement parameters if you want the mesh to be refined iteratively in areas of highest error.

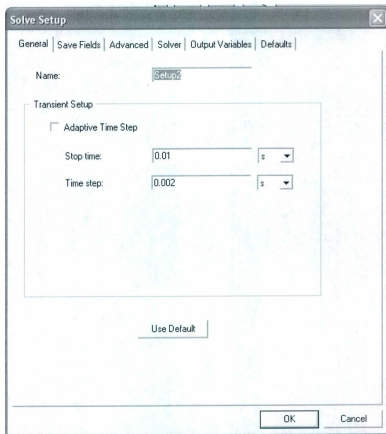


Fig A.9: Window for adding a solution setup

To add a solution setup to a design:

1. Select a design in the project tree.
2. Click Maxwell3D>Analysis Setup>Add Solution Setup or Maxwell2D>Analysis Setup>Add Solution Setup

- Alternatively, right click Analysis in the project tree, and then click Add Solution Setup on the shortcut menu.

The Solve Setup dialog box appears containing several tabs.

For Non-Transient Solutions

The following tabs are present for non-transient solutions:

General	Includes general solution settings.
Convergence	Includes settings for convergence.
Expression Cache	Contains an optional list of expressions that you can specify for convergence criteria.
Solver	Includes settings for nonlinear residual and matrix solver type.
Frequency Sweep	Includes setting for varying the frequency of an Eddy Current or AC Conduction solution. NOTE: This tab is present only for Eddy Current and AC Conduction solutions.
Defaults	Enables you to save the current settings as the defaults for future solution setups or to revert the current settings to Maxwell's standard settings.

For Transient Solutions

The following tabs are present for transient solutions:

General	Includes general solution settings.
Save Fields	Enables you to create a time point list for saving field solutions.
Advanced	Supports user control program, magnetization and import options, and computing various data for links.
Solver	Includes settings for nonlinear residual solver type.
Expression Cache	Contains an optional list of expressions that you can specify for evaluating solutions.
Defaults	Enables you to save the current settings as the defaults for future solution setups or to revert the current settings to Maxwell's standard settings.

For Electric Transient Solutions

The following tabs are present for electric transient solutions:

General	Includes general solution settings.
---------	-------------------------------------

Solver	Includes settings for initial condition, temporal tolerance, computing power loss data, importing a mesh, and enabling thermal feedback from ANSYS Mechanical.
Expression Cache	Contains an optional list of expressions that you can specify for evaluating solutions.
Defaults	Enables you to save the current settings as the defaults for future solution setups or to revert the current settings to Maxwell's standard settings.

3. Specify the desired settings on the tabs.
4. If you want to disable an individual analysis, uncheck the Enabled checkbox. Refer to Disabling and Enabling an Analysis Setup for additional information.
5. If you want to use the default values, click Use Default.
6. Click OK.

10) Optimetrics (Optional)

Optimetrics enables you to determine the best design variation among a model's possible variations. You create the original model, the nominal design, and then define the design parameters that vary, which can be nearly any design parameter assigned a numeric value in Maxwell. For example, you can parameterize the model geometry or material properties.

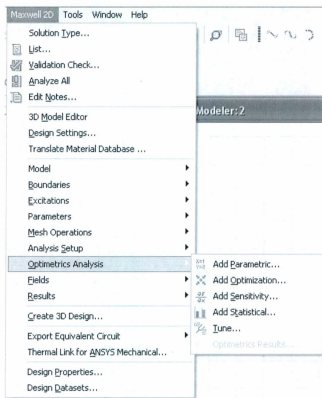


Fig A.10: Menu for adding a Optimetrics solution

You can then perform the following types of analyses on your nominal Maxwell design:

Parametric	<p>In a parametric analysis, you define one or more variable sweep definitions, each specifying a series of variable values within a range. For example, you can parameterize component values. (See Variables in Maxwell for more information.)</p> <p>Optimetrics solves the design at each variation.</p>
------------	--

	<p>You can then compare the results to determine how each design variation affects the performance of the design. Parametric analyses are often used as precursors to optimization solutions because they help to determine a reasonable range of variable values for the optimization analysis.</p>
Optimization	<p>For an optimization analysis, you identify the cost function and the optimization goal. Optimetrics changes the design parameter values to meet that goal. The cost function can be based on any solution quantity that Maxwell can compute.</p>
Sensitivity	<p>In a sensitivity analysis, you use Optimetrics to explore the vicinity of the design point to determine the sensitivity of the design to small changes in variables.</p>
Tuning	<p>Tuning allows you to change variable values interactively while monitoring the performance of the design. If you want to ensure that tuning does not resolve variations already solved by parametric setup, you must check Save Fields Mesh in the Options tab of the optimetrics setup.</p>
Statistical	<p>In a statistical analysis, you use Optimetrics to determine the distribution of a design's</p>

	performance, which is caused by a statistical distribution of variable values.
--	--

11) Running Simulations

After you specify how Maxwell is to compute the solution, you need to begin the solution process. In general, the Analyze command applies to the selected setup and associated sweeps, if any, or to a select sweep. To use this command, right-click on a setup or sweep in the Project tree, and click the command on the context menu. The Analyze All command applies to all enabled setups at or below the level invoked in the Project tree. To use this command, either click Maxwell 2D or Maxwell 3D>Analyze All or right-click on the Analysis icon in the Project tree and select Analyze All from the popup menu.



Fig A.11: Menu for running simulation

What do you want to do?

- Solve a single setup with or without sweeps
- Solve a specific sweep
- Enable a queue so that multiple simulations can run sequentially as resources become available.
- Run more than one simulation, whether multiple setups, or multiple sweeps under a single setup, or setups with dependencies.
- Monitor queued simulations
- Configure and run remote analysis
- Configure and run distributed analysis
- Monitor the solution process
- Change a solution priority for system resources
- Abort an analysis
- Re-solve after modifying a design
- Re-Solving after ANSYS Thermal Link Feedback

12.1 Viewing Solution Data

While Maxwell is generating a solution, or when it is complete, you can view the following information about the solution:

- Convergence information.
- Computing resources, or profile information, that were used during the solution process.
- Output Variables computed during each adaptive, non-adaptive, or sweep solution.
- Output Parameters and Matrix Data computed during each adaptive, non-adaptive, or sweep solution.

- Mesh data.

Note

Since adaptive mesh refinement is not performed for transient solutions, convergence data is not available for Transient analysis.

- The state of solved solutions.

To access the Solutions dialog box, in which the information above can be accessed, do one of the following:

- Click Maxwell3D, Maxwell2D, or RMXprt and then select Results>Solution Data.
- Right-click Results in the project tree, and then click Solution Data on the shortcut menu

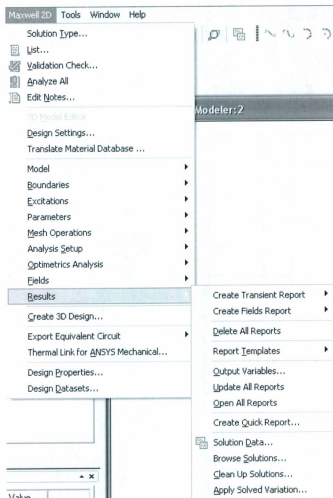


Fig A. 12: Menu for showing a result

12.2 Post Processing and Generating Reports

When Maxwell has completed a solution, you can display and analyze the results in the following ways:

- View solution data including the following: convergence information, computing resources that were used during the solution process, mesh statistics, and matrices computed during each adaptive, non-adaptive, or sweep solution.
- View analysis results for Optimetrics solutions.
- Plot field overlays - representations of basic or derived field quantities on surfaces or objects.
- Create 2D or 3D reports of RLC matrices and basic and derived field quantities.
- Plot the finite element mesh on surfaces or within 3D objects.
- Create animations of field quantities, the finite element mesh, and defined project variables.
- Use the Fields Calculator to perform computations using basic field quantities.

12.3 Creating Reports

After Maxwell has generated a solution, all of the results for that solution are available for analysis. One of the ways you can analyze your solution data is to create a 2D or 3D report, or graphical representation, that displays the relationship between a design's values and the corresponding analysis results. You create reports using either the Create Quick Report command, or the Create <type> Report commands. The Quick Report feature lets you select from a list of predefined categories (such as S-parameters) from which to create a rectangular plot.

For each solution type (Electrostatic, Magnetostatic, AC Conduction(2D only), DC Conduction, Eddy Current, Transient , or Electric Transient(3D only), the Results menus present a list of Create <type> Report commands based on the solution data of direct interest for the design. For example, for the Magnetostatic solution type, the Results menu contains templates for Magnetostatic Parameters and for Fields. These appear on the menus as Create Magnetostatic Report and Create Fields Report. Each of these Create <type> Report menu items includes a further cascading menu that lists the Display Types available for that report.

If you have created custom report templates (for example, including your company name or other format changes), you can also create a report based on that template by selecting Maxwell 2D, Maxwell 3D, or RMXprt>Results>Report Templates>PersonalLib><templateName>.

12.4 Plotting Field Overlays

Field overlays are representations of basic or derived field quantities on surfaces or objects for the current design variation. You can set the design variation via the Set Design Variation dialog. This dialog box is accessible from the Solution Data window via by clicking the ellipsis button on the right of the Design Variation field, and via the Results>Apply Solved Variation command.

To plot a basic field quantity:

1. Select a point, line, surface, or object to create the plot on or within. You may also select a plane or object list in the History Tree.

Note

For 2D Designs, a plane selection must be consistent with the drawing plane or an error will result.

If it does not exist, create it.

2. Click Maxwell3D or Maxwell2D and then select Fields>Fields.

A submenu appears.

3. On the Fields submenu, click the field quantity you want to plot.

If you select a scalar field quantity, a scalar surface or volume plot is created. If you select a vector field quantity, a vector surface or volume plot is created. If the quantity you want to plot is not listed, use Calculating a Derived Field Quantity.

The Create Field Plot dialog box appears.

The Specify Name field shows a name based on the field quantity you selected, and the Quantity list shows the field quantity selected.

4. To specify a name for the plot other than the default, select Specify Name, and then type a new name in the Name box.
5. To specify a folder other than the default in which to store the plot, select Specify Folder, and then click a folder in the pull-down list. Plot folders are listed under Field Overlays in the project tree.

Note:

All plots (field overlays) in the same folder have the same scale settings. To plot the same field with a different scale, you can create or move the new plot to a separate folder. By default, current density plots are stored in a folder called J, but you can specify a different or new folder. Plots in different folders have a different plot keys.

6. Select the solution to plot from the Solution pull-down list.
7. Select the field type to plot in the Field Type pull-down list.
8. Under Intrinsic Variables, select the time at which the field quantity is evaluated.
9. Select the field quantity to plot from the Quantity list.
10. Select the volume or surface (region) in which to plot the field from the In Volume list.

This selection enables you to limit plots to a volume or the intersection of a volume and the selected object. You may select multiple volumes in the list by holding down the Ctrl key while clicking.

Note:

The In Volume list should be used when plotting on a surface which has a discontinuous field solution across the boundary to select the object on one side of the surface.

11. Optionally, you may select the Plot on surface only checkbox to obtain a plot around the out-side edge of selected objects.
12. Click Done.

The field quantity is plotted on the surfaces or within the objects you selected. The plot uses the attributes specified in the Plot Attributes dialog box.

The new plot appears in the view window. It is listed in the specified plot folder in the project tree. If you have created a field plot on a simulation in progress, the field plot is updated after the last adaptive solution.

If you want to update the field overlay before then, to view progress in the solution, select the Field icon in the Project tree that contains the field plot of interest, right-click to display the short cut menu, and select Update Plots.

To turn off the display of the plot, right click on the plot and select Plot Visibility from the short-cut menu. Unchecking Plot Visibility turns off the plot display.

13) Exporting Equivalent Circuit Data

You can export lumped R, L, C data from a Maxwell solution to Ansoft SIMPLORER or Saber format. Importing the new data file to SIMPLORER or Saber enables you to include wave effects in the circuit simulations.

An equivalent circuit can be exported from a parametric solution or from an imported table.

Note:

You can only export an equivalent circuit from a parametric solution when the following two criteria are met:

- The solution type is Magnetostatic or Electric.
- A parametric setup exists.

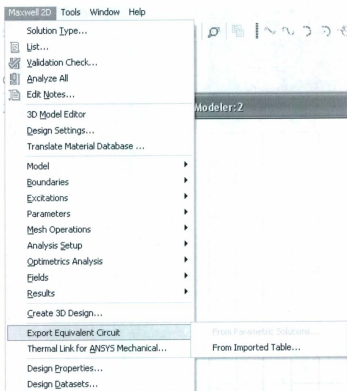


Fig A.13: Menu for Exporting solution data

Appendix B

Results from Published Literature

In their paper “High-Efficiency Line-Start Interior Permanent-Magnet Synchronous Motors” [39], Dr. Kazumi Kurihara and Dr. M. A. Rahman ran a series of simulations on a partial V-shape interior permanent magnet synchronous motor. The photograph of the experimental motor is given in Fig B.1.



Fig B.1: Experimental rotor.

The specification and results from simulations of the experimental motor are given below:

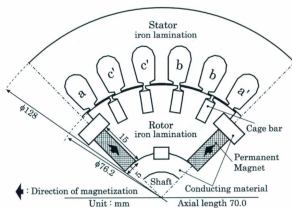


Fig B.2: Cross-section of experimental motor

Stator:	Outer diameter	128.0mm
	Inner diameter	77.0mm
	Stack length	70.0mm
	Number of slots	24
	Conductors per slot	56
Rotor:	Outer diameter	76.2mm
	Core length	70.0mm
	Inertia	0.0015kgm ²
Load:	Inertia	0.0263kgm ²

Fig B.3: Design data of experimental motor

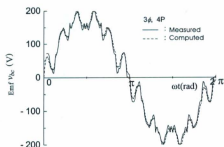


Fig B.4: EMF generated by PMs.

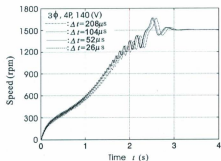


Fig B.5: Computed speed-time response at various time-steps

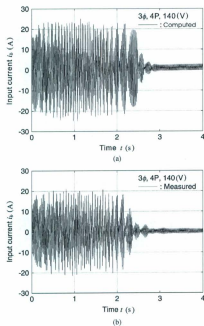


Fig B. 6 Input Current vs. time response in computed and measured results

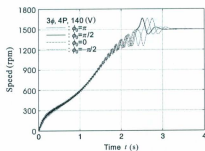


Fig B.7: Computed speed-time response at various initial angles

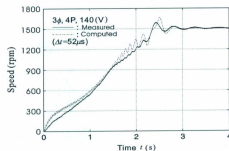


Fig B.8: Comparison between measured and computed speed-time response

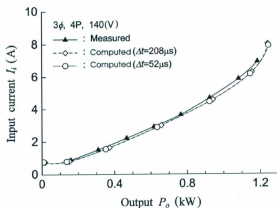
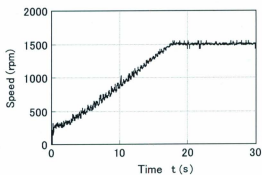
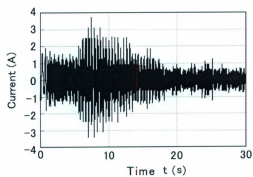


Fig B.9: Computed and measured results of input current versus output power.



(a)



(b)

Fig B.10: Measured results of run-up responses under V/f control.

(a) Speed response. (b) Current response.



